Final technical report

Partners:	Contract number:
DLR, Institute for Solar Research (DLR) (former DLR, Institute of Technical Thermodynamics) **University of Applied Science Aachen, Solar Institute Jülich (SIJ)** **RWTH Aachen University, Institute for Automation Control (IRT)** **RWTH Aachen University, RWTH Aachen University, Institute for Power Plant Technology, Steam and Gas Turbines (IKDG)** (former Institute of Steam and Gas Turbines, IDG) **K.U. Leuven, Electrical Engineering Department, Leuven, Belgium (OPTEC)**	**VH-VI-208**

Name of the project:	
vICERP: Virtual Institute of Central Receiver Power Plants	
Project duration: **Jan 1, 2008 – October 31, 2011**	Report period: **January 1, 2008 – October 31, 2011**
Confidentiality: **Public report**	
Date: **March 27, 2012**	
Version: **Final version**	
Authors: **Tobias Hirsch, Editor (DLR)** **Nils Ahlbrink (DLR)** **Jan Gall (IRT)** **Vera Nolte (IKDG)** **Cristiano Teixeira-Boura (SIJ)** **Joel Andersson (OPTEC)**	
Approved by: **Robert Pitz-Paal (DLR)** **Spiros Alexopoulos (SIJ)** **Mathias Hakenberg (IRT)** **Philipp Vennemeier (IKDG)** **Till Doerbeck (KAM)** **Moritz Diehl (OPTEC)**	

This page left blank.

Table of Contents

I. Aim and structure of the project

I.1. Market situation for solar tower systems

While the first round of solar thermal power plant construction mainly in Spain was dominated by parabolic trough systems, solar tower plants are gaining more and more attraction. The motivation behind this development is the potential for further cost reduction which is estimated to be higher than the one for line focusing systems. The first commercial tower plants are in operation in Spain (PS10-10 MW, PS20-20MW, Gemasolar 17 MW with 16 h storage) and in the US (e-solar). In the race for better cost efficiency a number of technologies is being developed or even projected in parallel. Among them are:

- Molten salt systems (Solar Two, Gemasolar)
- Saturated steam systems (PS10, PS20)
- Superheated steam systems (e-solar)
- Open volumetric air receivers (Solar tower Jülich)
- Closed air receivers for gas turbine integration (project Solugas)

The technologies differ in the temperature levels that are reached, the type of machine that is used (steam or gas turbine) and the way thermal storage capacities can be implemented. In terms of storage capacity, the concept with open volumetric receiver has some intrinsic advantages. With air at ambient pressure as a heat transfer fluid the fluid cycle and especially the storage can be designed in a cost-efficient way. A first demonstration plant has been erected in the German town Jülich near Cologne, see Figure I.1-1. The plant is equipped with a 1.5 MW_{el} steam turbine, a solar receiver and a 1.5 h storage system. Although the system feeds electricity to the grid it is mainly designed as a research and demonstration facility. Since 2011 the facility is owned by DLR.

In this concept, the heliostat field concentrates the solar irradiation onto the receiver arranged at the tower. There, the porous ceramic structure is heated and ambient air is suckd through the heated receiver. On its way through the receiver cups, the air is heated to about 680 °C. In the waste heat boiler, the air temperature air transfers its energy to the water-steam cycle, which then drives the steam turbine. During high solar irradiance periods hot air can be directed through the storage system. Heat generated in the solar receiver can be supported by heat from the storage during low irradiance periods. The cold (120 °C) return air from the storage and/or the boiler is transported through the receiver, and from there to the front of the receiver surface. It thus increases the air inlet temperature and thus the efficiency of the system. The thermodynamic parameters given in the scheme reflect the configuration of the Solar Tower Jülich.

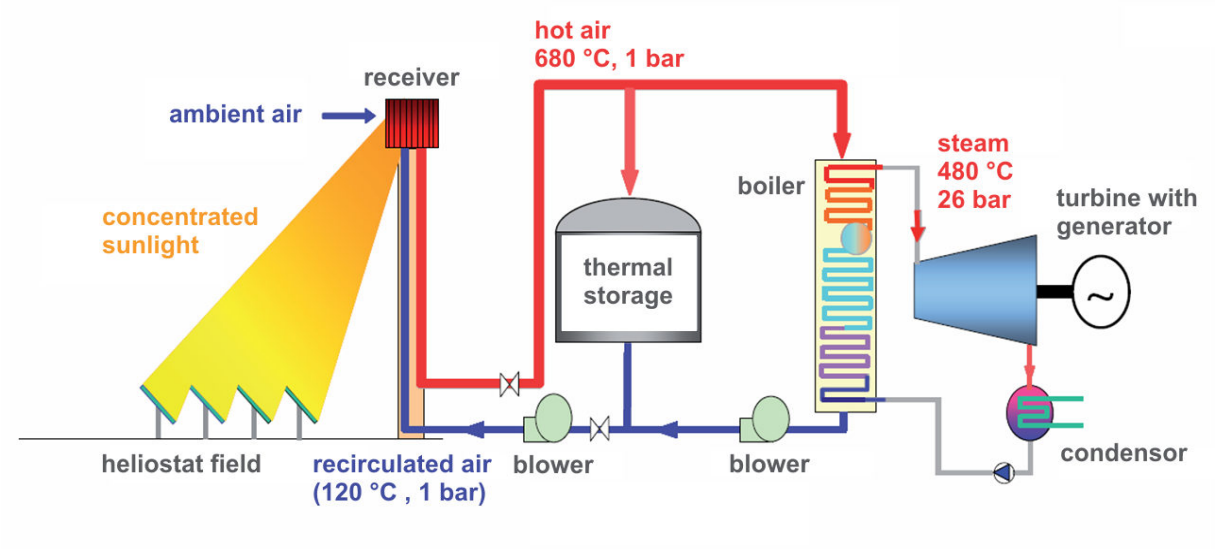

Figure I.1-1: Scheme of the Solar Tower Jülich demonstration plant

Experiences with existing plants show that, besides the improvement in cycle efficiency, transient effects significantly influence the operational behaviour and thus the economics of solar thermal power plants. For tower systems characterized by high flux densities in the receiver transients in the critical components should be carefully analysed prior to erecting a plant.

I.2. Aims of the project

The aim of the vICERP is to build up capacities in the field of dynamic simulation for solar tower systems. The initial phase of the project intends to bring together experts from different fields, create sensitivity for the special boundary conditions in solar thermal power plants, and set up numerical tools for investigation of dynamic effects. The activities were linked to the open air receiver technology since broad expertise in this concept was already available at DLR and SIJ. However, the models and methods developed are transferable to other tower technologies. The cooperation between the partners formed during this project is intended to be continued in follow-up activities to ensure continuity and dissemination of results. The main aims of the initial phase of the vICERP project can be summarized as:

- Development of dynamic simulation models for central receiver power plants
- Validation of the models by means of the Solar Tower Jülich plant as an example
- Analysis of design improvements.
- Development of innovative control concepts
- Development of numerical optimization tools especially for optimizing the dynamic behaviour.
- Establishment of a close cooperation between the participating institutions.
- Increase of human resource in the field of solar thermal power plants.

I.3. Consortium

The vICERP consortium is composed of five partner institutes. Their contributions to this project were:

- DLR Institute of Solar Research (formerly Institute of Technical Thermodynamics, department Solar Research)
  - co-ordination
  - heliostat field modelling and validation
  - receiver modelling and validation
  - coordination of system model
- University of Applied Science Aachen, Solar Institute Jülich (SIJ)
  - thermal storage modelling and validation
  - interface to operational data from the Solar Tower Jülich plant
- RWTH Aachen University, Institute of Power plant technology, Steam and Gas Turbines (IKDG)
  - Modelling and validation of the water-steam cycle
- RWTH Aachen University, Institute of Automation Control (IRT)
  - Development of advanced control concepts
- Katholieke University of Leuven (Belgium), Optimization in Engineering Department (OPTEC):
  - Development of numerical optimization tools

II. Results of WP 1 – Transient model library development

II.1. System level model

In order to make use of the flexibility an object-oriented modelling approach offers the model structure has to be well defined. On the top level, the main components like solar receiver, storage system and water-steam cycle are connected by fluid streams. The model structure should allow for

- Easy replacement of component models without changes in the rest of the top level model
- Extension of the layout by new components
- Different degrees of detail of the component models in one plant model
- Robustness in boundary conditions

For the vICERP project a structure based on the staggered grid approach is applied. This will be described in the following.

A common way of modelling 1-dimensional thermo-fluid flows is to use the finite volume method. A special case of this method is the so called “staggered grid“ method, where all fluxes are calculated on the border of a control volume and the intensive quantities are calculated in the center of a control volume [1]. It is the only reasonable method, if lumped and distributed models are used within one library [2]. Its major advantage is that component equations and the media models are decoupled by the use of capacitive and non-capacitive elements. This approach is demonstrated for a pipe section, see Figure II.1-2.

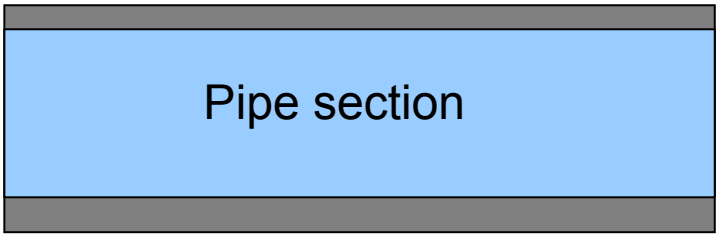

Figure II.1-2: Pipe section

The fluid inside a pipe section is discretized with the finite volume method with two control volumes. By applying the staggered grid method all fluxes are calculated on the border of a control volume and the intensive quantities are calculated in the center of a control volume. In the following equations the mass flow rate $\dot{m}$, the enthalpy flow rate $\dot{H}$, pressure p, pressure drop dp, mass m, internal energy U, and the specific enthalpy h are used to demonstrate a possible set of balance equations.

A dynamic version of the energy and mass balance can be formulated and solved for these control volumes, as all terms appearing in these balance equations are either constants, or fluxes calculated on the border of the control volume, or the considered derivative with respect to time.

The momentum balance, however, is formulated for a control volume, which is shifted half a control volume. For the shifted control volume, the intensive quantities are known on the border of the control volume. As the intensive quantities like pressure are used in the momentum equation, this balance equation can be solved only for a shifted control volume.

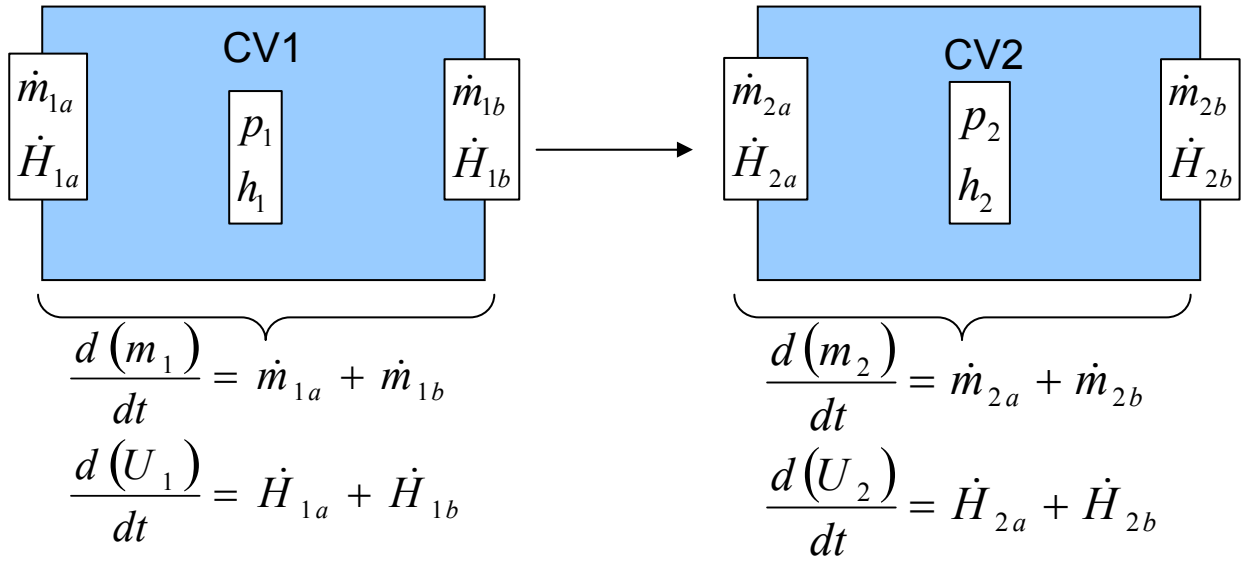

Figure II.1-3: Discretized pipe section with two control volumes

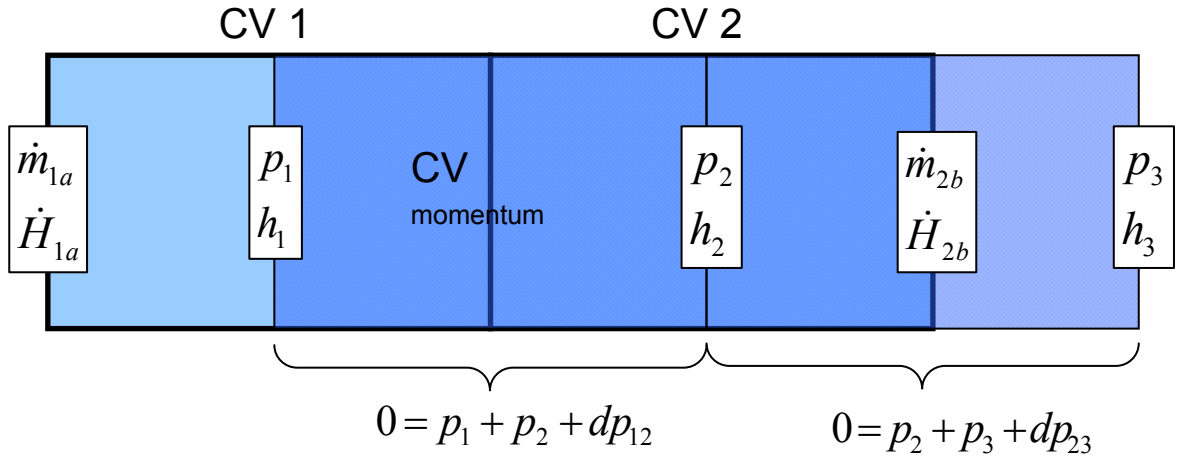

Figure II.1-4: Demonstration of the shifted control volume in the "staggered grid" method

This approach results in two different elements if implemented in Modelica. Connectors are used to link the models. One element, which is called capacitive or volume element, includes the dynamic mass and energy balances. The pressure is held constant over the control volume. The intensive quantity pressure is calculated in the centre of the volume element and is given to the connector. Therefore, its value is known on the border of the adjacent flow element as demanded by the staggered grid method.

In the other element, which is called non-capacitive or flow element, the momentum balance is implemented. A static set of mass and energy balance is used. They are set up in an alternating sequence to obtain a full set of balance equations resulting in the described staggered grid method.

The described pipe section can be modelled with an alternating sequence of volume and flow elements. To obtain a symmetric component, the last flow model can be devided into two half elements, whereas one half is moved to the inlet of the component.

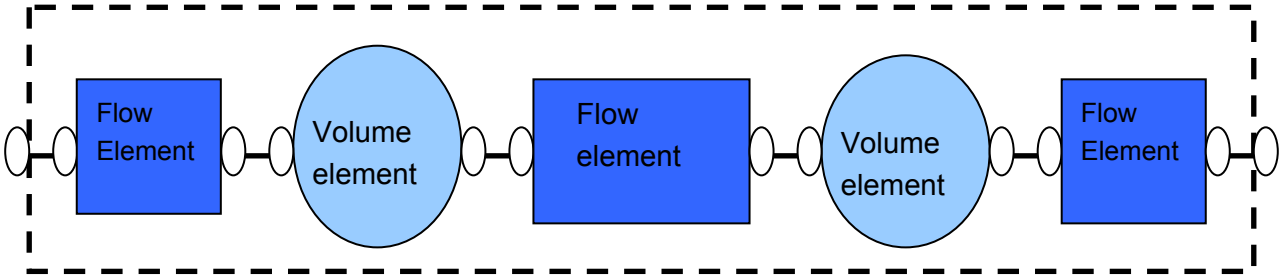

Figure II.1-5: Modelica model of the fluid section

This method is not only valid for a single pipe section but also appropriate for a complete system. Models of a receiver, a storage tank or a boiler are built up of volume and flow elements applied alternatively. For example, the fluid pipe section model would be connected to one volume element either side.

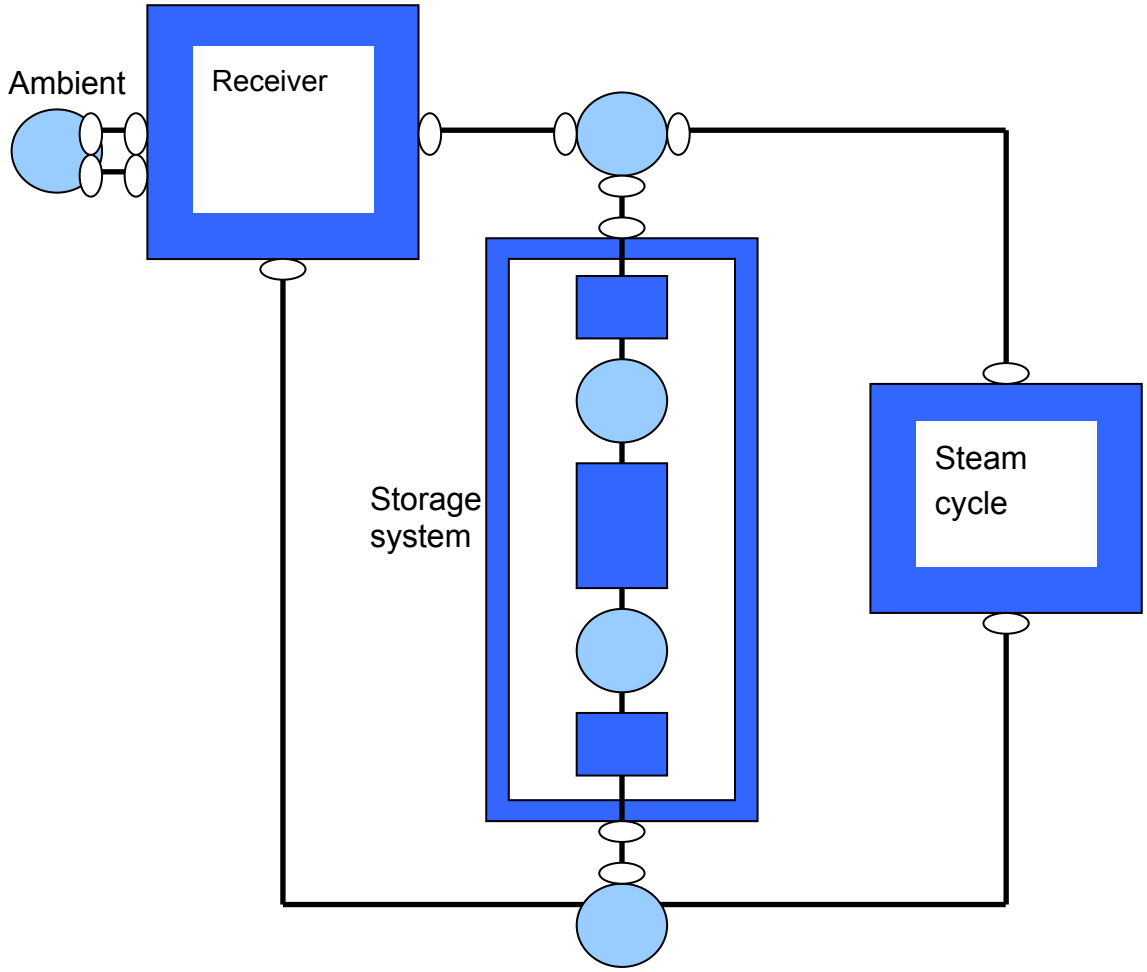

Figure II.1-6: Simple system setup using volume and flow elements

This approach is demonstrated with a simple system setup showing the central components receiver, storage system, and the steam cycle. The inside of the storage system model is shown, demonstrating the usage of the volume and flow elements in the storage system model itself and outside in the system. The central components are symbolized as flow elements because the closing elements at the border of these components are flow elements.

However, inside these components volume elements can be implemented as shown for the storage system.

II.2. Heliostat field model

The heliostat field is the first component in the energy conversion chain of the solar thermal tower power. Losses caused by the quality of the heliostat field or the operational strategy have a significant impact on the plant performance due to its position in the chain. Besides, the heliostat field plays a decisive role concerning the dynamic effects of the power plant. As the sun position changes and the direct normal irradiation (DNI) fluctuates during the day, the heliostat field and its operational strategy generate an altering flux density distribution in time and local distribution on the receiver surface.

The heliostat field model has to make an appropriate representation of these effects with adequate calculation effort. For this reason, the ray tracing software STRAL (Solar Tower Ray Tracing Laboratory) was chosen for modelling of the heliostat field [3], [4]. STRAL was developed for detailed modelling of solar thermal tower power plants and covers detailed modelling of heliostats, modelling of shading objects like towers, the implementation of user-written receiver models, and includes an optimization algorithm for aim point optimization. Additionally, it is able to be used in a co-simulation with other simulation tools due to its TCP/IP-interface. In STRAL, individual heliostat geometries can be generated or inserted from other tools. If existent, the detailed mirror surface consistence measured with methods like deflectometry can be imported and used in STRAL. Blocking and shading of the heliostats and the shading of the tower is considered using efficient algorithms. Although STRAL performs only single time step calculations, it can be used for the described tasks, as the transient behaviour of the heliostat field is much faster than the behaviour of the receiver. It is sufficient to perform a series of single time step calculations, in which the heliostat movement can be included with using STRAL functionality called tracking function. In these tracking functions, a model for actuators can be included. The new angular position of the heliostats is calculated depending on the time step, the actuator model and the previous angular position.

For the heliostat field of the Solar Tower Jülich, the position of the heliostats and its general geometry is known. Deflectometry measurements were accomplished for only a few heliostats. This complicates the modelling of the heliostat field, as the existent measurements can not be used as representative heliostats. For this reason, the heliostat field model is set up with the correct general geometry of the heliostats (holding structure, mirror height, mirror width) but with an assumed fixed mirror error for all heliostats. An actuator model is implemented for the elevation and azimuth axes in tracking functions.

In addition, a model of the tower is set up to include the shading impact on the reflected solar power. During ray-tracing simulation the rays are checked for collision with the tower.

The graphical representations of the heliostat field model, the tower model, and of the receiver model in STRAL are shown in Figure II.2-7.

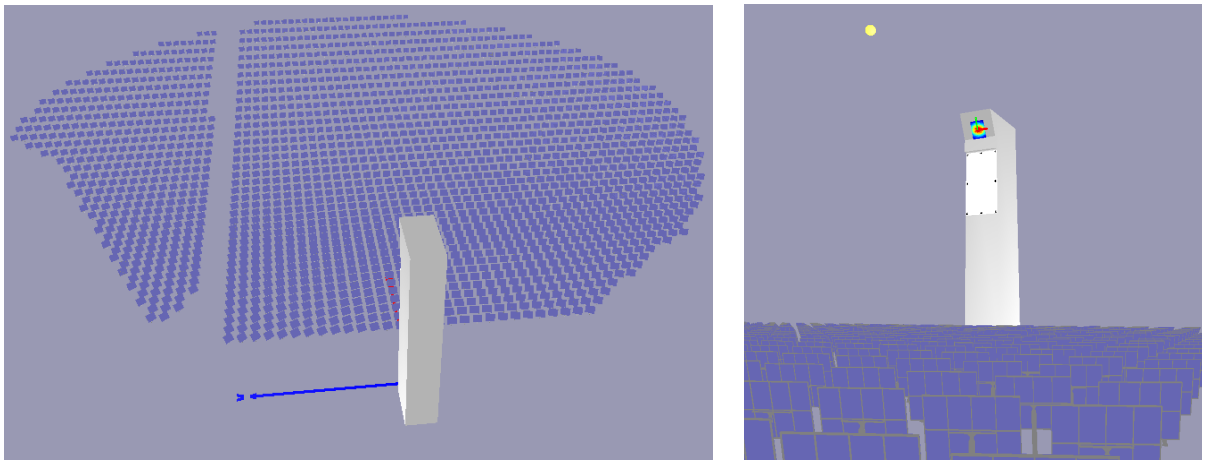

Figure II.2-7: Heliostat field and tower model of the Solar Tower Jülich in STRAL

II.3. Receiver model

One major goal of the vICERP project is to develop dynamic models of the power plant components. For the power plant model, the models should represent the major quantities of the component sufficiently. In the receiver, the solar energy is converted and hot air is provided to the power plant cycle. Therefore, the dynamic behaviour of the air at the outlet of the receiver has to be calculated in the model with the minimum number of state variables. Additionally, the critical quantities like the allowed upper temperature of the absorber combs have to be considered.

The receiver model is developed using the STRAL receiver model interface. The interface offers the possibility to include user-written receiver models of great detail. For the receiver of the Solar Tower Jülich, the central geometrical dimensions are represented like receiver height, width, and opening angle. The receiver model comes with a variable discretization to adapt to the existent receiver configuration using absorber modules. The receiver model evaluates the incoming rays in the ray tracing process and calculates a flux density distribution depending on the chosen discretization.

The thermal behaviour of the receiver is not included in this model but represented in a more complex dynamic model. For the dynamic model, the modelling language Modelica and the simulation environment Dymola are used for its good possibilities to model dynamic systems of different engineering systems. The two receiver models interface the flux density distribution calculated in STRAL via the TCP/IP-interface in a co-simulation. The co-simulation was developed and tested successfully [5]. Its setup is shown in Figure II.3-8.

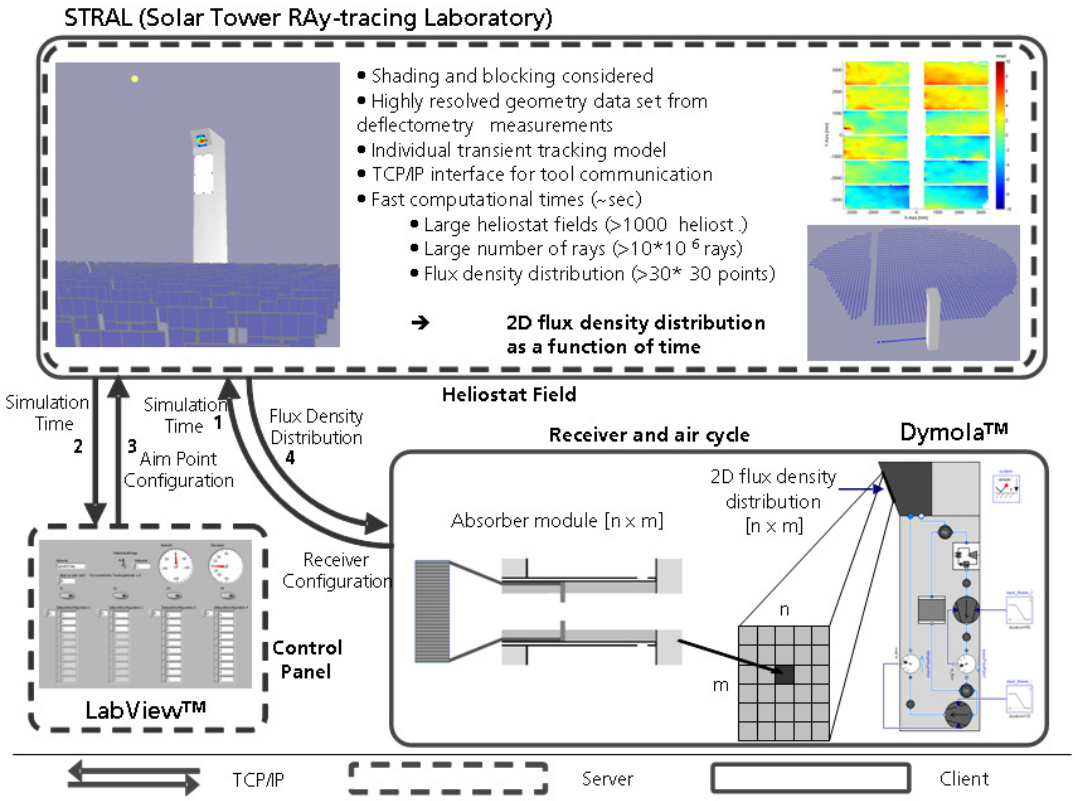

Figure II.3-8: Setup of the co-simulation of STRAL, Dymola, and additional simulation software (Labview exemplary used for the implementation of an aim point strategy)

The crucial component of an open volumetric air receiver is the absorber module consisting of the absorber comb, the holding structure, the piping, and a fixed orifice. The incident solar radiation is absorbed in the channels of the absorber comb. The air mass flow rate through the absorber comb is mainly dependent on the orifice installed in the piping of the absorber module as the mass flow rate is distributed depending on the pressure drop of the modules. Besides, the still warm air coming from the steam generator is led back to the receiver to increase the efficiency of the power plant, passes the absorber module and is blown out in front of the absorber comb. The interaction of the returning air, flux density on the absorber comb and the mass flow rate through the comb have a big impact on the absorption efficiency and on the plant performance, respectively. An outline of the actual design of an absorber module is shown in Figure II.3-9.

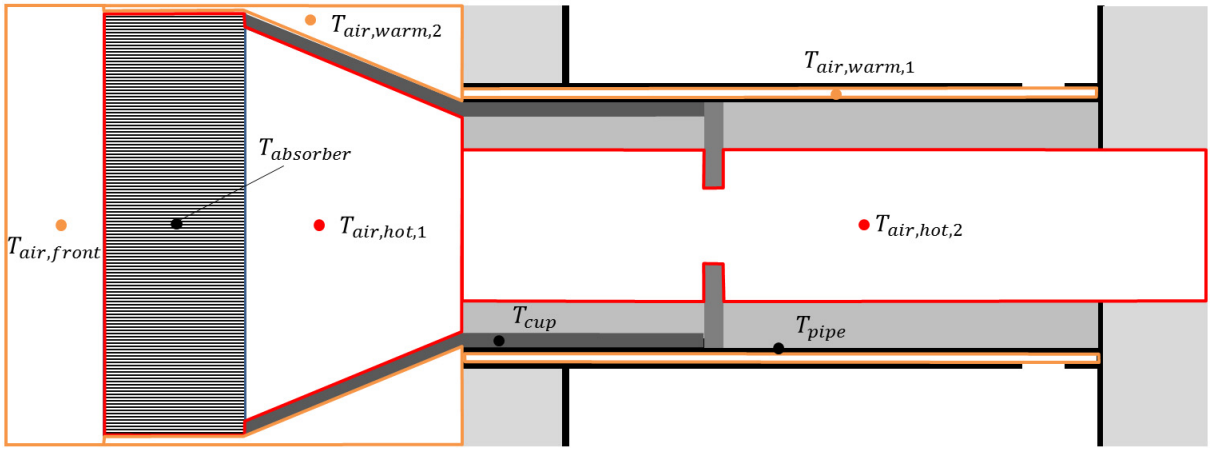

Figure II.3-9: Sketch of an absorber module and the used states/control volumes

Similar to the physical design of an open volumetric air receiver, the model is setup out of absorber modules models as the smallest modelling unit. A more detailed modelling increases the calculation effort to an unrealistic level without increasing the scientific findings for a system simulation in the same manner. However, a more detailed model is developed for the absorber channels to create an absorber efficiency lookup table depending on the air inlet temperature, flux density, and the air mass flow rate. By that, the essential effects of the absorption process can be implemented into the receiver model keeping the computational effort acceptable.

The model of the absorber module is developed to deliver a precise representation of the air mass flow rate and the corresponding specific enthalpy at the outlet of the module. Therefore, the absorber module is divided into a minimum number of control volumes to secure the modelling goal and to keep the calculation effort low. The number was determined by reducing the number of temperature states/number of control volumes of a more detailed model comparing the results at the same time. The chosen temperature states and the control volumes can be seen in Figure II.3-9.

The energy balance equation is formulated dynamically for each control volume. The convectional heat exchange terms are formulated using standard heat exchange correlations from the VDI heat atlas for air flow through pipes and annular gaps. Conductional heat transfer is described using Fourier's law for heat conduction.

Storage of mass in the air control volumes of the absorber module is neglected, as the volume is much smaller than the volume inside the header of the subreceiver or the receiver. A steady state formulation of the mass balance equation is applied. In terms of model structure the absorber module is of type "flow" and calculates the mass flow rate out of the pressure drop. The momentum balance in the absorber module model is reduced to a pressure drop equation providing the relation between pressure drop and mass flow rate.

The outlet of the absorber modules correlates to the inlet of the subreceiver header. The mass flow rates of all modules of the subreceiver are merged in this header. The absorber modules of each subreceiver are dependent of each other due to the pressure drop over the modules. It can be assumed that the pressure drop over the absorber modules of each subreceiver is identical. The mass flow distribution in the subreceivers changes, if one of the absorber modules changes its performance for example due to an altering flux density. The mass flow distribution can be calculated using the pressure drop over the absorber modules.

A crucial control volume is the one in front of the absorber comb. It is difficult to model but has a big impact on the module performance. The warm return air is blown out in front of the

absorber comb. Currents in front of the receiver mix the air streams with each other and with the ambient air. It is difficult to model these effects with an adequate calculation effort. Thus, a fraction value called Air Return Ratio (ARR) is established. ARR describes the fraction of the warm return air mass flow rate sucked into the absorber comb again. ARR equal to zero is equivalent to an air inlet temperature identical to the ambient temperature, whereas an ARR equal to one represents the complete feedback of the warm return air. In most cases, the ARRs have to be assumed based on operating experience.

Besides the model for absorber modules, models for headers, air piping, and distributors are developed. The level of detail is chosen much lower, as the components have less impact on the receiver performance. A scheme of the receiver model is shown in Figure II.3-10.

For the different headers the same model can be used adapting the geometrical parameters. As the header volumes are large and their pressure drop is low compared to the absorber modules, the models are designed to be lumped volumes models. Pressure drop is neglected for that type of model. Mass and energy balance equations are formulated dynamically using pressure and temperature as state variables.

The basic structure of pipe models is of type “flow”. However, pipe models are distributed models using a finite volume approach with an altering sequence of flow and volume models [2]. For the air piping, there are differences between the hot air side carrying the heated air from the receiver and the warm air side directing the warm air from the steam generator or storage back to the receiver. The hot air piping is equipped with inner heat insulation, whereas the warm air piping has insulation installed on the outside of the pipe.

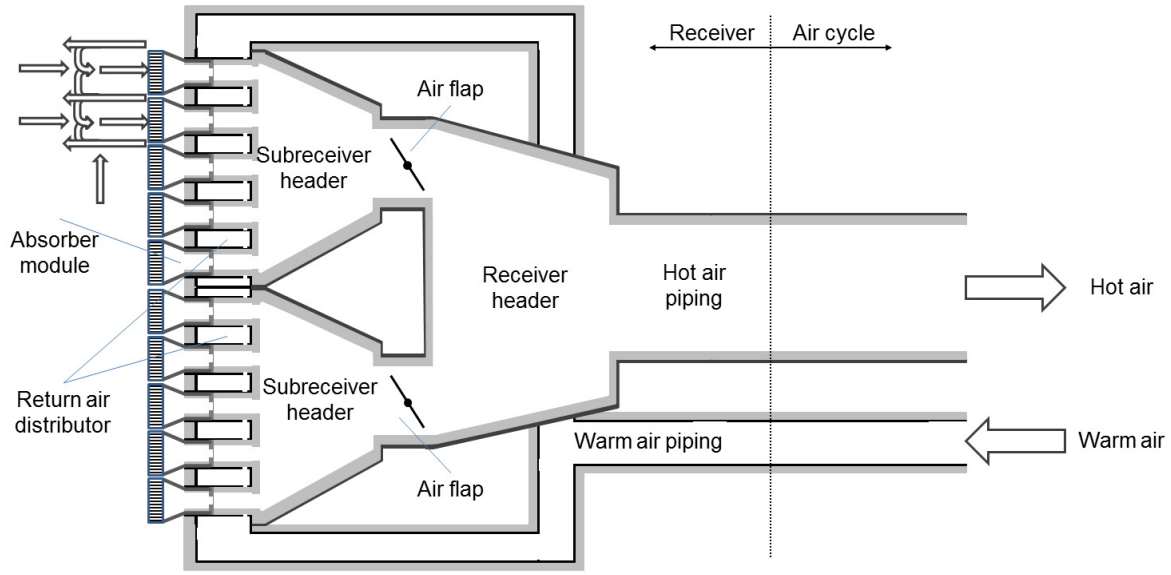

Figure II.3-10: Sketch of the receiver components

Thus, two variants of the piping model are developed. Convectional heat transfer is considered on the inside of the pipe/ inner insulation, as well as on the outside of the pipe/ outer insulation depending on the type of the pipe model. Conductional heat transfer is implemented only radial to air flow. Pressure drop of the pipes is considered using a quadratic correlation

The return air is distributed to the absorber modules using boreholes of different diameters in the return air piping. A lumped model is setup to represent the distributor. Instead of a detailed model taking the current fluid flow into account, a fixed distribution of the air flow is implemented depending on the design distribution. The influence of the mass flow rate distribution of the return air is analyzed in a sensitivity analysis, which supports this model approach. Besides the distribution of air, the heat exchange between the warm return air and the hot air inside the subreceiver headers is considered using a simple heat exchange correlation.

The model of the whole receiver is finally composed of the component models. Due to the modelling concept, it can easily be integrated as a flow model into the power plant model with different levels of detail. Depending on the simulation goal, the discretization of the receiver model can be changed. The number of equations can be reduced by substituting a couple of adjacent absorber modules with one representative absorber module. The discretization of the flux density distribution, the orifice diameter distribution, or the distribution of the return air remains untouched by the user, as the conversion is considered in the receiver model to ease the use of the model.

II.4. Thermal storage model

A thermal storage system is used as a buffer that stores energy in times of high irradiances and enables operation of the plant after sunset or during periods of reduced solar radiation. The storage behaviour of the solar tower Jülich is similar to that of a regenerator. The following figures show the storage construction and the functioning.

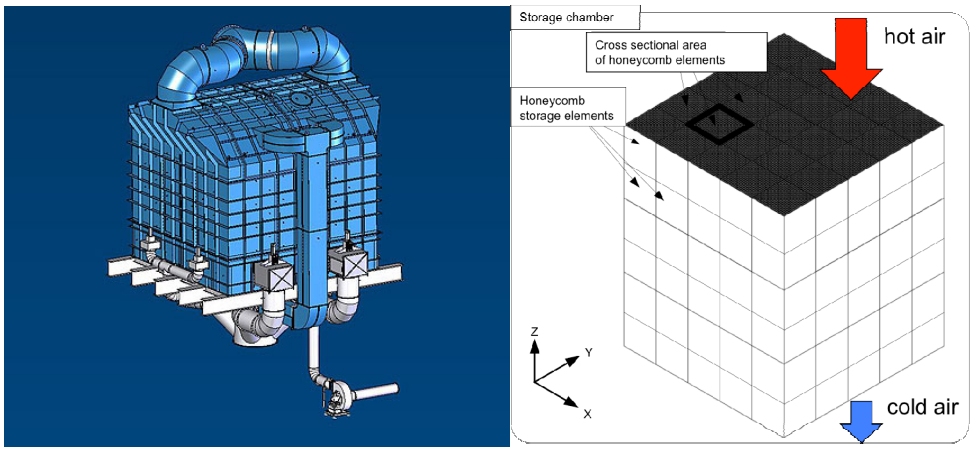

Figure II.4-11: Heat storage, honeycomb elements and storage chamber of the Solar Tower Jülich

The storage chamber consists of honeycomb storage elements. These elements are stacked, so that a cubic like storage chamber results. The hot air flows through this package of storage material and heats it up. During discharge air flows in reverse direction and cools it down. Inside the storage a temperature profile is generated, as presented in the following figure.

The storage in Jülich has a capacity for 1.5 hours. It has his maximum load when the air outlet temperature achieves the permitted maximal air outlet temperature. This is always a lower temperature than the inflow air temperature. An exemplary temperature profile for a loaded heat storage is the 100% curve in the figure Figure II.4-12 .

Intention of the modelling was to submit a dynamical state simulation of the thermal storage system during load and discharge process as well as to switch between these processes in a continuous simulation run. The storage unit in Jülich is often used as a buffer storage [6]. Thus, the ability to simulate charge and discharge states within one simulation is of crucial importance.

Each MWh of storage causes a finite quantity of exergy destruction because of air pressure drop during storage processing.

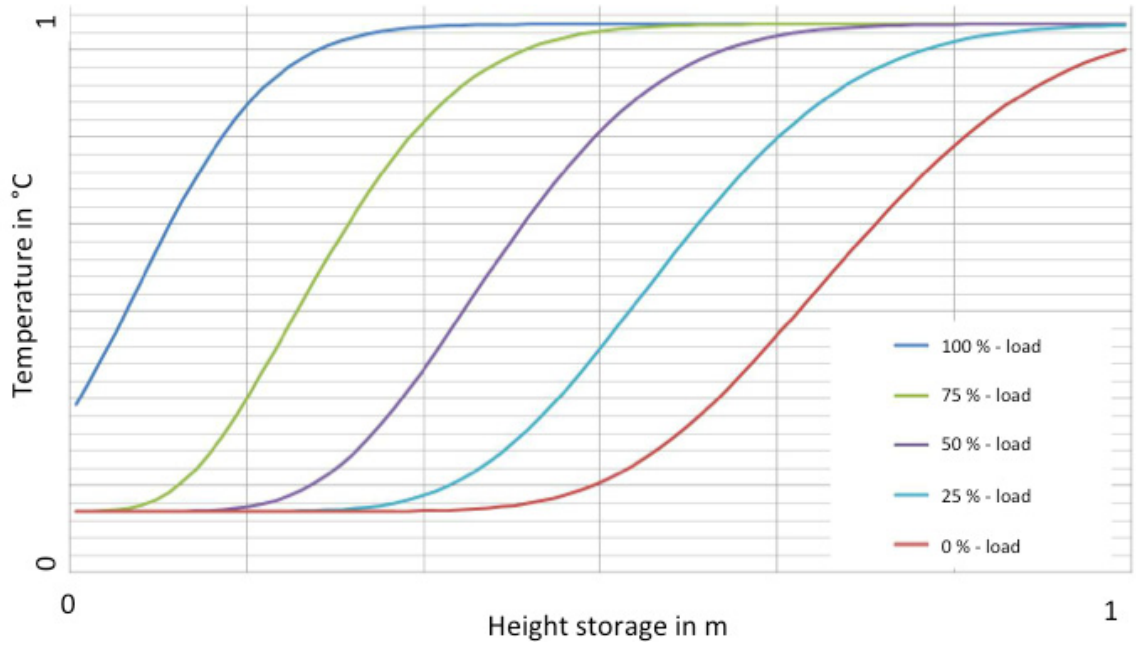

Figure II.4-12: Example for characteristic storage temperature profile

On the one hand, the outlet temperature of this kind of storage is directly dependent on the temperature profile inside the storage (e.g. figure below). On the other hand, the temperature profile is influenced by time dependent boundary conditions and different characteristic parameters. These are the inlet temperature, fluid mass flow, solid geometry, solid material, initial material temperature and initial fluid medium temperatures.

The storage needs to be loaded and discharged several times, proceeding with continuous mass flow and inlet temperature, before the inside temperature profile reaches an equilibrium steady state. After reaching this state, the temperature profile stays constant if the boundary conditions remain unchanged.

In order to describe numerically the storage unit, it is divided in discrete elements (cells) in which the energy and momentum balance is solved. The next figure presents a exemplary 3D-discretisation

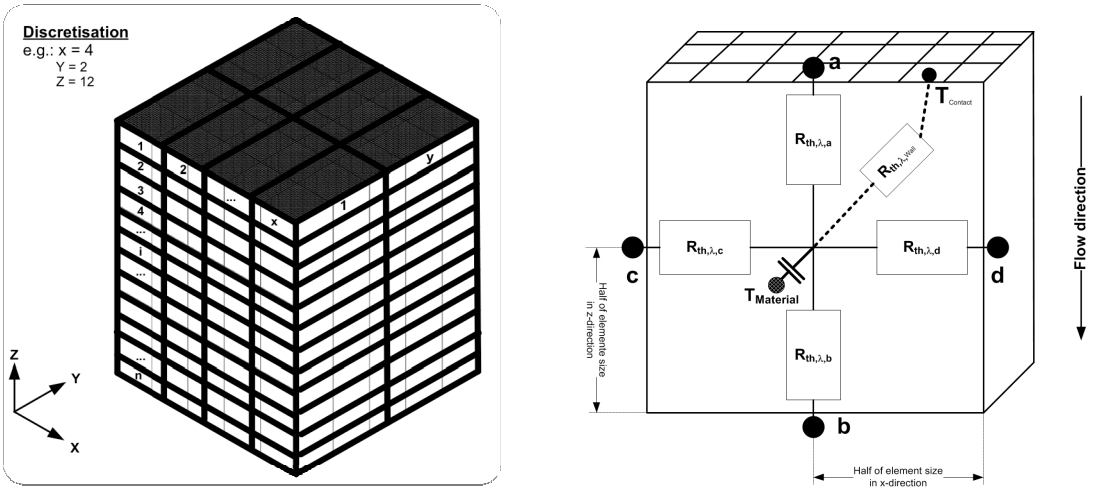

Figure II.4-13: Storage discretisation (left) and the thermal resistor diagram of a discrete element/cell (right)

The number of discrete elements (cells) is variable and is set as a parameter. The temperature profile and pressure drop inside the storage cells is calculated for each time step.

For the energy balance, the required heat transfer coefficient is calculated thermodynamically by storage and honeycomb geometry and by flow parameters. The heat conduction in three dimensions is considered and implemented as well [7]. The thermal resistor diagram (figure above) shows the heat conduction considered within the storage model.

The conventional heat flow rate in a solid $\dot{Q}_{Solid}$ can be computed by means of the thermal resistance in each cell. The thermal resistance $R_{th,a}$ depends on the direction and the geometry of the cell. The heat flow rate $\dot{Q}_{Fluid}$ between fluid and material is computed from

$$\dot{Q}_{Fluid} = \alpha A (T_{Fluid} - T_{kontakt})$$

where α is the heat transfer coefficient, A is the heat transfer area, $T_{kontakt}$ is the wall temperature, and T_{Fluid} the temperature in the fluid control volume.

The heat transfer coefficient α can be determined from Nusselt correlations. All temperature dependent values are computed with the Modelica fluid library.

The Nusselt number can be computed depending on the flow regime. In the case investigated, a constant Nusselt number of Nu=3.61 can be used for laminar flow. Shah gives a correlation for the Nusselt number that is valid for the laminar flow regime.

For pressure drop calculation a special equation for laminar flow trough rectangular ducts is used [9], [10]. For the description of the pressure drop, the pipe friction factor ζ_λ is used as a proportionality factor.

The model allows computing the outlet temperature of the thermal storage at any process time. Further more the model is capable to take into account flow direction changes inside the storage.

II.5. Water-steam cycle model

The layout of the water steam cycle in the solar tower power plant in Jülich is similar to the one in conventional power plants with a single steam pressure level. Due to the small power of 1.5 MW for this demonstration plant a multiple pressure system has not be realized. For larger systems, typical HRSG power plant designs withtwo or three pressure levels could be used for higher thermal efficiency. A simplified scheme of the steam cycle of the solar tower power plant is shown in Figure II.5-14.

In the power plant of the vICERP project in Jülich, steam is generated in the steam generator (station point 4 to 1, SG) by means of hot air. The steam generator is divided into three subcomponents (stages). The three stages are in the sequence of water/steam flow direction:

1. the economiser, where boiler water is heated to saturation conditions,
2. the boiler, where the water is vaporized and
3. the super-heater, where steam is heated to the turbine inlet conditions.

The superheated steam drives a turbine, which provides mechanical power to an electric generator (station point 1-2). The subsequently positioned condenser converts the expanded steam into liquid water by removing the vaporisation heat (station points 2-3). The feed pump increases the water pressure level to the boiler inlet conditions (station points 3-4).

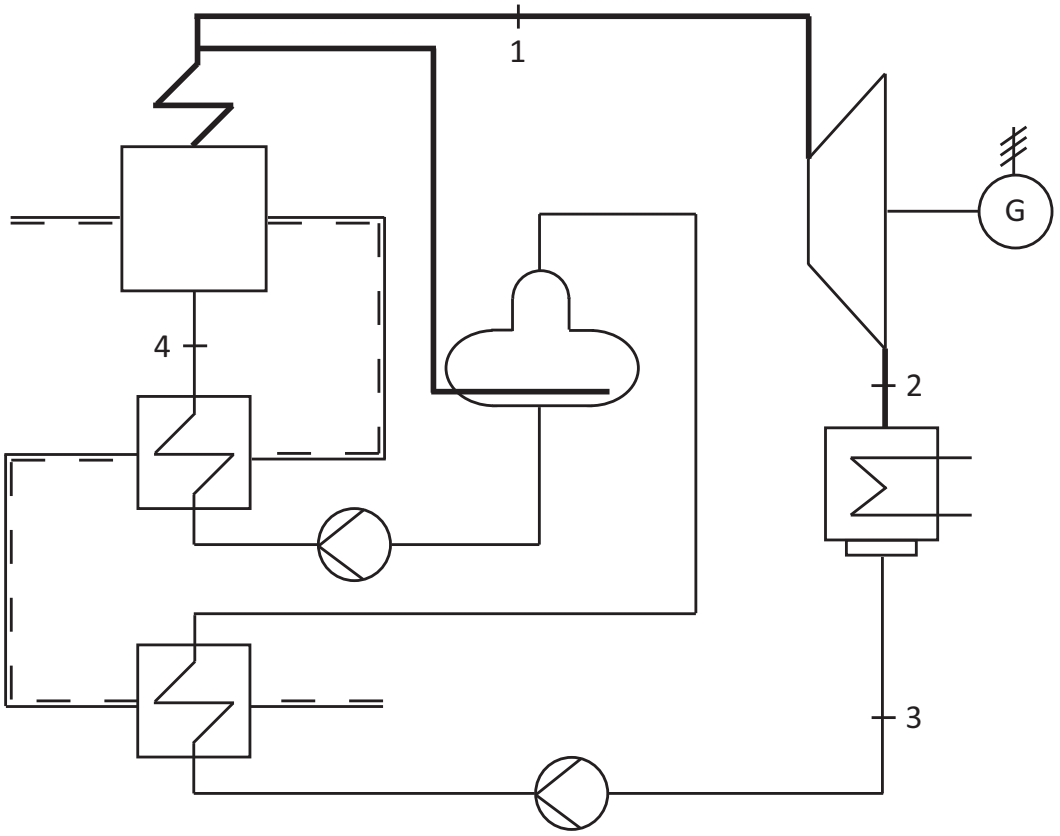

Figure II.5-14: Simplified scheme of the Solar Tower Jülich demonstration plant

The models developed for the vICERP project enable transient process simulations. The software tool *Modelica* allows to model components of the water steam cycle separately and to connect these single models using so-called ports. The *Modelica* media library contains fluid models for air and water that are used for the simulation.

For the simulation of the pre- and super-heaters (sub-components of the boiler) a simple heat exchanger model was developed. This model can be used for the calculation of the different heaters in the water steam cycle by simply adjusting the governing parameters. The heat exchanger model consists of a tube bundle and a shell.

The bundle of tubes consists of several finite volume “dynamic pipe” models from the *Modelica* library. The model considers pressure losses and heat transfer relations. A heat flow from the outside to the fluid can be assigned through a so called heat port. This port is connected with a mathematic model that describes one dimensional heat flow through a cylindrical wall including heat storage. Inflow losses and losses caused by bendings etc. are not considered.

The shell model consists of one dimensional energy, impulse and mass balances which are functions of the inlet and outlet values.

Energy balance: $$\frac{\partial m}{\partial t} = \dot{m}_{out} + \dot{m}_{in}$$

Impulse balance: $$\frac{L}{A}\frac{\partial \dot{m}}{\partial t} + (p_{out} - p_{in}) + \Delta p_{fric} + \Delta p_{stat} = 0$$

Mass balance: $$m\frac{\partial u}{\partial t} + \dot{m}(h_{out} - h_{in}) = \dot{Q}$$

The models for pressure losses and heat transfer with the tube bundles are exchangeable. The shell is not segmented but calculated as a whole, because the correlations for pressure losses and heat transfer in the “VDI Wärmeatlas” [11] contain average values for the complete heat exchanger.

The boiler in the Jülich solar tower is a fire tube boiler. It consists of tube bundles in a cylindrical shell. The shell is similar to the drum of a circulation boiler. Therefore, the model for this component is based on the work of *Casella* [12] and *Leva* [13]. In this case, it is important that the air charged tube bundles are always completely covered by water. Figure II.5-15 shows the principle setup of a fire-tube boiler.

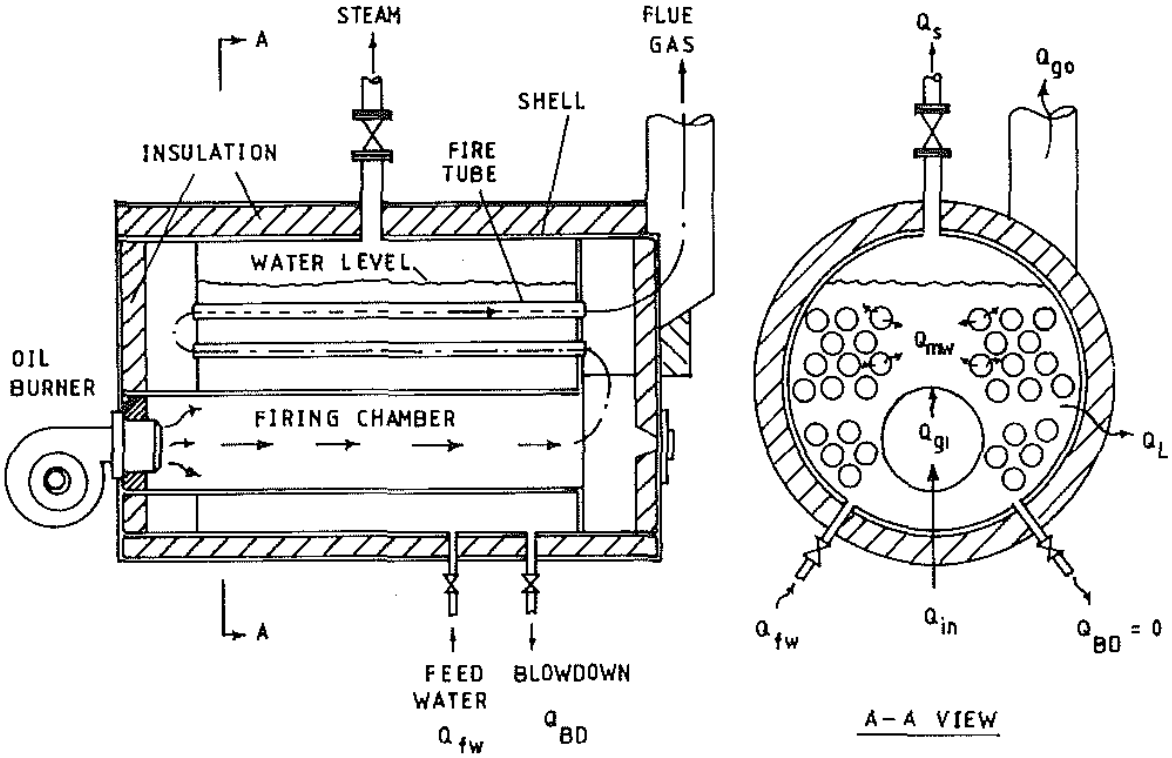

Figure II.5-15: Schematic of a fire-tube boiler (Source: Huang & Ko 1994)

The two fluid phases inside the boiler (water and steam) are modelled with a non-equilibrium model. In consequence, there are two separate balance equations for liquid water and steam and there is no coupling condition in form of a saturated steam phase required.

The water surface separates the boiler into two volumes. The volumes are connected by models for mass and convective heat transfer. The mass transfer model considers three different phenomena, depending on steam mass fraction and temperature of the two phases. The scenarios are evaporation, surface condensation on water surface and condensation.

Furthermore, the boiler model considers heat transfer and heat storage in the metal wall of the shell, convective heat transfer from both phases into this wall and out of the wall to the environment.

Liquid water and steam are regarded as individual volumes. This is the reason, why density and temperature gradients as well as the mixing of in- and outgoing fluids are not taken into account. Displacement of the tube bundles is also disregarded in the model.

For the tube bundles the model developed for the heat exchangers is used. According to the high mass of water inside the shell, saturation temperature can be assumed. Therefore, a model for saturated reservoir boiling has been developed to design the heat transfer between the shell and the tube bundles, according to *VDI* [11]. Additionally, it is possible to replace this model by a more complex model for undercooled reservoir boiling.

This is not important for the simulation, as water is considered to be an ideal liquid. However, the feed of hot steam accompanied by heat supply into the feed water tank has to be regarded. The drum model used for the boiler considers this.

The mass transfer model is replaced by a model for convective mass transfer as the following:

$$\dot{m}_{konv} = KA\left(T_{vap} - T_{liq}\right)$$

K is the mass transfer coefficient. Its value is governed by the mass flows, the steam and water distribution and the geometric boundary conditions.

The turbine is modelled for steady state, because heat and mass storage in this component is negligible compared to boiler and feed water tank.

The turbine is divided into n stages. For each stage the steady state energy balance is formulated:

$$a + q = h_o - h_i + \frac{c_o^2 - c_i^2}{2} + g\left(z_o - z_i\right)$$

The mass flow attains a value depending on the pressure at inlet and outlet condition, according to the *Dampfkegelgesetz* of Stodola:

$$\frac{\dot{m}^2}{\bar{\mu}} \sum_{1}^{N} \frac{1}{2s^2 A^2} = \frac{n}{n-1} \frac{p_i}{v_i} \left(1 - \left(\frac{p_o}{p_i}\right)^{\frac{n+1}{n}}\right)$$

Torsional moment and angular velocity are obtained from the *Modelica* library to represent the mechanical turbine shaft properties. The connection between the specific enthalpy at in- and outlet of the turbine is modelled with the method of *Zweifel* and the assumption of a constant polytropic efficiency in all turbine stages.

$$\eta_T = 1 - \frac{\sum_i \Delta s_i}{\sum_i (\Delta s)_{ist}}$$

Furthermore, the model contains the option of a moisture dependent efficiency correction with the *Baumann* factor:

$$\eta = \eta_0 \cdot (1 - \alpha \cdot (1 - x))$$

For part load operation no further efficiency adjustments are implemented.

The condenser model has been separated into three parts, the shell, a wall model and the tube bundles as can be seen in Figure II.5-16.

The shell contains a condensation model and a model for the steam sided pressure loss. It is separated into n segments in which the steam mass fraction is calculated. Condensate and steam mass flow for the mass and energy balances can be determined with reference to the mass fraction.

$$\frac{dm}{dt} = \dot{m}_{steam,in} + \dot{m}_{liq,in} + \dot{m}_{steam,out} + \dot{m}_{liq,out}$$

$$mu = m_{steam} h_{steam,sat} + m_{liq} h_{cond,sat} - pV_n$$

$$\frac{dmu}{dt} = \dot{m}_a h_{inflow,a} + \dot{m}_b h_{inflow,b} + \dot{Q}$$

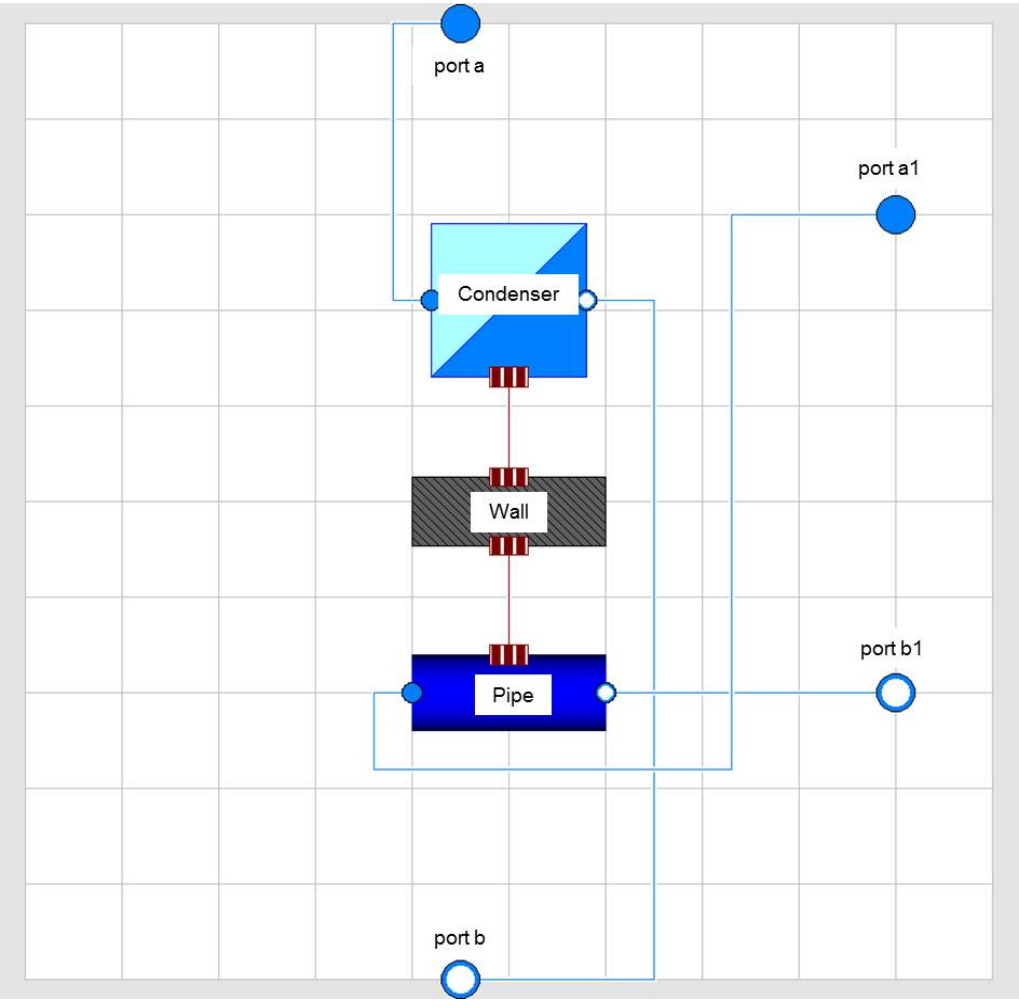

Figure II.5-16: Condenser in Modelica

The wall temperature for each segment is assumed to be constant. Each segment is connected to the wall with a model for convective heat transfer.

The convective heat transfer to the wall is described by the following fequation.

$$\dot{Q} = \alpha_{cond} \frac{A}{n} (T_{wall} - T_{sat})$$

The heat transfer coefficient α_{cond} is determined with the equation for film condensation obtained from the *VDI Wärmeatlas* [11].

The wall model represents the heat resistance of the tube walls. It acts as heat storage during part load operation. To be compatible with the shell the model is separated into n segments as well. The temperature over each segment of the wall is calculated with the energy balance.

$$\dot{Q}_{\frac{in}{out}} = \frac{2\pi L\lambda \left(T_{\frac{in}{out}} - T\right)}{n \frac{\ln r_a}{r_i}}$$

The tube bundles model is designed referring to the “dynamic pipe” model from the *Modelica* library. This model is according to the shell and wall model also separated into n segments. The model contains mass, energy and torque balances for one dimensional fluid flow.

Equal to the turbine the pumps are represented by a stationary model. The mass flow is calculated referring to the pressures at the ports.

The pump model is controlled by speed frequency and a deposited characteristic chart for part load operation. The controlled pump model is shown in Figure II.5-17.

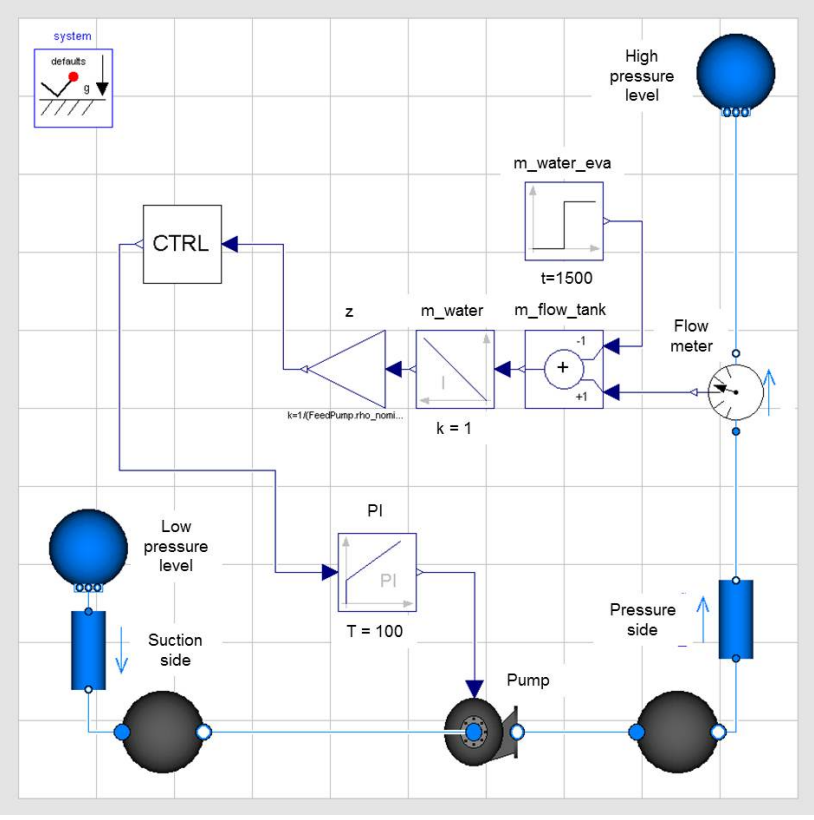

Figure II.5-17: Controlled pump in Modelica

The air cooler model consists of three sections of tube bundles, wall and fan (Figure II.5-18). For the tube bundles and the wall the same models as for the condenser were used.

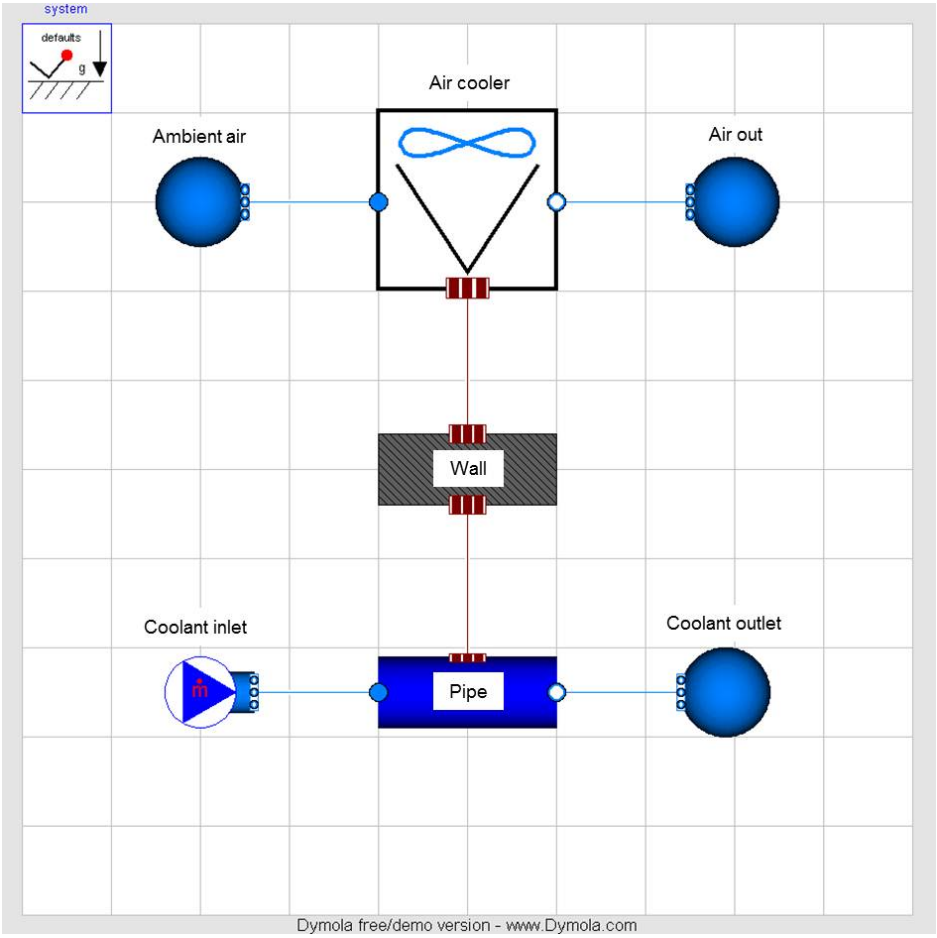

Figure II.5-18: Model of the aircooler in Modelica

The fan model is separated into two segments. In the first segment the heat transfer from the tube bundles to the air flow is calculated. In the second segment the conversion of the mechanical fan power into enthalpy of the fluid is modelled.

$$P = \dot{m}\left(h_{out,2} - h_{in,2}\right)$$
$$-\dot{Q} = \dot{m}\left(h_{out,1} - h_{in,1}\right)$$

The volume flow through the fan is determined using the equation below.

$$P = P_{nenn}\left(\frac{\dot{V}}{\dot{V}_{nenn}}\right)^3$$

This equation provides a relation between power and nominal power referring to the appropriate volume flows.

Furthermore, an alternative equation based on the relation between power and speed frequency is implemented.

III. Results of WP 2 – Model validation

III.1. Heliostat field model

A validation of the heliostat field could not be performed due to several aspects. First of all, the quality of the heliostat mirror surfaces is not known up to now. Deflectometry measurements were performed for some of the heliostat and showed a diverse picture, which prevented for using the measured mirror surfaces as representatives for other heliostats. In the future, it is planned to measure the quality of the mirror surfaces for all heliostats. This is a pre-condition for a validated detailed heliostat field model. However, the feasibility of a heliostat validation was already shown using deflectometry measurements of the SSPS-CRS field of the Plataforma Solar de Almeria, Spain. Excellent agreement between measured and simulated flux density distributions could be demonstrated [3].

Secondly, at the Solar Tower Jülich it is not possible by now to log the heliostat-aim point configuration during operation. The only information available is the number of heliostats aiming at the receiver. The heliostat field can not be validated without the missing information even if every heliostat is validated for itself, because the aim point strategy has a big impact on the flux density distribution on the receiver surface.

Finally, the flux density measurement method needs to be validated as well. At the site in Jülich, a new indirect flux density measurement system using a CCD camera is installed [14, 15]. In the near future, it is validated using a moving bar system.

III.2. Receiver model

The validation process of the receiver model is divided into two validation sections using different data and level of detail. The first section contains the validation of a single absorber module using data from the absorber test rig of the OVABSOL project [16], [15]. The second section uses the power plant data of the Solar Tower Jülich to validate the complete receiver model [17].

The absorber test rig of the OVABSOL project was constructed to test different types and geometries of absorber combs. The setup of the test rig is outlined in Figure III.2-19. The geometry of the absorber module used in the Solar Tower Jülich does not agree exactly with the one used in the test rig. However, the absorber cup holding the absorber comb and the comb itself are of the same type. As the main losses occur in the comb (1) and the cup (2), the setup can be used for a meaningful validation of the absorber module. The losses of the air in the pipe (3) are much smaller as the pipe is equipped with insulation on the inside.

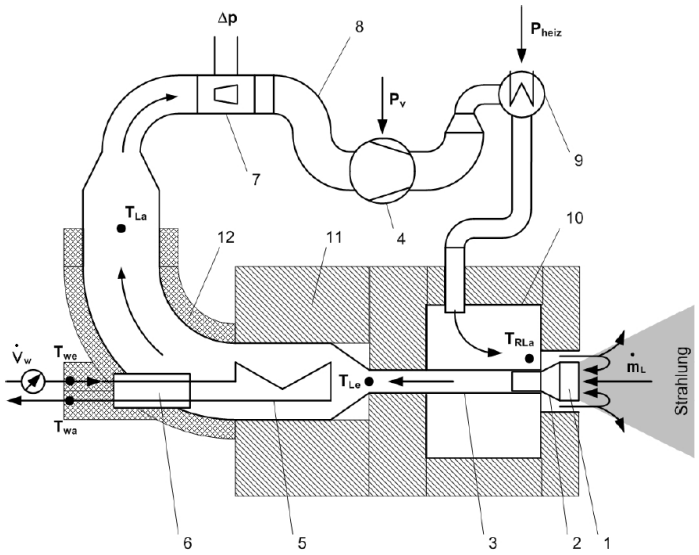

Figure III.2-19: Sketch of the OVABSOL test rig

The main advantage of the test rig is the opportunity to test a single module beforehand and compare the results with the simulation results instead of using full receiver setup from the beginning. That way differences can be indicated much faster. Additionally, the test rig offers the possibility to test with and without the warm return air. Without the return air, the air inlet temperature of the absorber comb can be directly determined as the ambient temperature. It is much more complicated with return air blown out in front of the comb. The air inlet temperature is dependent on the amount of return air fed back to the absorber comb. This fraction is described as the Air Return Ratio (ARR) and has to be assumed for the most cases.

The test rig delivers the following quantities, which can be used as inputs for the simulation or as base quantities of the validation:

1. Ambient air temperature (2 sensors, simulation input)
2. Air mass flow rate (pressure detection, simulation input)
3. Return air temperature at the outlet of the chamber (5 sensors, simulation input)
4. Flux density distribution (moving bar system, simulation input)
5. Air temperature at the outlet of absorber cup (3 sensors, validation base quantity)

The measurement errors are in the range of +/- 4°C for the temperature sensors (depending on the temperature level). Larger measurement errors occur for the mass flow rate measurement using a pressure detection system and the flux density measurement using a moving bar system. The measurement error of the air mass flow rate measurement is stated with 1.08%, whereas the error for the flux density measurement system is declared with 3.5% [16]. The overall measurement error of the test rig concerning the absorber efficiency is calculated to 3.8%. It has to be mentioned that the flux density measurement system interrupts the operation due to the rotary arm swinging the reflecting surface in front of the absorber comb. Additionally, the flux density distribution is not homogeneous as assumed in the simulation instead it shows strong inhomogeneous distribution.

The data of three tests are used for the validation to cover the meaningful temperature and mass flow rate interval with and without return air. The first test was carried out without return air. The flux density distribution was measured at two instants of time. The mean value was determined to around 500kW/m². The flux density distribution is assumed to be constant during the rest of the test except for the start up and the shut down of the lamps. Both can be seen in Figure III.2-20 showing the comparison of the mean air temperature at the outlet of the cup. As the starting procedure as well as the shut down of the lamps is not known, the flux density is unknown leading to major differences compared to the simulation results. Besides, small peaks in the measured curve of the air outlet temperature indicate the time instant of a flux density measurement procedure influencing the operation.

The error between both curves is calculated using the specific enthalpies instead of temperatures. A positive value expresses an overestimation of the simulation data compared to the measurement data and vice versa. It can directly be seen that there is a good agreement between the two curves. The dynamic behaviour as well as the absolute values match for the complete time interval except for the start up and shut down of the lamps, which was not considered in the simulation. The error adds up to 0.66% for the first steady state point (shortly before the flux density measurement) and 0.18% for the second point at a higher temperature level.

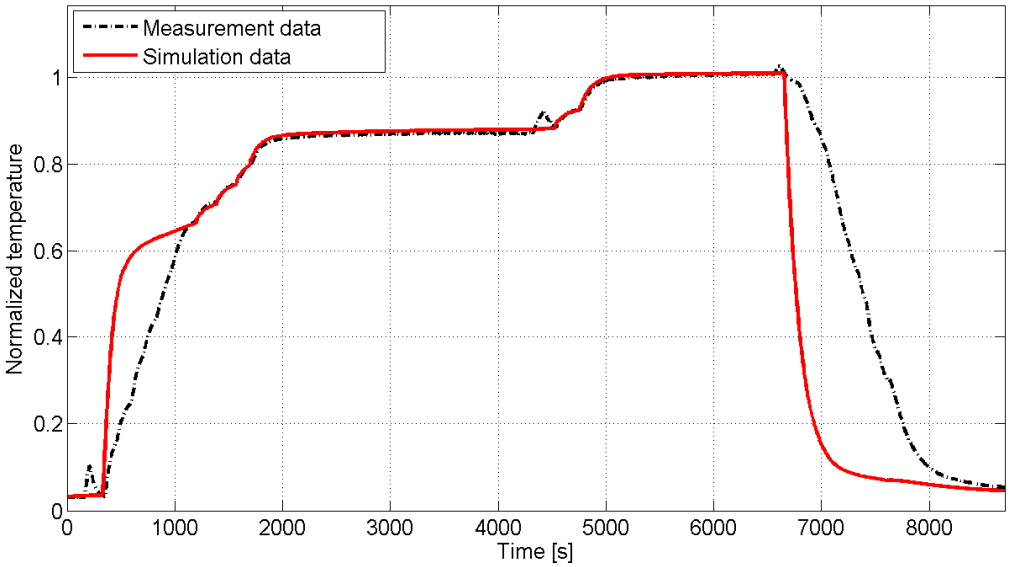

Figure III.2-20: Comparison of the air temperatures at the cup outlet for the first test without return air.

The second test was performed without air return as well but at higher temperature levels with a mean flux density of around 500kW/m². The flux density level was decreased in the second part of the test to around 100kW/m². An overestimation of the model in comparison to the measurement results can be found in the first part having errors of 2.93% and 4.43% at steady state points (Figure III.2-21). In the second part applying a lower flux density level, an underestimation of the model can be seen. Errors of -2.88% and -6.29% are obtained. The main source of error is assumed to be the flux density measurement and the inhomogeneous flux density distribution as well as the low mass flow rate level to reach the high temperatures.

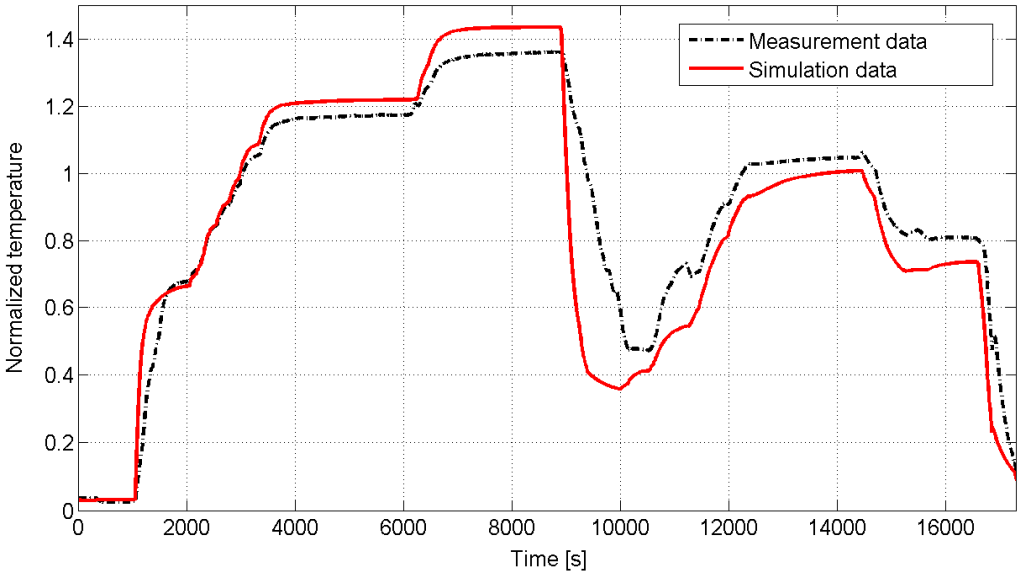

Figure III.2-21: Comparison of the air temperatures at the cup outlet for the second test without return air

In the third test, the same temperature levels are tested using a mean flux density of 500kW/m² but using the return air. The air return ratio is assumed to be independent of the mass flow rate level and set to 40%. Simulations with an ARR of 0% and 100% are carried out to analyze the limitations of the simulation. First of all, the dynamic behaviour of the ab-

sorber modules can be represented precisely using the developed model. A good agreement can be found between the measured and simulated curve shown in Figure III.2-22 except for the start up/shut down of the lamps and the flux density measurement points. The absolute level differs in the same manner seen in the first two tests. Errors in the range of -4.3% up to 5.28% indicate the underestimation of the model at lower temperatures and the overestimation at higher temperatures. A likely source of error is the mathematical model of the absorber channel including the absorption process and heat transfer from the comb to the air. The correlation for the calculation of the convectional heat transfer between the absorber channel and the air might cause the under-/overestimation.

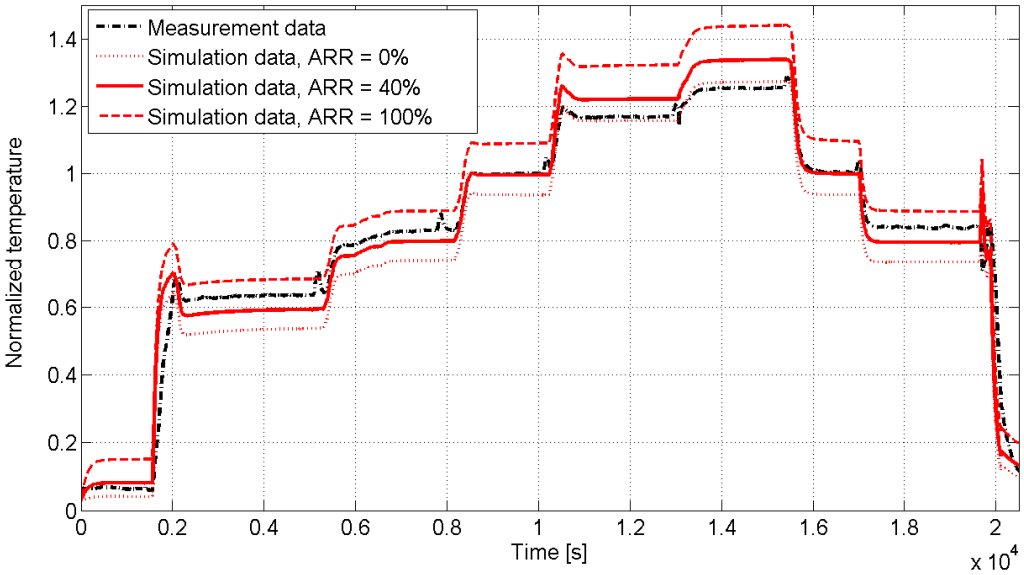

Figure III.2-22: Comparison of the air temperatures at the cup outlet for the third test with return air

Altogether, the first validation section showed a good and satisfying agreement between the simulation results and the measurement data. Improvements like a homogenization of the flux density distribution, a more precise flux density measurement, and improvements of the absorber channel model and the modelling of the air in front of the receiver would most probably lead to an even better agreement.

These tests did not cover the validation of the pressure drop over the module. Appropriate tests for a single orifice and for a single absorber comb were performed beforehand in the design phase of the Solar Tower Jülich. The results were used in the development of the pressure drop function for an absorber module.

In the next step, the full receiver model was validated using the power plant data of the Solar Tower Jülich. Most of the data was gathered by the process control system of the power plant except for the flux density distribution. The following data was used as inputs for the simulation or as base quantities of the validation:

1. Ambient air temperature (simulation input)
2. Air mass flow rate of the receiver (simulation input)
3. Return air temperature before the receiver (simulation input)
4. Flux density distribution (simulation input)
5. Air temperatures at the outlet of absorber modules (validation base quantity)
6. Air temperatures at the outlet of subreceivers (validation base quantity)
7. Air temperature at the outlet of the receiver (validation base quantity)

The flux density measurement uses a new measurement approach, in which the flux density is calculated using a CCD camera system. The method still has to be validated with state of the art technology, which is planned for the near future. However, the first checking of the energy balances shows a good agreement [14].

For the simulation, the model is adapted to the receiver geometry using the original data like orifice diameters or pipe lengths if available. Simulations are performed with different level of discretization. The discretization is chosen from a raw partition with one module per subreceiver to a complete partition with the original number of modules per subreceiver. Simulations are performed with assumptions for Air Return Ratios (ARR). Different ratios are tested for the four subreceivers of the Solar Tower Jülich to analyze the effect of the air return ratio on the simulation results. In whole, six days are used for the validation. The results of two representative days are shown.

The simulation results are compared for the air outlet temperature of the subreceivers and the receiver with the experimental data. For the calculation of an error between simulated and measured quantities, the specific enthalpy of the air at the accordant position is utilized. Positive values area again overestimations of the simulation data compared to the measurement data and vice versa.

For the first day, the subreceivers are simulated with ARRs of 40% to 60%. Different air return ratios are chosen due to cover the effect of natural draft lifting warm air from the bottom to the top. No further assumptions or additional models are used to represent the natural draft, wind direction, wind speed, or turbulences in front of the receiver. An appropriate model with an adequate calculation effort is not available and has to be developed in the future. The measured and simulated air outlet temperature of the upper left subreceiver is shown in Figure III.2-23 for a representative day and a discretization of 5x6 modules per subreceiver.

Figure III.2-24 displays the measured and simulated air outlet temperature of the same day with a discretization of 1x1 modules per subreceiver, 5x6 modules per subreceiver and the original number of absorber modules (15x18 modules per subreceiver) and a fixed ARR of 50%. The temperature is plotted normalized due to confidentiality of the data.

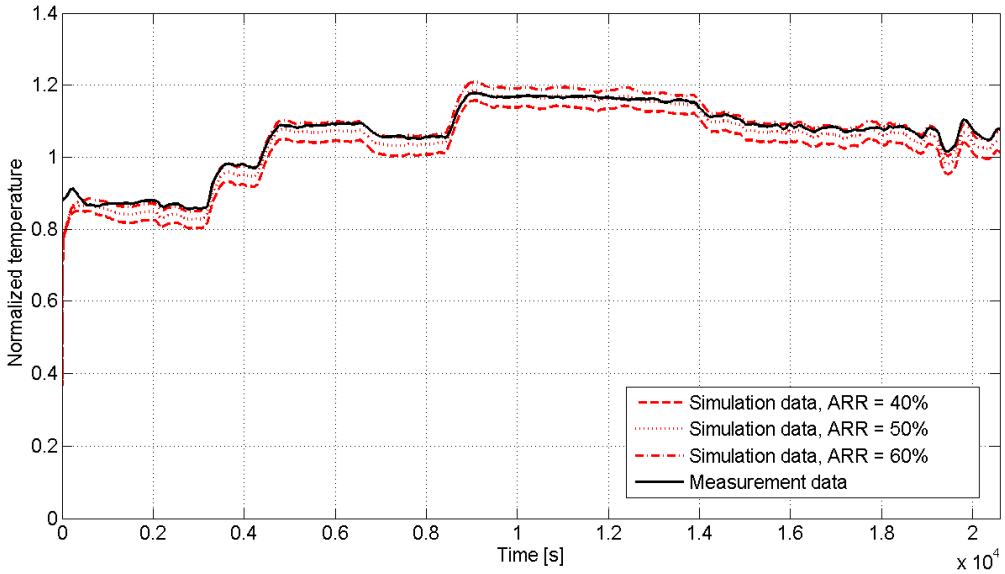

Figure III.2-23: Simulated air outlet temperature of the upper left subreceiver for different air return ratios and 5x6 modules per subreceiver compared to the measurement data for the first day

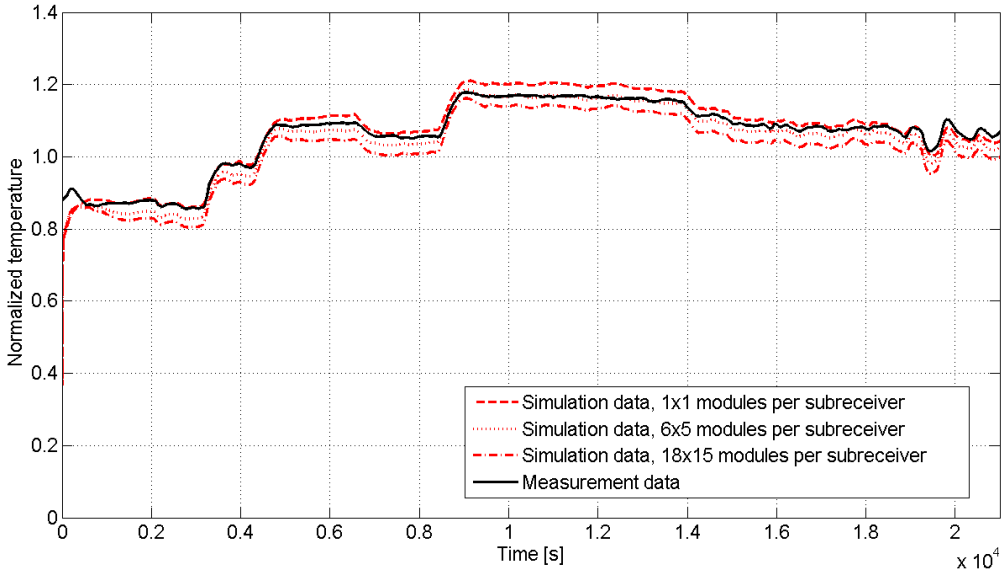

Figure III.2-24: Simulated air outlet temperature of the upper left subreceiver for different levels of discretization and an air return ratio of 50% compared to the measurement data for the first day

The two plots indicate a good agreement between measured and simulated air outlet temperature for the subreceivers using different discretization levels and air return ratios. Both, the absolute values as well as the dynamic behaviour, show a very good performance in the most sections. The errors calculated out of the specific enthalpies are in the range of ±5%. A very detailed simulation with 15x18 modules per subreceiver, which corresponds to the original number of absorber modules, does not improve the simulation results significantly compared to a simulation using 1x1 or 5x6 absorber modules per subreceiver. The curve is shifted to lower temperatures on the whole with increasing number of modules. The effect of an inhomogeneous flux density distribution and the corresponding absorption efficiency affects the simulations results using different levels of discretization. For the air return ratios, the curve is shifted towards higher temperatures with increasing ARR as air inlet temperature increases.

Figure III.2-25 shows the air outlet temperature of the receiver for the same day. The simulation results are generated using a discretization scheme of 5x6 absorber modules per subreceiver and different ARR from 30% to 70%.

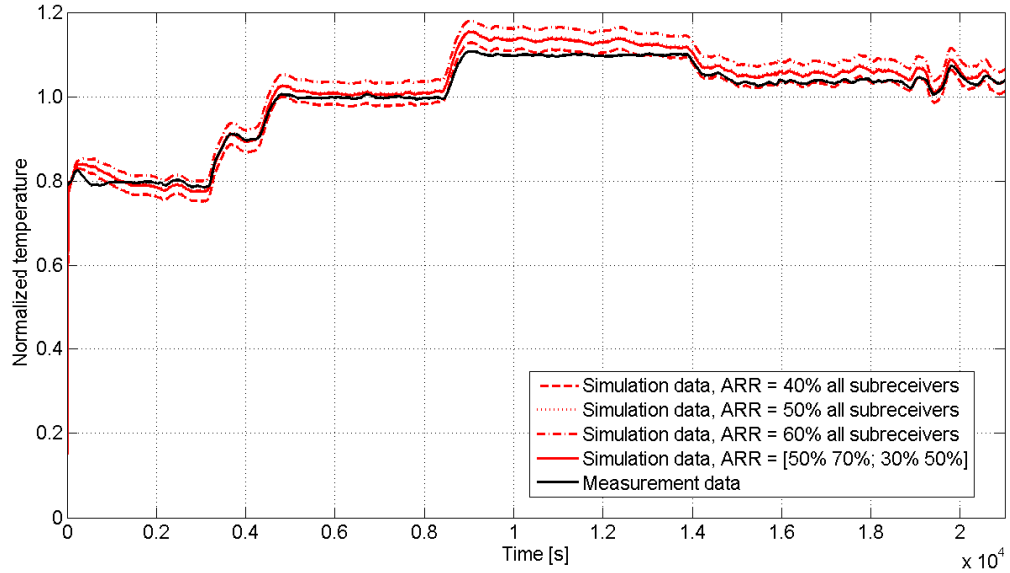

Figure III.2-25: Simulated air outlet temperature of the receiver for different air return ratios and 5x6 modules per subreceiver compared to the measurement data for the first day

The same good agreement can be seen for the receiver. The dynamic behavior as well as the absolute values fit to the measurement results. The error is in the range of ±5%. The dynamic behavior is obviously not affected by the ARR ratio as the curves are only shifted on the whole.

Figure III.2-26 and Figure III.2-27 shows the measured and simulated air outlet temperature of one subreceiver and the receiver for an additional day, but with a similar result. The dynamic behaviors as well as the absolute values are in a reasonable range for the simulation and a good agreement can be obtained compared to the measurement data except for the last part of the plot. Differences between simulation results and measurement data could be due to wind effects, as the AAR is a function of wind velocity, which is not included in the simulation.

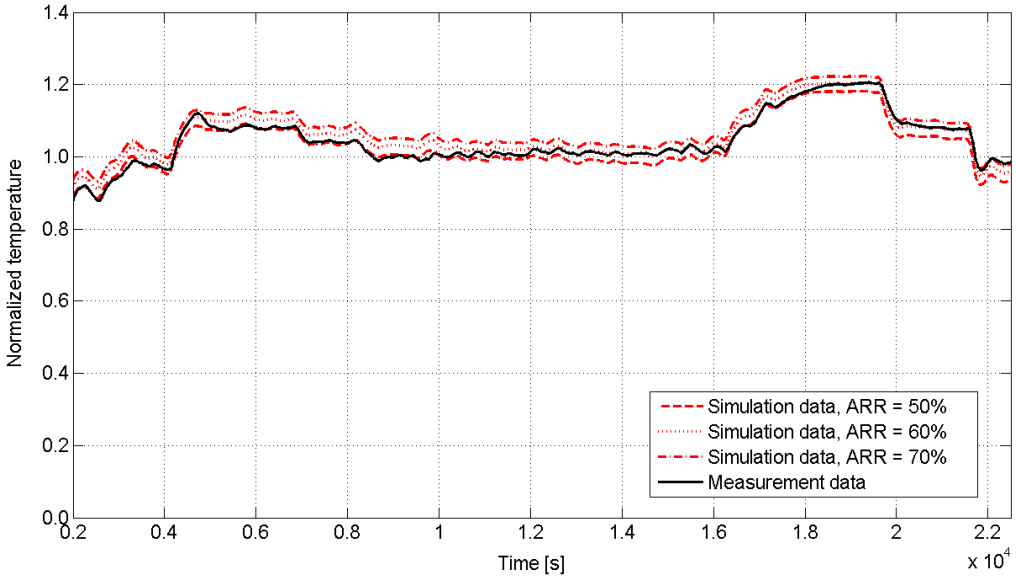

Figure III.2-26: Simulated air outlet temperature of the lower left subreceiver for different air return ratios and 5x6 modules per subreceiver compared to the measurement data for the second day

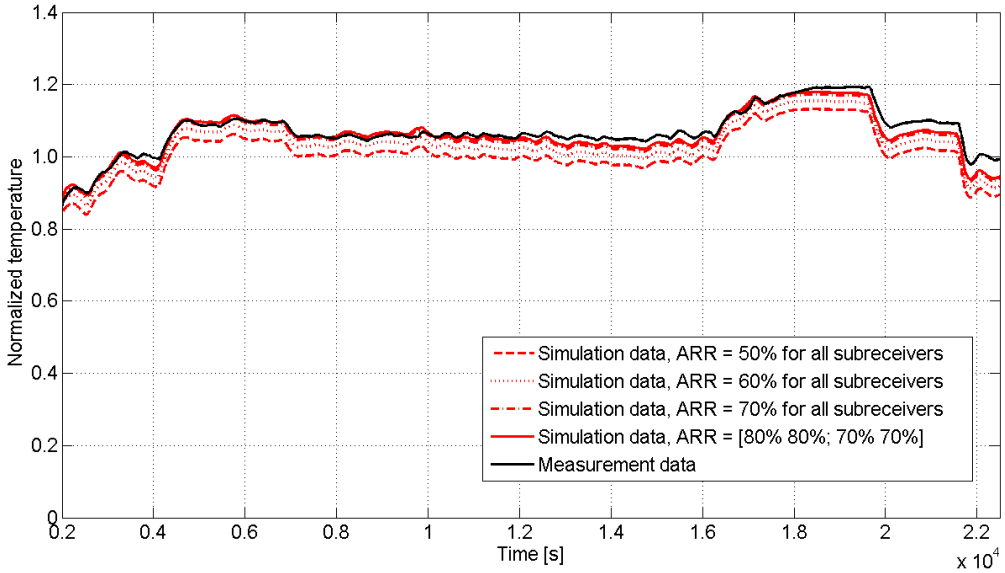

Figure III.2-27: Simulated air outlet temperature of the receiver for different air return ratios and 5x6 modules per subreceiver compared to the measurement data for the second day

In summary, the validation of the dynamic receiver is successful. A good agreement in the dynamic behavior and for the absolute values can be demonstrated. Improvements can be achieved, if the effects of wind and air flows in front of the receiver could be model in more detail. However, it is necessary to keep the calculation effort in feasible range. In addition to the performed validation, the mass flow rate distribution and the air inlet temperatures of the absorber modules should be analyzed in more detail. The model in the current state can simulate the air outlet temperatures of the subreceivers and the receiver in an adequate way. It can be used in the complete power plant simulation to represent the dynamic behavior of the solar receiver.

III.3. Thermal storage model

The following figure shows exemplarily the measurement positions of one chamber at the research storage at Solar Tower Jülich (STJ). The pressure drop is measured on top of and above the storage material. There are eight levels with three temperature measurements each, generating a representative average level temperature. On top and above the storage material is also one temperature measurement.

These temperature values are used to validate the storage model, represented by crosses in the following figures. All results were generated with a storage discretization level of 450 elements in airflow direction. The presented validation was made while solar operation for one load/discharge-sequence and uses one storage chamber. The test boundaries, e.g. mass flow, inlet temperature and inlet pressure, are the nominal solar tower process values. Air inlet temperature and mass flow values fluctuate in a small range while validation, because of the solar operation. The fluctuation inlet values are also used as the simulation input values. The real temperature of the storage at the beginning was interpolated and used also as initial conditions of the model.

At the beginning of the validation the storage has a homogeneous temperature of approximate 150°C. First the storage is loaded till maximum (100%-Charge) and than the air flow direction is changed immediately. Thus the discharge operation starts. For discharging operation a constant but higher mass flow is used till the storage reaches 0%-Charge. A compu-

tational time of 20 seconds, on an actual ordinary notebook, was needed to simulate 4 real-time hours.

Airflow pressure drop comparison between measurement (--) and simulation is presented in the next figure. The continuous line represents the measured pressure profile.

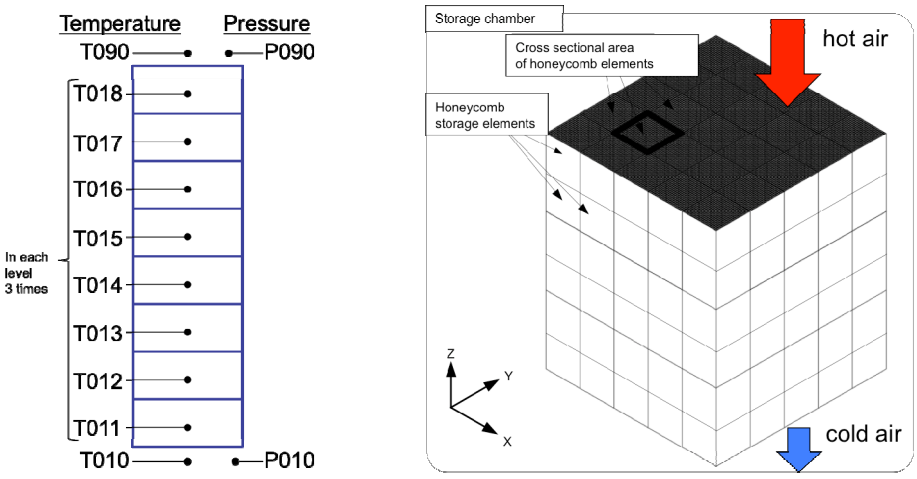

Figure III.3-28: Temperature measurement test rig (left) and exemplary framework construction of the storage chamber (right)

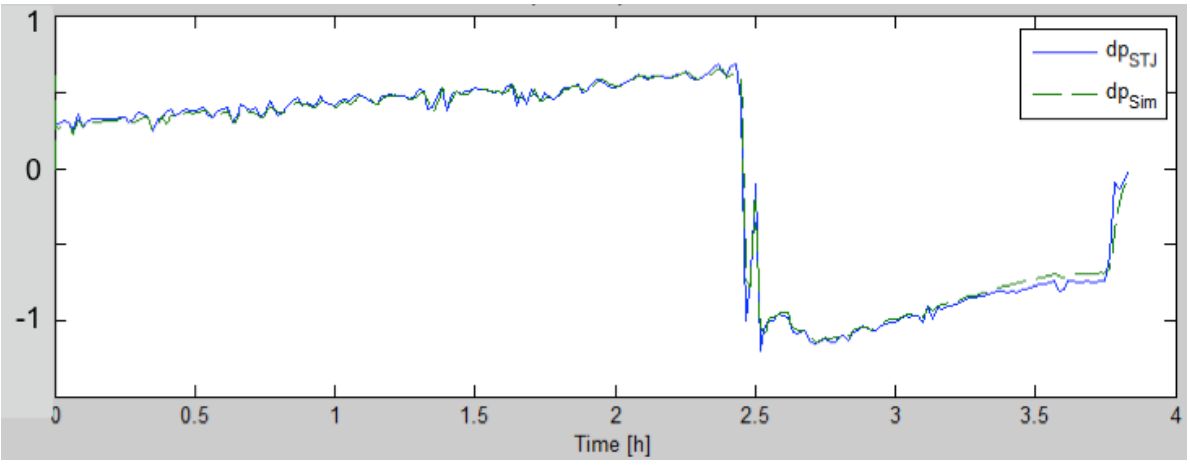

Figure III.3-29: Normalized pressure drops from measurement and simulation (right)

The simulation results for the pressure are close to the measured values. The pressure drop rises up while loading because hot air has to pass a longer time through a high temperature area. Thus, the pressure drop becomes less while discharging.

The following figures compare the simulated temperature with the measured ones at the beginning of the charge (Figure III.3-30), while charging (Figure III.3-31) and at the nearly end of the discharge process (Figure III.3-32). The dot dashed line describes the simulated value profiles.

The difference between simulated and measured temperature profile is less than 5 %. This is within the acceptable range for the dynamic simulation of the storage system.

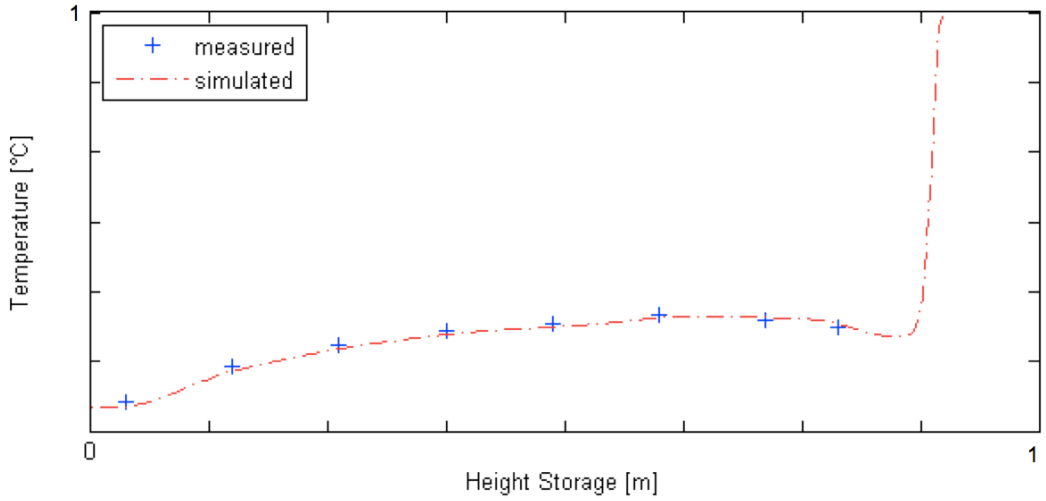

Figure III.3-30: Storage temperature profile at the beginning of load process (axes normalized)

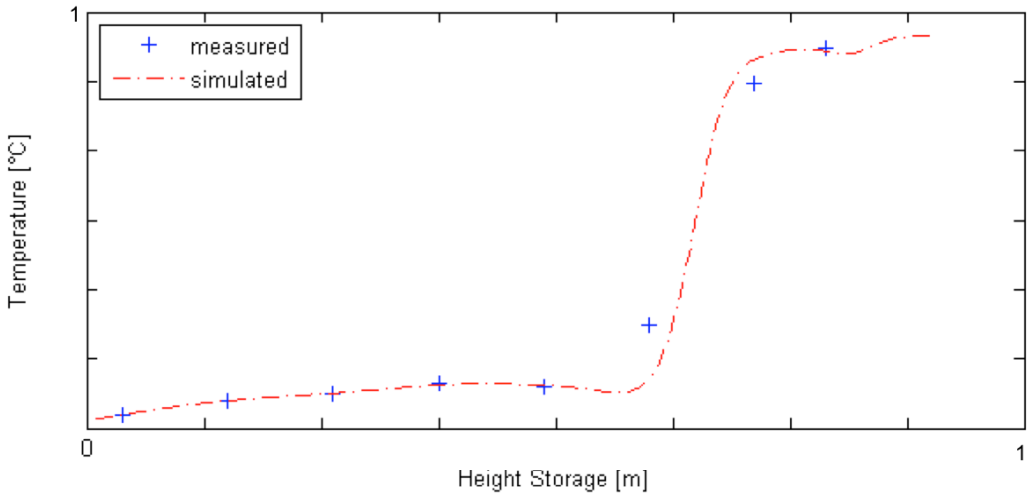

Figure III.3-31: Storage temperature profile during the load process; after 1 hour (axes normalized)

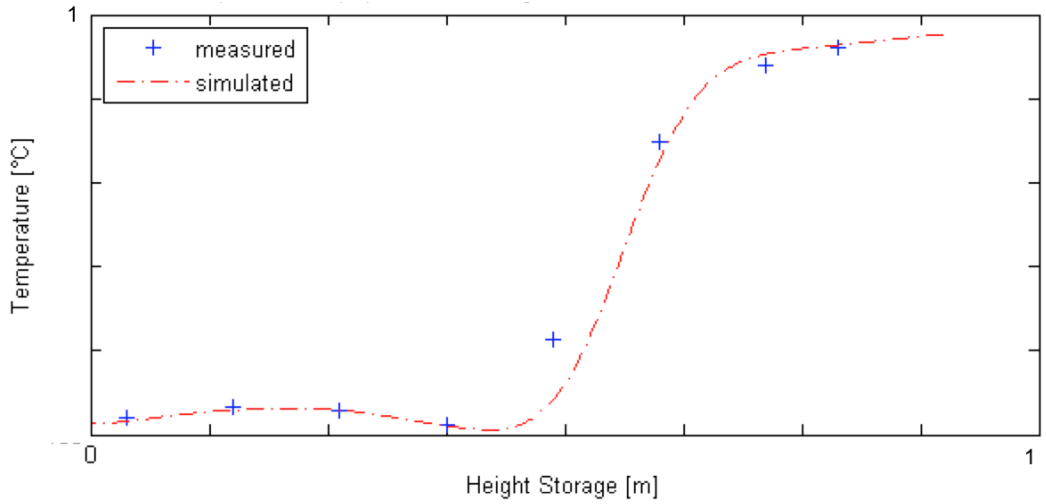

Figure III.3-32: Storage temperature profile at the end of the discharge process; after 3.2 hours (axes normalized)

III.4. Water-steam cycle model

For the validation of the water-steam cycle component, measured data from the solar tower Jülich were used. For the validation of the complete cycle some sensors are missing since they are not required for the plant operation. Unfortunately, a complete validation of some parts of the cycle was not possible without this information. This is the case for some fluid streams and temperatures inside the cycle. For confidentiality reasons this report does not provide the details of available measurement locations.

Due to the missing data only single components of the cycle can be validated. The function of the complete cycle was tested in a second step, not relying on complete cycle operation data from the solar tower Jülich. The component models have been validated with design data, data of quasi-stationary operation and data from start-up tests performed at the solar tower Jülich.

The tests were conducted using a gas burner instead of the solar energy receiver to guarantee heat supply at controlled temperature. As the “EEG” prohibits electricity production in the Jülich power plant without application of solar energy, operation including the turbine was not possible.

The temperature values from the boiler validation with design data differ in the range of 0.01%. Only the air outlet temperature shows too high values with a discrepancy of 23.26%. In the validation with data from quasi stationary operation this difference is reduced to 14.48%. The other values are in the same range as before.

During the start-up of a water-steam cycle the temperature in the steam generator is increased stepwise to preheat the components and to prevent the material from invalid thermal stresses.

One possible start-up strategy for the Jülich plant foresees increase of the hot air temperature depending on the boiler pressure. The following section refers to this start-up option, although other are conducted as well. In normal operation mode the temperature is maintained constant, while the air mass flow rate differs. To simulate the start-up behaviour of the boiler test environment as displayed below has been set up (Figure III.4-33).

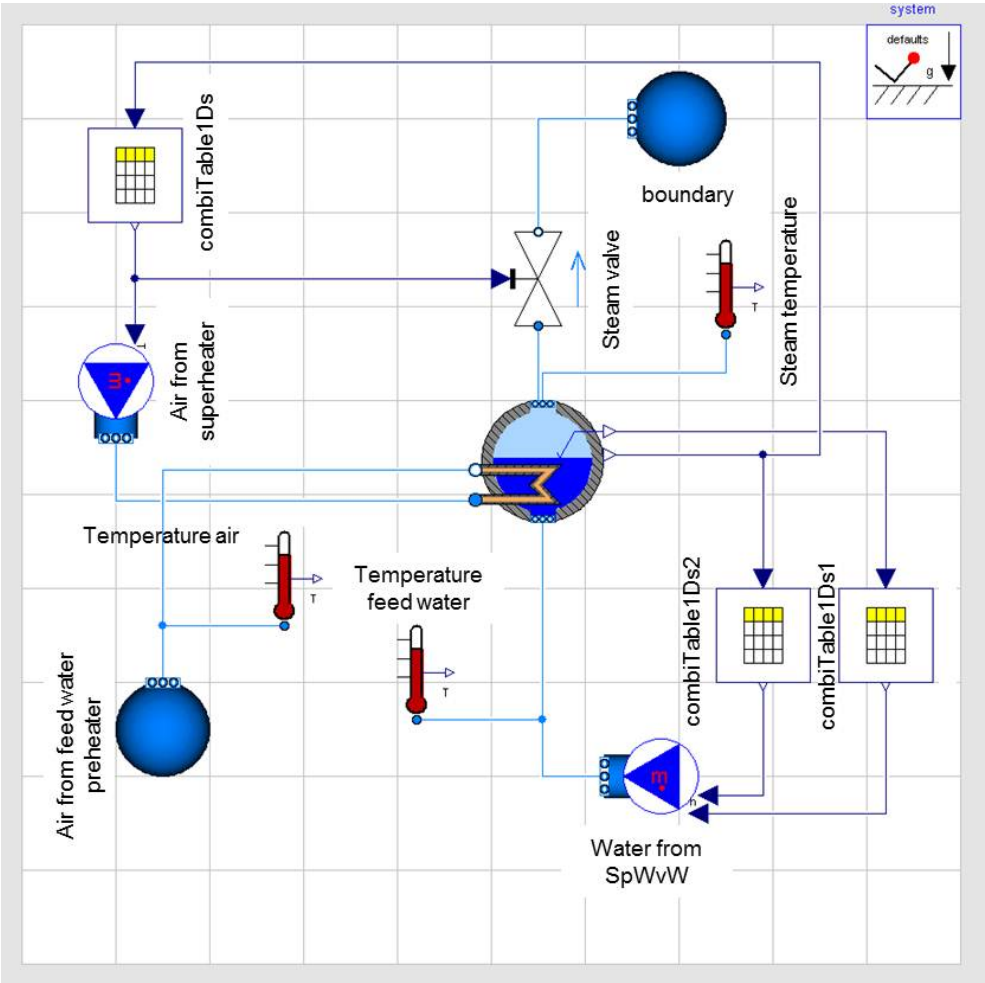

Figure III.4-33: Start-up test environment for the boiler

Pressure and water level inside the boiler are measured. Both values are used to control the mass flow rate of the feed water pump considering tables. Besides, pressure is used to control the air inlet temperature which in turn controls the valve position at the steam outlet. At start of the simulation start the water level in the interior of the boiler was estimated.

Figure III.4-35 and Figure III.4-35b compare measured boiler values during start-up with simulated values.

As one can see, the simulated pressure rises slower than the measured one, but reaches the same level in the same time.

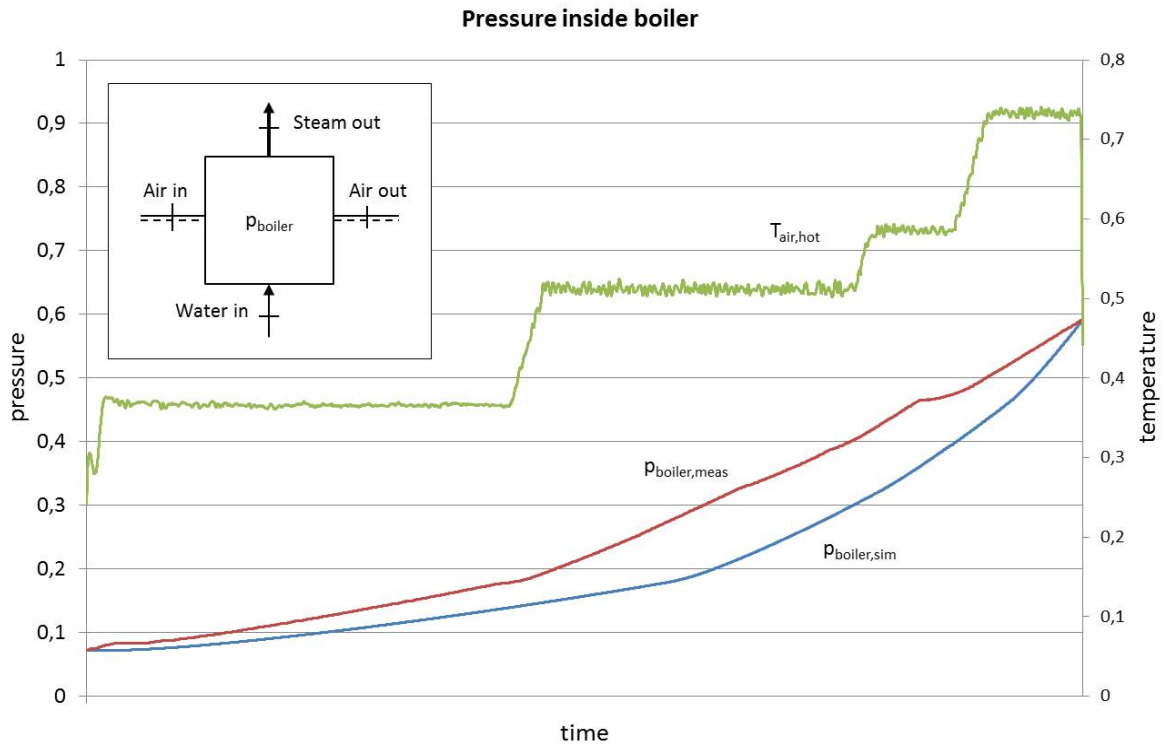

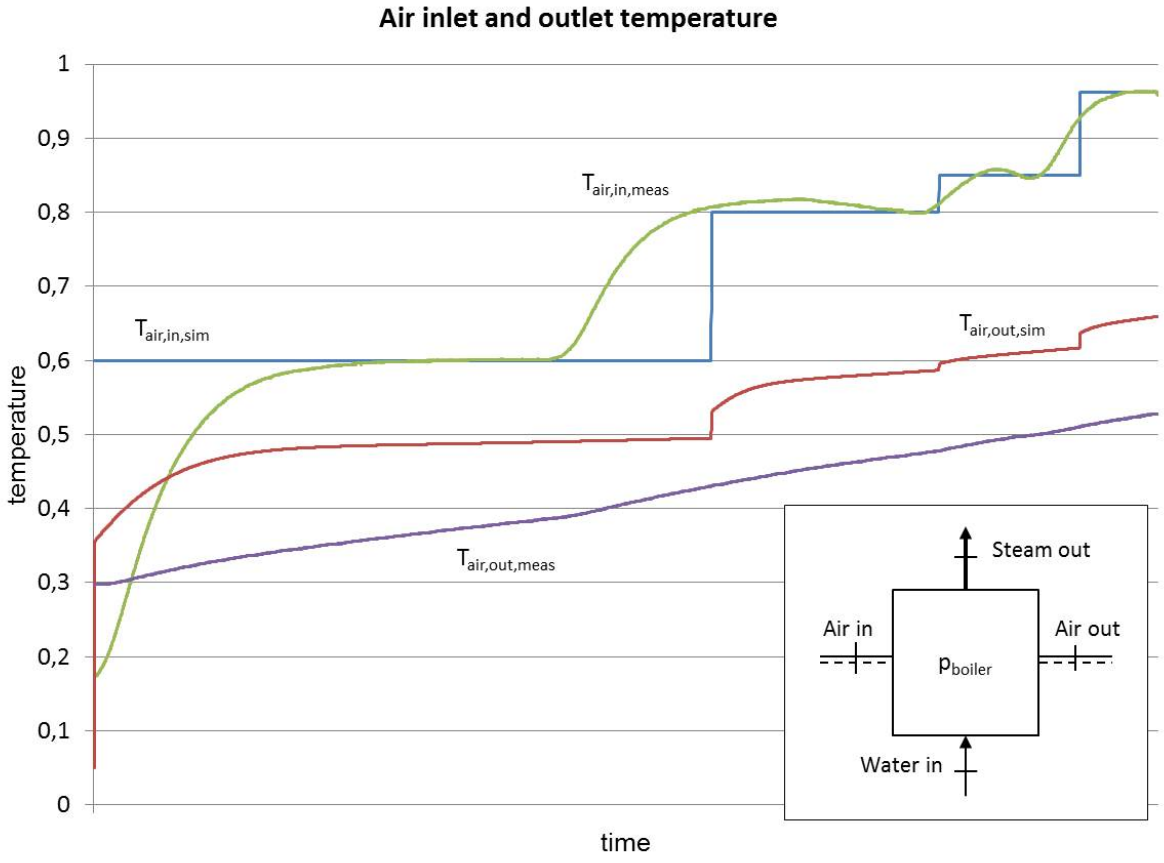

Figure III.4-34: Characteristics of boiler values during start-up

The air temperature is increased with the reach of certain pressure values. As the steam mass flow is controlled by the air temperature it also rises slower in the simulation. Additionally, the steam mass flow rate is dependent on the boiler pressure. As the simulated pressure is lower than the measured one, the steam mass flow is lower as well. Due to the inertia of the components (super heaters) the measured air inlet temperature of the boiler changes steady not stepwise.

In the simulation, however, it was only possible to model the rises stepwise. The outlet temperatures deviate almost parallel. The simulated temperature is higher as well as in the stationary validation. The trend of the graphs for the feed water and steam temperatures are similar. The discrepancies can be explained referring to the differences described before.

The preheaters show better results for the validation with operation data than with design data just like the boiler. The condensate preheater has a maximum temperature difference for the validation with design data of 14.1%. In the other case the maximum difference is 12.11%. As no detailed geometry data was available the simulations were made with adjusted tube lengths. The maximum temperature difference for the validation of the feed water preheater with design data is 10.53%, while comparison with operation data resulted in a maximum temperature difference of 3.69%.

In the test environment for the start-up simulation of the preheaters the air inlet temperature cannot be controlled by the steam pressure. Therefore, the changes in air temperature as well as the enthalpy and pressure of the feed water are triggered. The test environment is shown in Figure III.4-36.

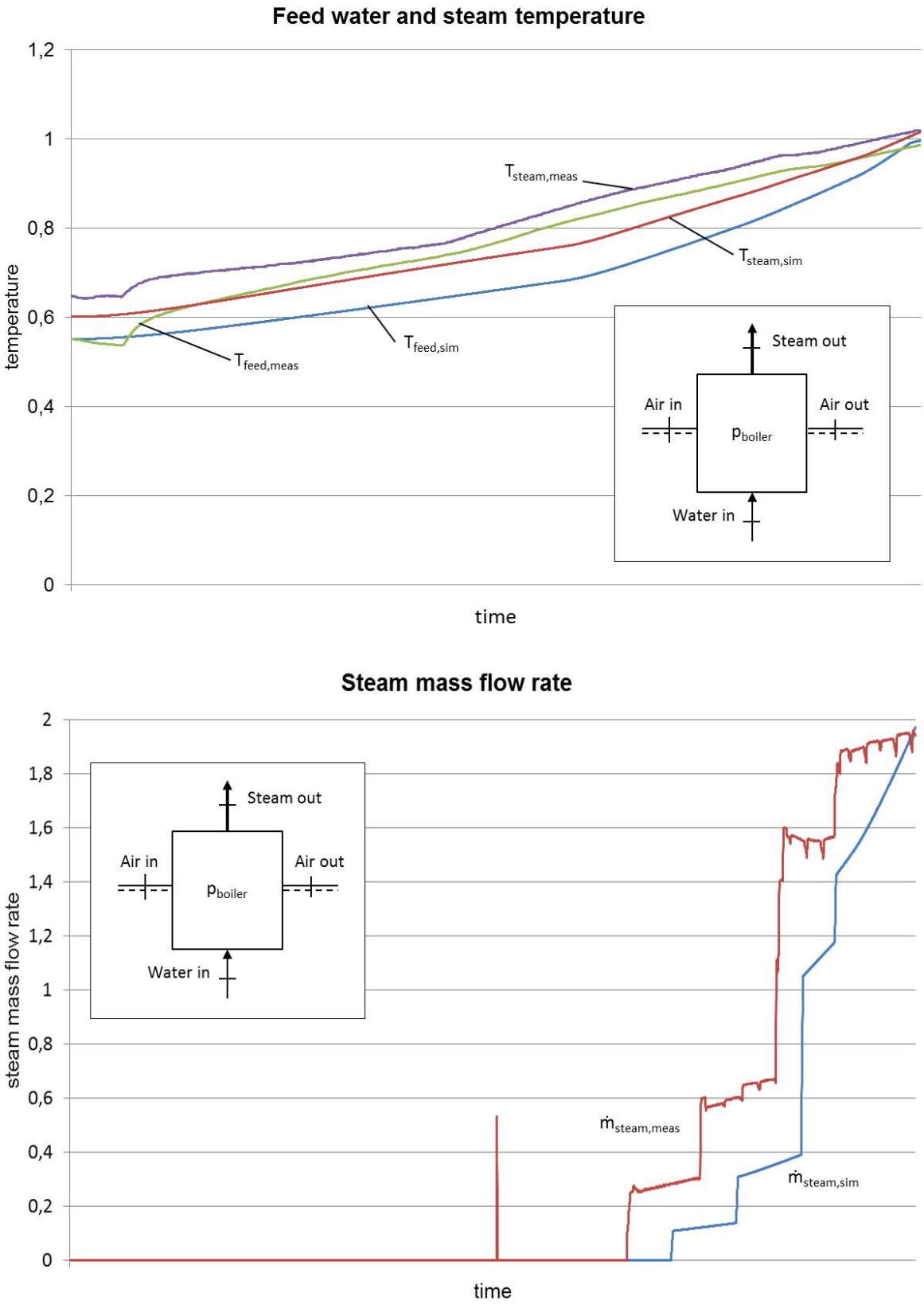

Figure III.4-35: Characteristics of boiler values during start-up

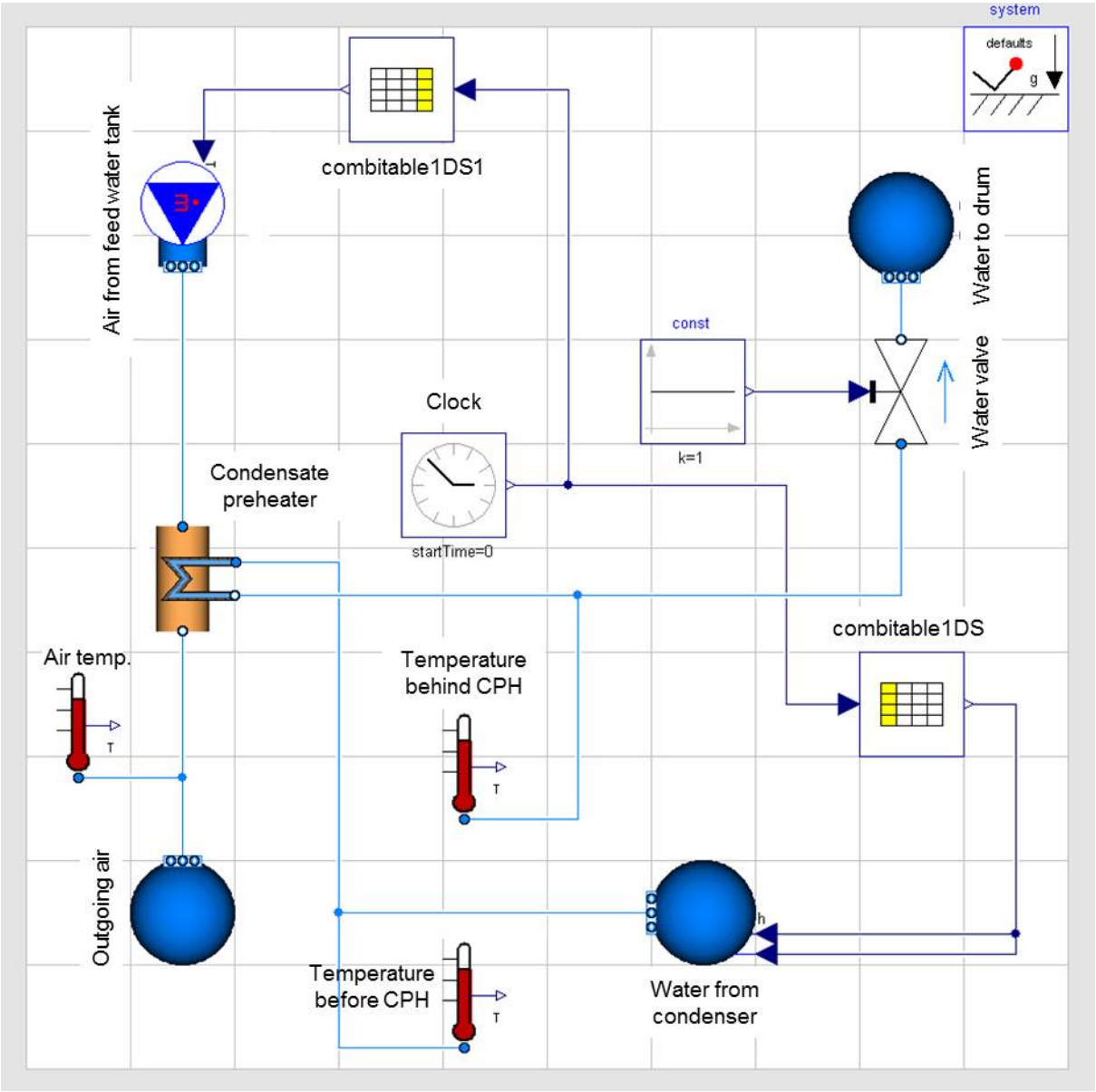

Figure III.4-36: Start-up test environment for the preheaters

Due to the mentioned inertia of the components the measured values of air and water temperatures in the preheaters show no linear characteristics, as can be seen in Figure III.4-37.

Nonetheless, the simulated air temperatures converge towards the same values as the measured characteristics. The water inlet temperatures are identical at start, but differ strongly in progress. In comparison to that, the outlet temperatures show a better accordance.

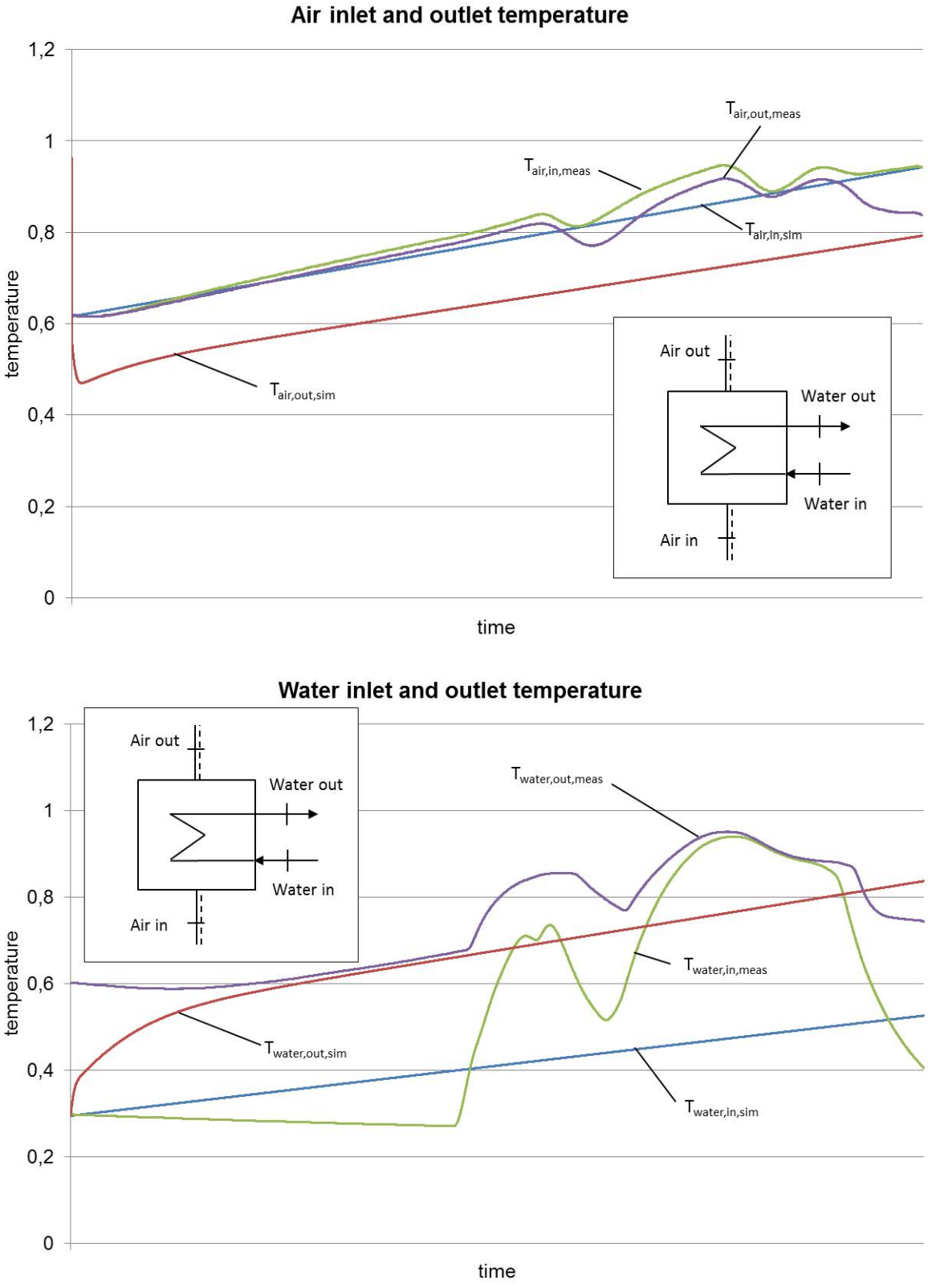

Figure III.4-37: Characteristics of preheater values during start-up

The super-heater section shows good results for the validation with design data with maximum temperature differences of 4.61%.

Equal to the start-up simulation for the preheaters a clock is inserted in the test environment for the super-heaters to replace the missing pressure input of the boiler. The clock triggers the enthalpy and pressure values of the steam at the inlet. The pressure of the steam at the inlet controls the air temperature as well as the valve position and in consequence the steam mass flow rate (Figure III.4-38).

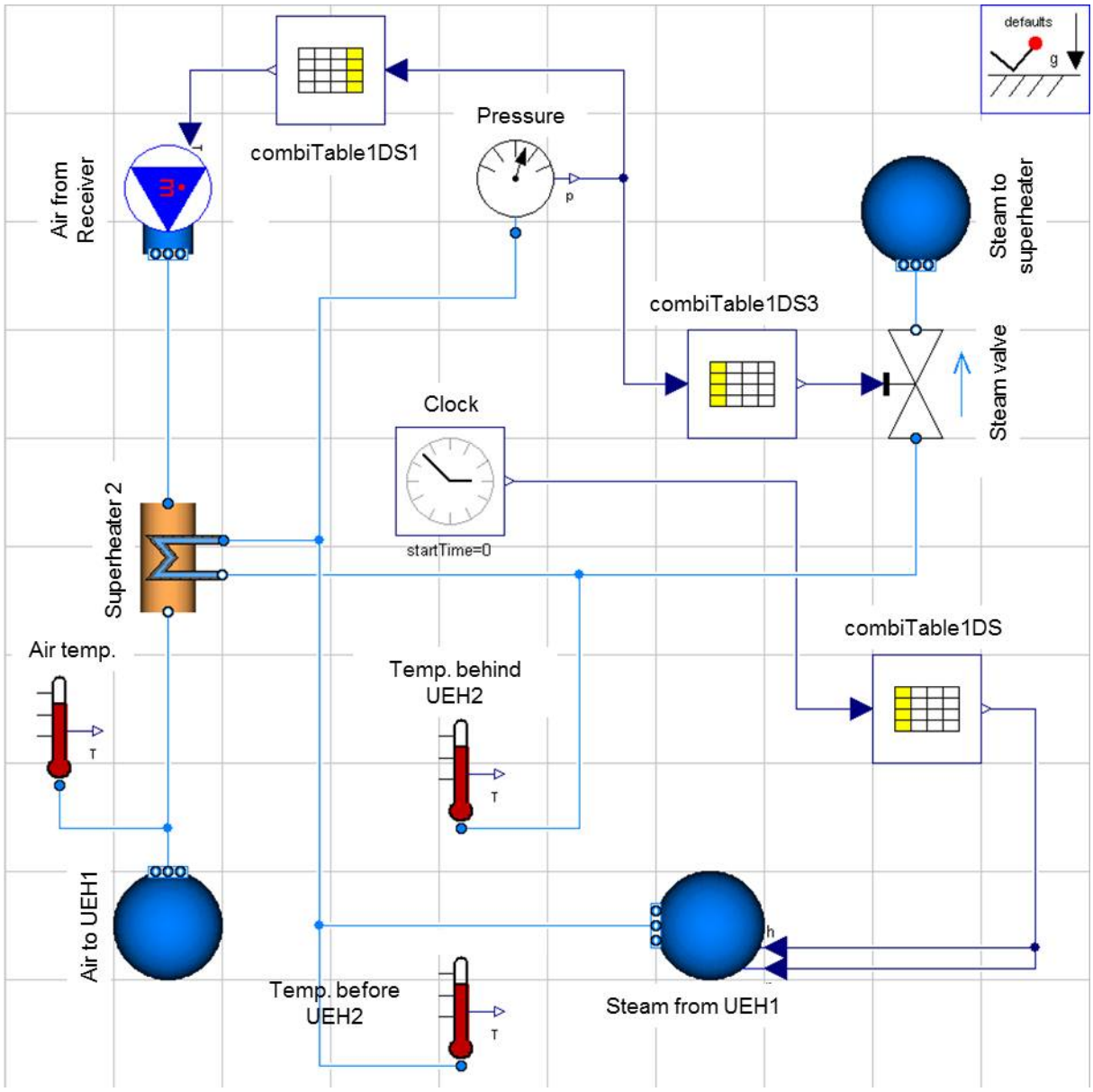

Figure III.4-38: Start-up test environment for the super-heaters

Contrary to the real start-up procedure the simulation needs to be supplied with a mass flow rate through the super-heater at any simulation time. This explains the differences in the steam outlet temperature, especially, at the beginning of the simulation. The characteristics of the inlet temperatures are identical (Figure III.4-39).

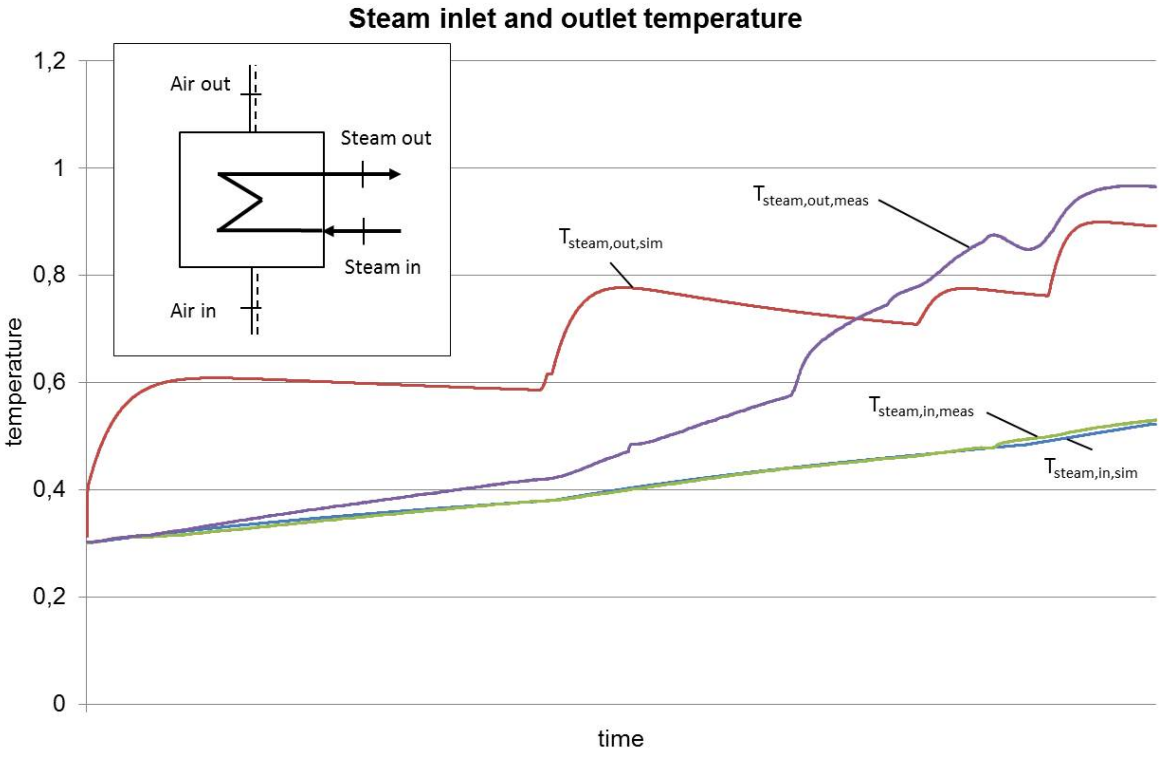

Figure III.4-39: Characteristics of super-heater values during start-up

The characteristics of the air temperatures are not displayed as the incoming air is derived from the measured values. The values of the outgoing air cannot be compared due to the fact that on this position no measurement point is installed and in consequence measured data are not available.

As explained above a validation of the complete water-steam cycle is impossible because of the missing data at certain positions. Instead, the functionality of the modelled cycle is tested with a fictional scenario. The values used for the scenario do not match the data from the solar tower Jülich.

Figure III.4-40 shows the *Dymola* model of the complete cycle. The program distinguishes between mass flow rate and volume models. These two model types should be used alternating. As this condition cannot always be met, volume models are added in between some of the cycle components. The volumes are small enough to not affect the inertia of the steam generator.

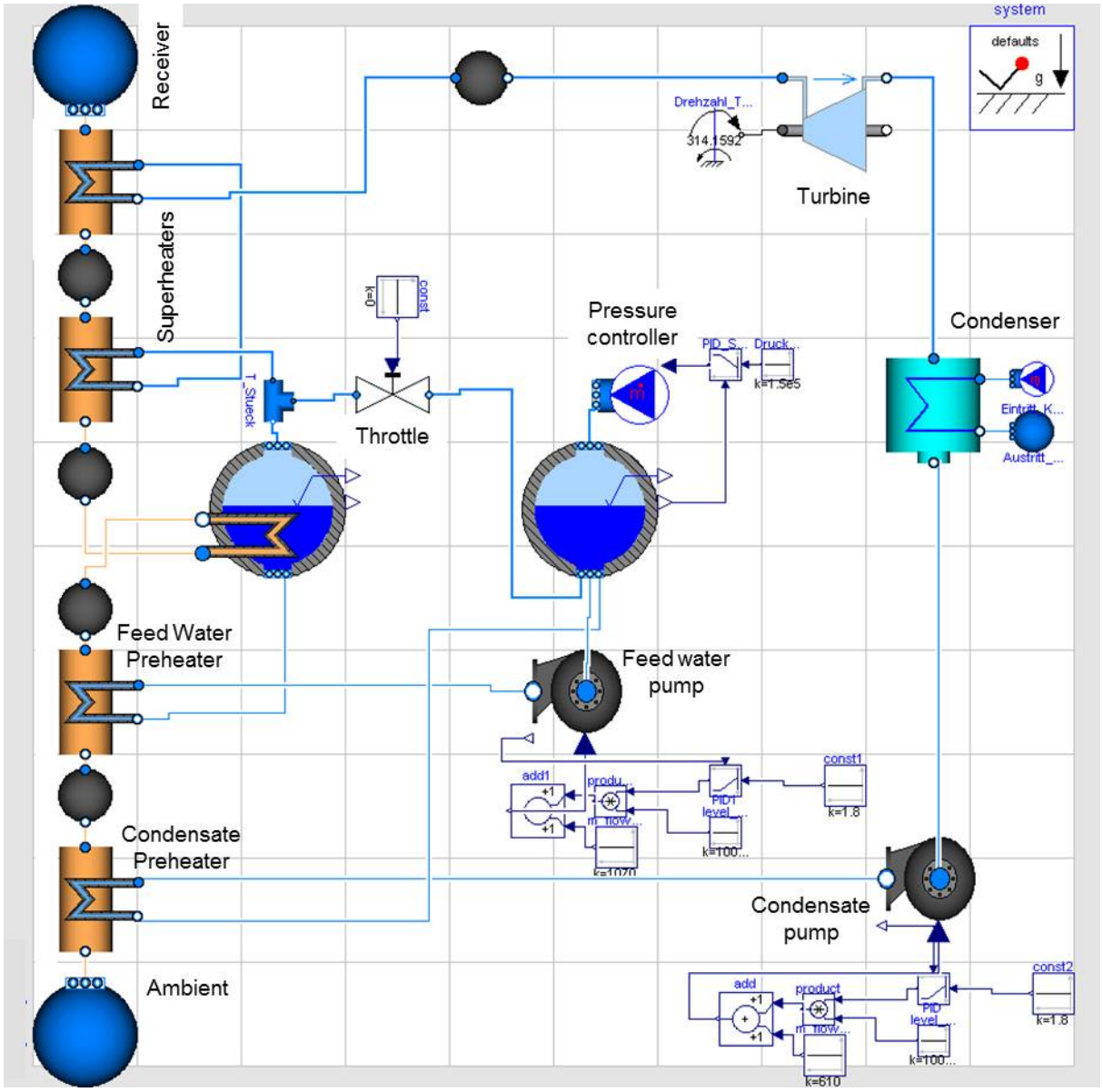

Figure III.4-40: Connected complete water-steam-cycle

The cycle test is performed with a drop of the hot air mass flow rate which represents the normal operation of a solar tower. The remaining boundary conditions are kept constant to minimize calculation time. Air inlet temperature as well as in- and outlet pressure are defined. Figure III.4-41 shows the drop of the mass flow rate versus time.

The boiler has the biggest inertia and therefore dominates the cycle behaviour. Figure III.4-42 shows the boiler reaction to the mass flow rate drop. Due to the reduced heat transfer the steam mass fraction in the liquid phase drops. This causes an increase of the density of the liquid phase. Together with the constant boiler volume this initiates a pressure drop, which in turn leads to a lower steam saturation temperature.

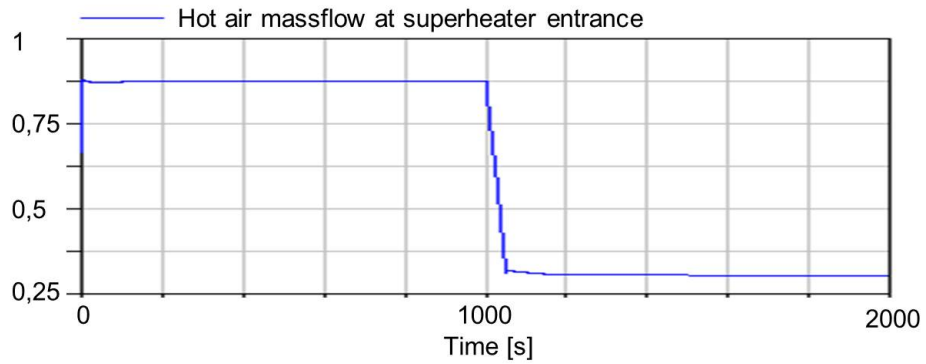

Figure III.4-41: Drop of hot air mass flow rate at steam generator entrance

The produced steam mass flow also decreases according to the reduced steam mass fraction. The boiler water level rises because of the reduced steam mass flow rate while the feed water mass flow rate is constant. This contributes to the temperature reduction and as a result to the drop of the steam mass fraction in the liquid phase.

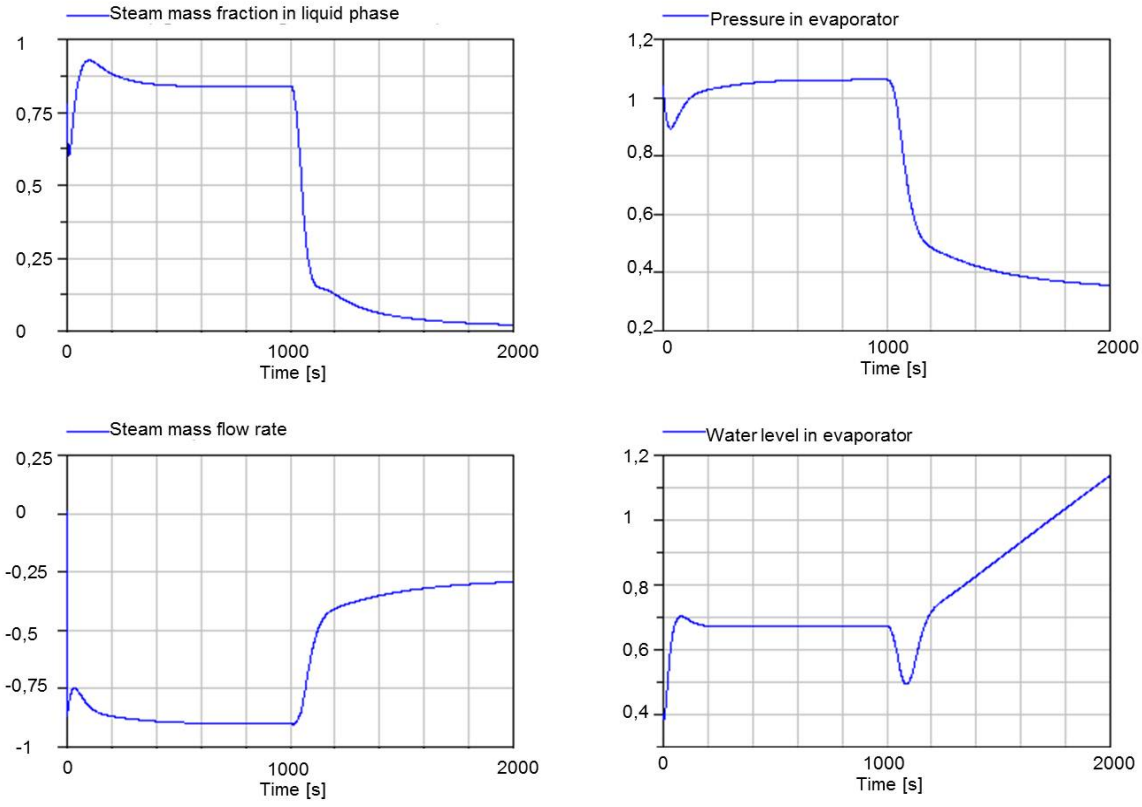

Figure III.4-42: Boiler reaction to drop of air mass flow rate

The sudden drop in the super-heater temperatures, as seen in Figure III.4-43, originates in the momentarily steady steam mass flow with a concurrently reduced air mass flow rate.

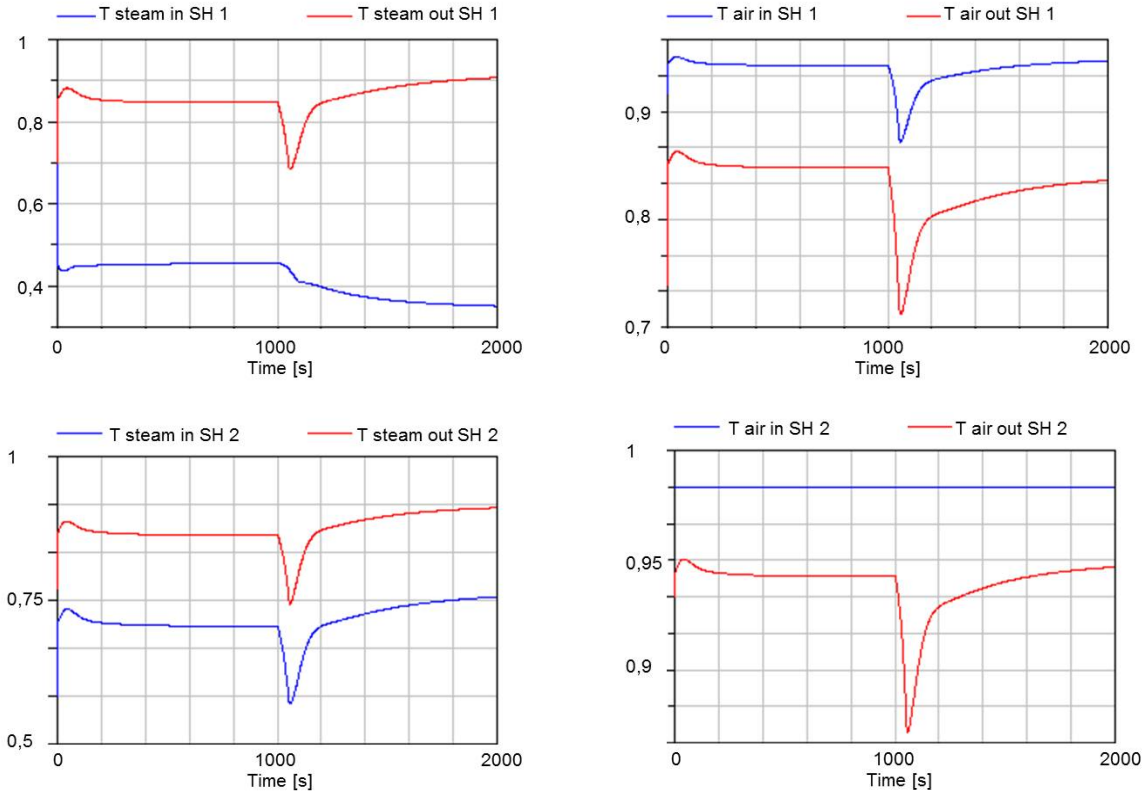

Figure III.4-43: Reactions of the super-heater temperatures

Due to the reduced steam mass flow rate from the steam generator the mass flow from the turbine to the condenser is reduced, too. Together with the constant feed water flow rate this triggers a declining condensate level inside the condenser (Figure III.4-44). This in turn leads to a pressure drop in the condenser.

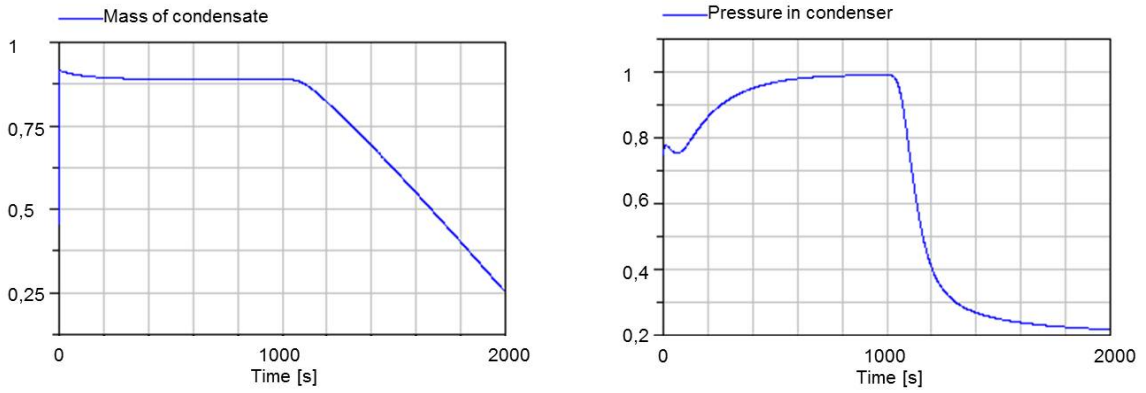

Figure III.4-44: Reactions of the condenser

Figure III.4-45 shows the temperature reactions in the preheaters. The water temperature drops since the water mass flow rate stays constant while the air flow rate is reduced. In addition, the reduced condenser pressure causes a drop in the water inlet temperature.

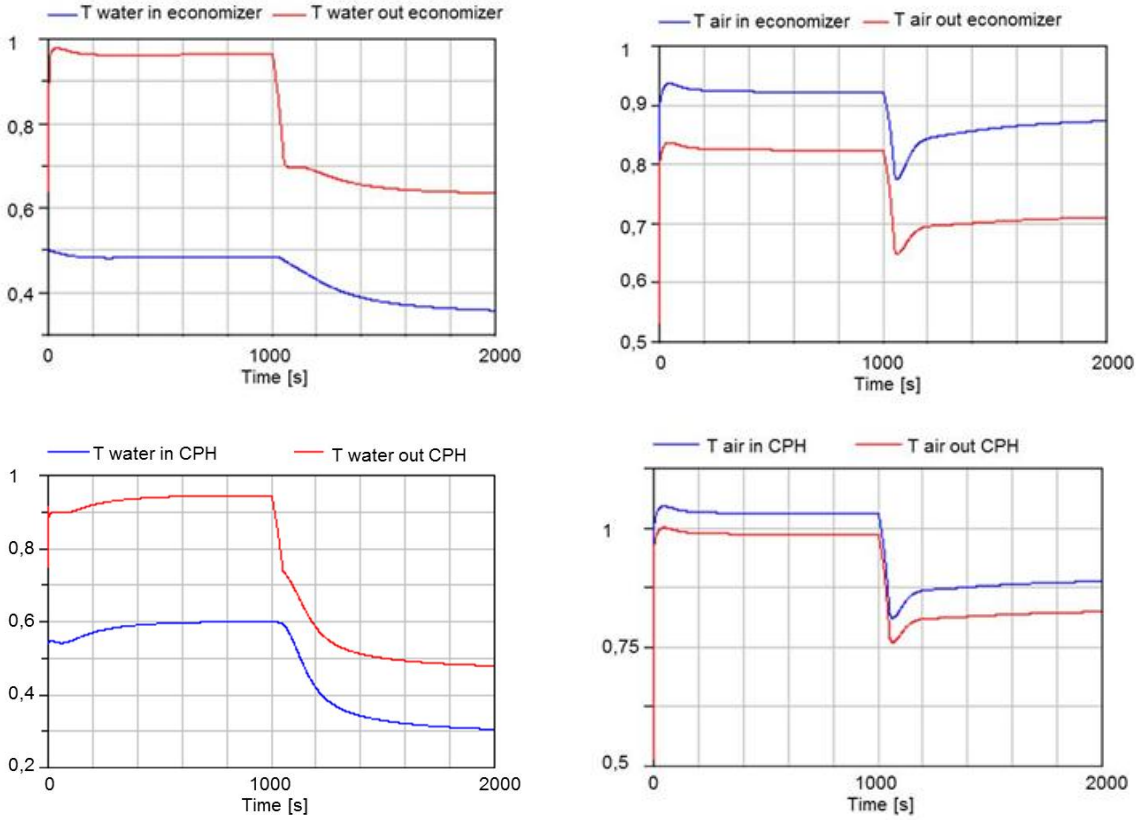

Figure III.4-45: Reactions of economizer and condensate preheater

The power output of the turbine is reduced due to the decreased steam mass flow rate and pressure (**Figure III.4-46**).

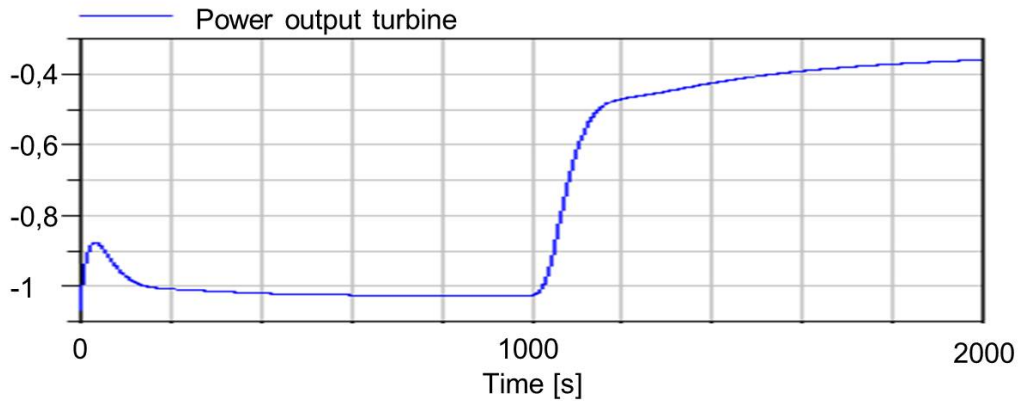

Figure III.4-46: Turbine reaction

IV. Results of WP 3 – Optimization of power plant operation

IV.1. Basic control scheme

This chapter describes the development and simulation tests of a basic automation scheme of the air cycle of the tower power plant. The developed automation concept, based on classic PID-controllers, should guarantee safe operation of the plant with regard to changing ambient conditions and setpoint changes. It also serves as a benchmark for further, more complex controllers, for instance, the model-based predictive control.

The main focus of the control scheme lies on the air cycle, since the control of the conventional water-steam cycle is already state of the art.

Solar thermal power plants have two major differences as compared to fossil fueled power plants. The first one consists in the fact that the fuel mass flow rate, i.e. the energy input into the system in form of solar radiation, is not a manipulated but a disturbance variable. The second difference lies in the use of the thermal energy storage which offers an additional degree of freedom in order to enhance the efficiency of the overall process.

The primary goal of the control is to keep the air outlet temperature at the receiver at 680°C under changing ambient conditions. Some examples of changing ambient conditions, which are disturbance variables of the process, are fluctuating solar radiation, wind speed and wind direction or ambient temperature. In addition, operator's actions can be taken into account, although the idea of this concept is to reduce them to the minimum and thus provide interacttion on a high level. This means that setpoints by the user concern, for instance, the amount of the energy to be fed into or withdrawn from the storage, but not the required manipulated values for the valves or blowers.

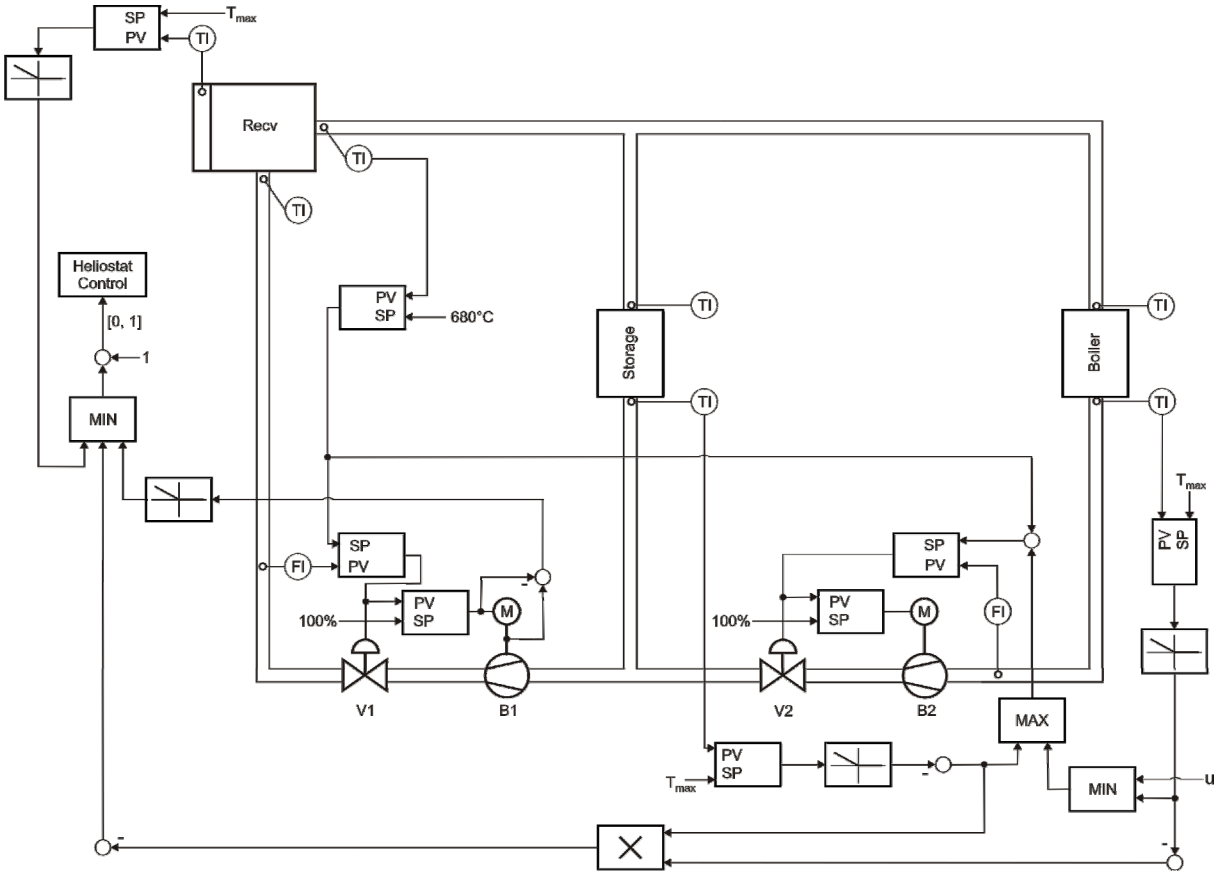

Figure IV.1-47: Basic automation concept

IV.1.1. Structure of the automation concept

The measured variables for the automation concept are various flow rates and temperature data, as shown in Figure IV.1-47, marked with FI (Flow Indicating) and TI (Temperature Indicating). Manipulated variables are valve and blower values. The primary goal of the control is to keep the air outlet temperature at the receiver at 680°C under changing ambient conditions. This is achieved by controlling the air flow through the receiver. In nominal operation, an increase of the air flow results in a reduction of the outlet air temperature.

Charging and discharging of the storage is executed through the interrelation of the air flow rates of both blowers B1 and B2. If the flow rate in B1 is greater than that in B2, the storage tank is charged. The hot air from the receiver flows from above into the storage tank, conveys its energy to the material of the storage and escapes through its lower, cool part. By discharge, the air flows in the opposite direction through the storage tank, which means that the flow through B1 is smaller than through B2. If both flow rates are equal, the air circulates only through the receiver and the steam generator. If B1 = 0, the process is driven entirely by the heat from the storage tank. Correspondingly, if B2 = 0, the entire heat is fed into the storage tank.

To define the energy input from the field of heliostats onto the receiver and thus in the air cycle, an additional block is introduced to control the heliostats. A value from 0 to 1 is assigned to the energy input as the input value, which reflects the percentage of the radiated power of the sunlight concentrated onto the receiver, as compared to the maximum possible power. During the operation of the power plant, this value should be equal to 1, since a smaller value means an energy loss.

IV.1.1.1. Overview

As it can be seen in Figure IV.1-47, the system is over-actuated in terms of the air outlet temperature as the most important process variable, which means that the system has more manipulated than process variables. The idea of the automation concept is an interconnection of different transfer blocks and controllers to achieve a successful cooperation of the actuators. It should control the air temperature at the receiver and comply with additional boundary conditions, such as maintaining the maximum temperature of the front side of the receiver or of the cool part of the storage tank.

The interconnection of various blocks is also shown in Figure IV.1-47. For technical reasons, the representation is slightly simplified and will be discussed below. The description of the following blocks will be presented in the next sections:

1. Controller
2. MIN- and MAX-blocks
3. Limiter
4. Multiplier

The main components of the automation concept are controllers of various types. Each controller has two inputs, namely the current process value (PV) and the setpoint (SP). Depending on the inputs, the controller calculates the control error ER = SP−PV and thus the current manipulated variable (MV) as the output. In the present concept, only P- and PI-controllers are used. Choosing the appropriate controller for certain process elements depends on the requirements to the related closed loops (for detail, see section IV.1.2).

Furthermore, there are various MIN- and MAX-blocks, each generating the minimum or the maximum value of the inputs.

The limiters serve to monitor the limit values. In these blocks, the interconnection of the input proceeds with no change if the input is greater or less than 0, depending on the block type. Otherwise, the output is equal to 0. However, it is assumed for this case that the output of the block does not influence the subsequent decisions concerning the minimum/maximum values. To avoid this, one can imagine that the block in the limit would output minus or plus infinity instead of zero. Another point of view is that in this case the signal is just irrelevant for

the subsequent minimum/maximum decisions. Therefore, these blocks restrict a signal to the strictly positive or strictly negative area.

Multipliers should be seen as real-valued AND-blocks. As abbreviated notations, they represent blocks which have an output signal unequal to 0 iff both input signals are unequal to 0. If at least one input signal equals 0, the block outputs zero too.

Pure proportional blocks have been omitted in Figure IV.1-47 for the sake of clarity of representation.

IV.1.1.2. Blowers & Valves

On the lowest level of the automation scheme, the different actuators, i. e. fans and valves, have to be controlled. This is performed by a modular approach, treating a single fan together with its downstream valve, e. g. B1 and V1, as one unit and connecting each unit identically to obtain the desired behaviour.

The main idea of the connection of one fan-valve-combination as depicted in Figure IV.1-47 is, that the developed wiring should ensure a fast adjustment of an arbitrary volume flow given as setpoint. To achieve this, two controllers are used. The first one compares a given volume flow as setpoint to the current volume flow, which can be measured, and adjusts the valve position appropriately to control the throughput of the valve. This obviously works only within the physical limits of the valve. If the valve is completely opened, it is not possible to increase the volume flow furthermore. For this reason, a second controller is used which actuates the fan to achieve a constant valve position. It means that this controller is used for disturbance rejection caused by the other controller.

The following example illustrates the behaviour of this structure. Assuming a stationary operation of the system with the valve completely opened, a negative step on the setpoint of the volume flow is performed. The first controller will close the valve to settle to the new setpoint. Noticing this, the second controller will decrease the rotational speed of the fan to bring back the valve position to be fully opened. After a transitional period (which is mainly determined by the mechanical inertia of the fan), again a stationary operation is achieved, in which the valve is again completely opened and the fan is rotating at an appropriate lower speed. Considering the other case, a stationary operation with a completely opened valve and a step on the volume flow in positive direction, the valve obviously cannot be “more opened”. However, the second controller notices the fact that the first controller demands an opening greater the maximal opening even though this cannot be reached by the physical valve. The second controller will then increase the fan speed to bring the manipulated value of the first controller back to the previous value, which results in an increasing volume flow through the fan. Notice that in this case, the position of the physical valve does not change at all; it remains completely opened all the time.

There are different benefits of this structure. The first one is the response time of the system to reach stationary volume flows when setting different setpoints. Since the inertia of the valve is less than that of the fan, the system is much faster compared to the case when the blower is used as a single actuator to control the volume flow. This obviously only holds if the valve can physically be set to a new position. However, in the other case, this structure is equivalent to a wiring where the fan is directly used to control the volume flow. Since during normal operation an additional pressure drop caused by a not completely opened valve in the air cycle of the plant has to be avoided, this benefit typically holds only for decreasing the volume flow. Nevertheless, with this structure it is possible to have a throttled operation by using the second controller to remain at a valve position which is partly closed. In this mode of operation, it is also possible to increase the volume flow very fast.

Furthermore, the fan itself has a low pressure drop during standstill periods such that an airstream just flows through it if the stream is generated by another fan installed in series (cf. Figure IV.1-47). For that reason, the valve V1 has to be closed when the plant should be operated only with heat from the storage. In this case without the valve, it would be impossible to get a zero volume flow through the receiver in this case. Additionally, the fans are lim-

ited to a minimal rotational speed. Therefore, the valves also have to be closed appropriately to set volume flows below the threshold given by the fan itself.

IV.1.1.3. Receiver

As mentioned above, the main goal of the automation scheme is to maintain the air outlet temperature at the receiver at a constant level about 680°C. The assumption is that an increasing volume flow through the receiver yields a decrease of the air outlet temperature. This assumption only holds for volume flows above a certain extent, so the controller of the receiver temperature is limited to a minimal flow greater than zero.

The temperature difference of the air outlet temperature from the setpoint is used to compute the necessary volume flow through the receiver. The demanded volume flow is fed into the structure for manipulating the actuators as described in the previous section. This results in a cascaded structure with the fan/valve control in the inner loop and the control of the receiver temperature in the outer loop of the cascade.

To consider the case when the fan operates at its upper limit and the outlet temperature at the receiver increases furthermore in periods of high irradiation, an additional feedback from the fan to the “Heliostat Control” is necessary to defocus some mirrors in that case. This is realized in the automation scheme by comparing the current setpoint of the fan B1 with its effective speed and use the difference to adjust some heliostat positions.

It is assumed that both fans reach their upper limit at about the same value for the volume flow. If B2 reaches the upper limit much before B1, this would yield in a somewhat hidden loading operation of the storage. If this assumption does not hold, an additional feedback from B2 has to be added in that way as described above for B1.

Additionally, care must be taken that the receiver’s front temperature does not exceed a given maximal value due to material properties, since this may irreparably damage the receiver. There are two possibilities to react on this situation:

1. Increase the volume flow through the receiver by decreasing the outlet temperature,
2. Defocus some of the heliostats.

The first solution, increasing the volume flow through the receiver, would be easily realizable by subtracting an additional term from the setpoint of the air outlet temperature of the receiver. This would imply an increasing volume flow by the control structure. However, since in any case an increasing volume flow through the receiver would result in a lower air outlet temperature, this solution has several drawbacks. The first disadvantage is that the boiler should be operated in its design point for the best efficiency factor, which would not be the case for more cold air. Furthermore, if the cold air is fed into the storage, this may destroy the temperature profile within this system. And as a last point, the reaction time might be quite slow until the fan is at a higher speed and the higher volume flow really cools down the receiver.

Therefore, in the automation scheme, the second approach is used. If a temperature above a given threshold is detected, this information is immediately used to defocus some mirrors by the “Heliostat Control” block.

Also, the inlet temperature of the receiver should not exceed a given limit, since this air is needed for cooling the construction of the receiver. This is accomplished in the automation scheme by the control of the storage and the boiler, which is described in the sections below.

It should be mentioned that up to now, without any user interaction, both units of fan and valve, i. e. B1/V1 and B2/V2, get the same setpoint. In this way, all air circulates through the receiver and boiler, the volume flow through the storage is zero.

IV.1.1.4. Storage

The operation of the storage, i. e. the decision when to load or unload the storage, should be carried out by the operator of the plant. As mentioned above, the controller of the receiver temperature accesses both fans/valves identically. To include a user input for the operation

mode of the storage, an additional input *u* is added to the volume flow setpoint of B2/V2. Adding the input at this point should be quite intuitive for the operator, since this signal has the physical unit of a volume flow and not something abstract like a valve position or blower speed. A value greater than zero results in unloading, smaller than zero in loading the storage. Note that there is no user interaction regarding the setpoints of B1/V1, since these are completely determined by constraints from the receiver control.

An additional condition regarding the mode of operation of the storage is that it should not exceed a maximal temperature at the cold end, since this can damage the construction. If this is the case, the cold air leaving the boiler should be used to cool down the storage at its cold end by flowing through it in upward direction. In other words, the storage has to be unloaded. Therefore, an input from an operator has possibly to be overdriven. This is accomplished by a controller for the storage temperature at the cold end, which is, due to the limiter, only active when it is really necessary. However, the controller does not overdrive the operator input in every case, but due to the downstream MAX-block only if the required volume flow to cool down the storage is above the one given by the operator. Due to this wiring, it is in this situation still possible for the operator to unload the storage with a higher volume flow, however, it is not possible to load the storage anymore.

The position of the temperature measurement has also to be considered. If the temperature is directly measured in the air flow and not in the solid material with thermal inertia, an additional hysteresis has to be used to avoid toggling of the system when small fluctuations around the maximal value occur.

IV.1.1.5. Boiler

For the boiler, a constraint is that the temperature at the cold end also does not exceed its design point, since this would mean that the boiler cannot cope with the delivered energy from the receiver. The approach here is similar to the one used for storage operation. If such a situation is detected, the user input will be overdriven in such a way, that the excessive energy will be used to load the storage. This is done in a similar way as mentioned above considering the storage.

However, it may happen during periods of high irradiation, that both the storage is full and the energy from the receiver cannot be dumped in the boiler. In this case, the presented automation scheme will cool down the cold end of the storage, since this is the crucial part compared to the boiler not operating at the maximal efficiency, but also will defocus some of the heliostats.

During start-up or shutdown of the plant, it must be possible to follow defined temperature profiles in the boiler independent of the solar irradiation, e. g. during start-up of the plant to heat up the turbine in a defined way. This is also covered by the presented automation scheme as it can be seen in section IV.1.2.4.

IV.1.2. Controller design

In addition to providing safe operation of the power plant, a further aim of the automation concept in Figure IV.1-47 is an easy implementability within the control system, which is possible due to the use of simple PID-controllers.

In the following sections, it is explained which controllers (P, PI, etc.) have been chosen for specific tasks and how the parameters have been determined.

IV.1.2.1. Types of Controllers

Since the overall automation concept should be simple to implement, this particularly holds for each controller.

When considering closed-loop behavior, one crucial point is stationary offset-free tracking of the controlled variable, i. e. the output should in stationary cases reach the setpoint without any steady-state deviation.

Considering the volume flow, offset-free tracking should be realized, because at this place user interaction comes into play. It is inconvenient for an operator if she sets a specific volume flow, but this value is never reached. The control of the valve should also be offset-free, since an open valve should really be opened to avoid additional pressure drops in the air cycle.

As mentioned above, the air outlet temperature of the receiver is the main controlled variable, so this should also reach its setpoint without deviation, because there will be direct (visual) feedback to the operator.

To accomplish offset-free tracking in the closed loop, the open loop system has to have integral behavior. A detailed analysis of the transfer functions of the above systems showed that none of them have integral behavior on their own, so the integral part has to be added in the controller. Therefore, the main controllers for operation of the plant have to be at least PI-controllers.

Recall that there is a cascaded structure concerning the control of the air temperature. From the consideration above one can see that there are controllers with integral action in the outer, as well as in the inner loop of the cascade, which is quite unusual.

For windup compensation, the integral part of the controllers will be continuously reduced if the controller saturates.

The other controllers are not used during “normal” operation of the plant, but are only active if some signals exceed their limits. Therefore, simple proportional controllers are sufficient. Furthermore, it would be nontrivial to decide when a controller saturates to choose adequate anti-windup measures.

IV.1.2.2. Determination of parameters

As a second part of the design process, the different parameters for each controller have to be determined. For the controllers of the volume flow, which is the part with the fastest dynamics in the plant, a response optimization approach has been carried out. For that, several steps of the volume flow with the non-linear model have been performed over a wide operating range of the system to find optimal controller parameters.

The optimization variables to be tuned by the optimizer are the controller parameters of the closed-loop system. By adding hard constraints to the optimization problem, it is possible to achieve a desired response time and damping ratio of the system.

The parameters of the other controllers were determined by variants of empirical formulas like the Ziegler-Nichols method or a T_u/T_g-model by Chien, Hrones and Reswick using the non-linear plant model.

IV.1.2.3. Feed-forward control

In a conventional power plant, the fuel flow rate in fuel combustion represents a manipulated variable, whereas the solar irradiation in a thermal power plant is a disturbance variable.

Since the latter variable is vital for the operation of a power plant, it should possibly be taken into account. One option is to measure the current direct radiation with a pyrheliometer and to calculate the radiant flux density at the receiver using a model of the field of heliostats. The radiant flux density can also be measured directly at the receiver. The obtained value can then be used in a feed-forward control to improve the performance of the system.

For that, a Hammerstein model is used, which consists of a static nonlinearity and a linear first-order lag element (PT1). The nonlinearity represents the static behavior of the receiver; the time constant of the PT1 corresponds to the delay of the receiver.

On the basis of the mean flux density at the receiver, the model calculates the required air flow rate to achieve the appropriate air outlet temperature of 680°C. It is an evident advantage of the feed-forward control that the information about the changing solar radiation is used immediately and not through the reaction on the change of the air outlet temperature

delayed by the inertia of the receiver. Section IV.1.3.3 shows a significant improvement of the control performance due to the above mentioned enhancement of the control scheme.

IV.1.2.4. Simulation results

IV.1.2.4.a. Control of volume flow

In Figure IV.1-48, the response to operator input is depicted. During stationary operation, the operator commands a change in the volume flow through the storage to (un)load it. The different subplots show the volume flow through each component, the velocity of the two blowers and the valve positions (from top to bottom).

Up to time *t = 10 s*, all air from the receiver is circulating through the boiler, i.e. *u* equals zero. Then, the operator performs a step in the setpoint of the volume flow of 2 m³/s; resulting in unloading the storage with this volume flow. As one can see, the speed of the fan B2 at the boiler is increased to reach the higher setpoint. Because of this, the volume flow through B1 at the receiver also increases, since the inlet pressure of the blower increases and there is a higher volume flow caused by this pressure differential. As a countermeasure, the valve V1 at the receiver is closed to keep the volume flow through the receiver constant until the speed of B1 has been decreased.

At time *t = 30 s*, the operator decides to load the storage and performs another step to the setpoint of the volume flow. To load the storage, the volume flow at the boiler has to be decreased, so the valve V2 is closed to bypass the time until the fan B2 has reached its new setpoint. However, as in the case above, the change of the volume flow through B2 also influences B1, therefore, the speed of this fan must be increased again.

As it can be seen in the figure, the closed-loop behavior of the blower/valve-combinations work as expected. Also note that the delay of the increase of the volume flow is caused by the inertia of the fan itself. The controller outputs the maximal manipulated value to increase the speed of the fan.

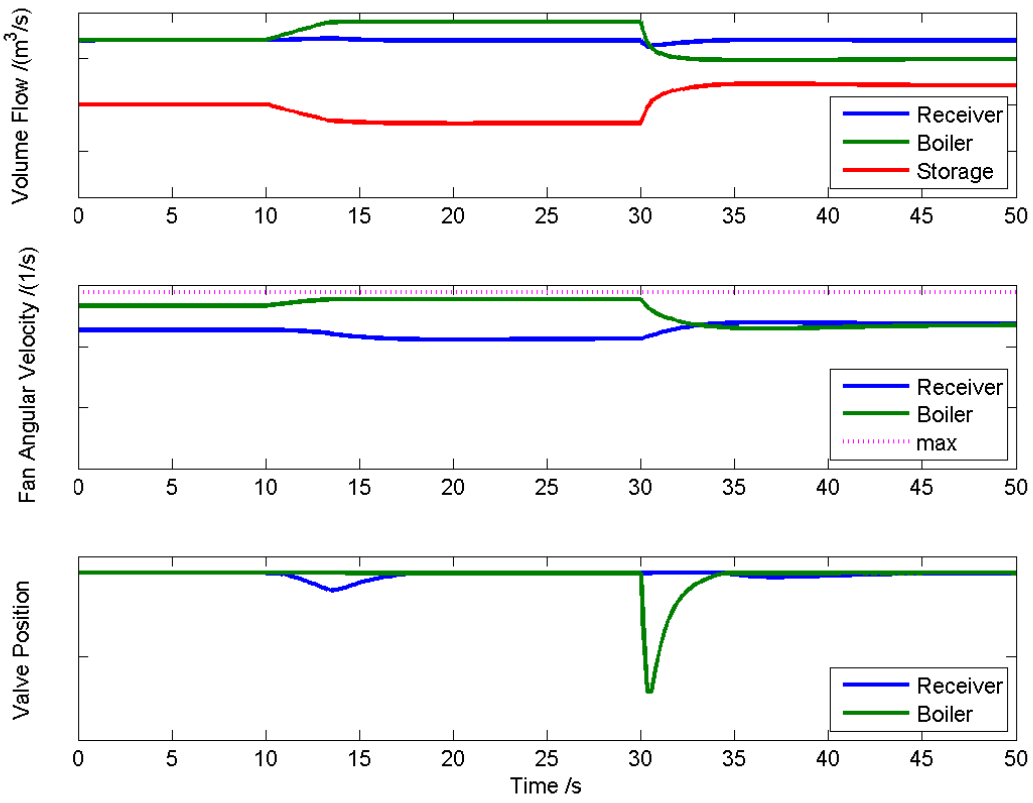

Figure IV.1-48: Operator Input

IV.1.2.4.b. *Start-up and Shutdown*

Figure IV.1-49 depicts the start-up and shutdown of the plant. During these periods it is important to follow given temperature profiles in the boiler to assure a defined heat-up of the turbine according to the rules of the manufacturer.

In the upper part of the figure, the outlet temperature at the receiver together with the actual setpoint is shown. In the lower part, the corresponding front temperature of the receiver is depicted. Note that in this simulation, a constant solar irradiation is assumed during the simulation run which allows full-load operation of the plant.

Due to the high irradiation during the start-up phase, the limit value monitoring of the blower defocuses some heliostats, since the fan is at its maximum speed.

At time $t = 2500\ s$, the feedback from the receiver front temperature gets active and defocuses some heliostats on its part, since the maximal value of this temperature is reached.

Afterwards, the system is cooled down again. This again requires the monitoring loop of the blowers to limit the amount of energy from the heliostat field.

As one can see, the system follows the trajectory of the air outlet temperature quite well, so it is assumed that the automation scheme can cope with transients in plant operation.

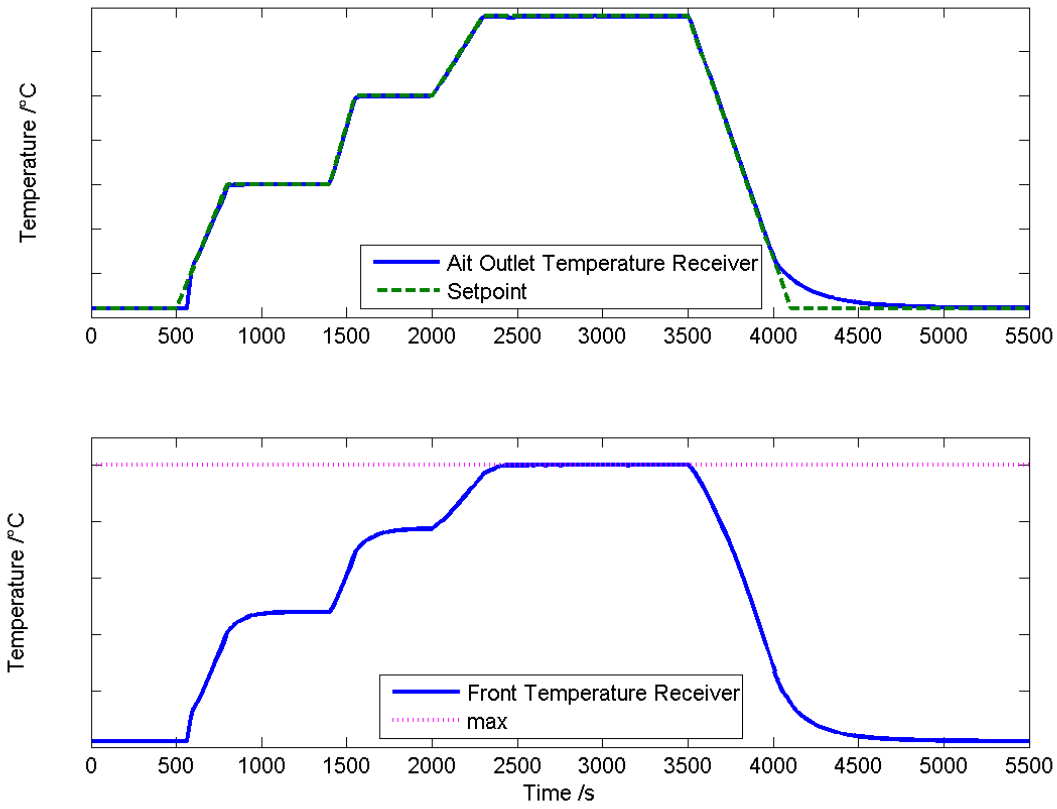

Figure IV.1-49: Start-up and Shutdown

IV.1.2.4.c. Control of the receiver temperature

Temperature control of the receiver, as the most important process variable given the varying solar radiation, is depicted in Figure IV.1-50 and Figure IV.1-51, including the results of the model-based predictive control (MPC) to be elucidated in the following sections.

Figure IV.1-50 depicts the receiver first in a steady operation point with constant radiation and the air temperature of 680°C. From the time point *t = 100 s*, a sinusoidal disturbance affects the radiation with an amplitude of 50% of the initial value and a period duration of 600 s. After 1200 s, the radiation remains constant. The radiation is depicted in the upper part of the diagram.

The lower diagram represents the air outlet temperature of the receiver. It is essential for the control to suppress disturbances, i.e. to keep the temperature as constant as possible by setting the volume flow through the receiver. The magenta line depicts a simulation of the behavior of the receiver without control, i.e. with a constant volume flow.

The blue line stands for the system response with the introduced PI-control. The green line depicts the control with an additional feed-forward control described in section IV.1.2.3. It is evident that it helps improve the performance significantly. The maximum deviation with the feed-forward control is about one-tenth compared to the simulation without feed-forward control.

Figure IV.1-51 illustrates the result of the control with a stochastic excitation of the process. The parameterization of the model for generation of the test signal for the radiation has been chosen so that the lower limit for the flow rate can be partly achieved during phases with little solar radiation.

It should also be noted that the models for the radiation refer to the mean flux density on the receiver surface. The spatial distribution of the heliostats induce a corresponding delay in the occurrence of disturbances, caused, for example, by clouds, since not the whole field is directly shadowed. Thus a low pass filtered signal reaches the receiver, which does not have such large gradients as the signal created by the model here.

Nevertheless, the advantage of the feed-forward control is also evident in this figure.

IV.1.3. Model-based Predictive Control

Model-based predictive control (MPC) is a control procedure based on an internal model of the process. The purpose is to predict the future process behavior using the internal model and thus to define optimal control actions for the desired system behavior.

The MPC relies on a discrete-time process model. Such model defines the system response over a prediction horizon at a time point *k* and compares it to a reference trajectory. The differences are weighted with a cost function; the optimal control actions over the control horizon are computed by minimizing this function. Furthermore, it is possible to penalize absolute values and changes of the inputs in order to consider the required energy of the actuating elements. In addition, these values, like the outputs, can be constrained to a permissible area during the optimization process.

For a closed-loop MPC, only the first value of the computed optimal trajectory of the actuators is introduced into the process, and the above described optimization for the next time step is iterated. This principle is known as *receding horizon*.

IV.1.3.1. Offset-free tracking

An important criterion of efficiency in the assessment of process control is offset-free tracking. In other words, it is the capacity of a closed loop to achieve a predetermined setpoint for time *t* towards infinity with no remaining deviation. Since the applied process model in the MPC contains inherent model inaccuracies, it is important to eliminate such "faults" with appropriate measures and thus provide steady-state precision

The MPC offers a number of options for that. The easiest method is an adjustment of the reference trajectory. The measured process output of the previous time step is compared to the output of the prediction model and the difference is subtracted from the reference trajectory. Here, it is assumed that the deviation between the real process and the model, given a constant reference trajectory, is caused by an additive disturbance at the output. Such extension of the MPC can be regarded as supplementary feedback over a discrete-time integrator in order to obtain steady-state precision for asymptotically stable systems.

IV.1.3.2. Disturbance prediction

Similar to the feed-forward control introduced in section IV.1.2.3, the MPC also allows consideration of the measurable resp. known disturbances. In contrast to the conventional automation scheme, in the MPC the future trajectories of predictable disturbances can also be specified over the prediction horizon. In case the future development of the disturbance is unknown, it is often assumed to be constant over the horizon.

IV.1.3.3. Simulation results

Figure IV.1-50 and Figure IV.1-51 demonstrate a comparison of the conventional automation concept with a MPC for the regulation of the receiver temperature. The MPC was implemented in Modelica. To solve the Quadratic Program arising in the MPC, qpOASES, which uses an Online Active Set Strategy and is intended particularly for the application of a MPC, was linked to Dymola.

As seen in the figures, advanced control methods help obtain better system performance. Nevertheless, plausible results can also be provided by means of PID controllers with structural improvements, such as a skillful interconnection of the controllers and an appropriate feed-forward control. Notably, the PID-based control combined with the feed-forward control

provides better results than the MPC without consideration of disturbances and is rather robust if parameterized appropriately.

To sum up, the employment of a MPC for the air cycle of a power plant seems not to be justified in every case, judging on the effort and costs of modeling, implementation and putting into operation. In particular, it seems less reasonable, since the aim of the control in normal operation is suppression of disturbances and no change in operation point occurs.

To enhance the efficiency of the overall system, it is worth regarding operation plans for the thermal storage tank.

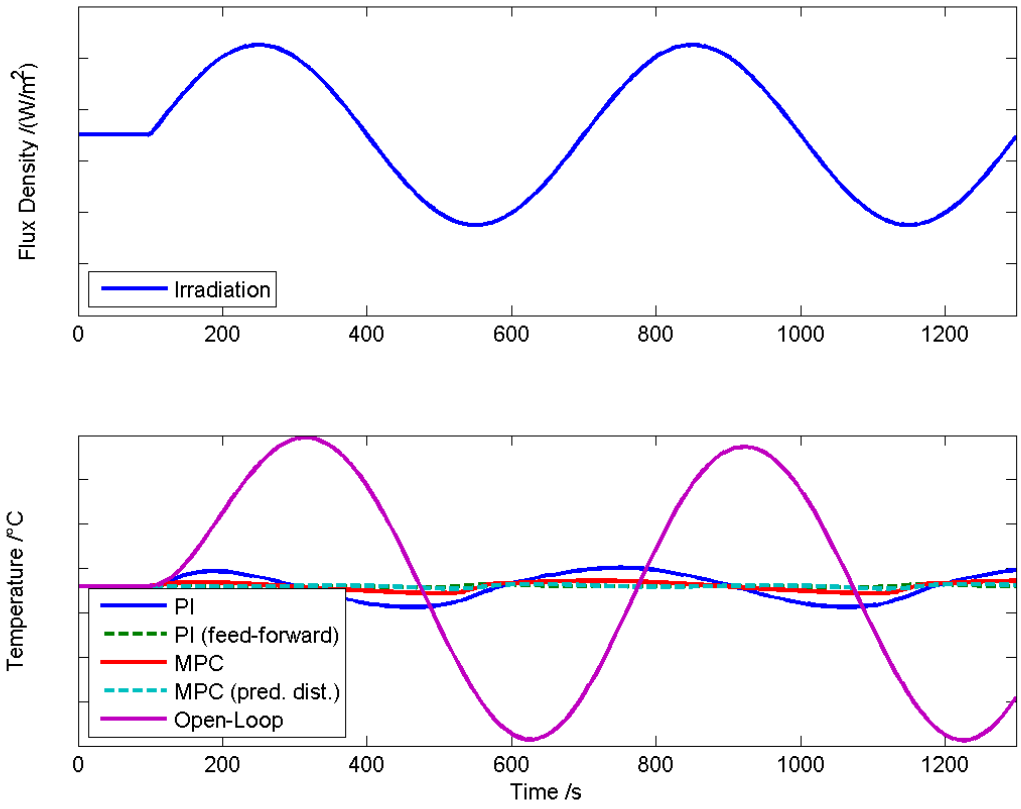

Figure IV.1-50: Sinusoidal disturbance

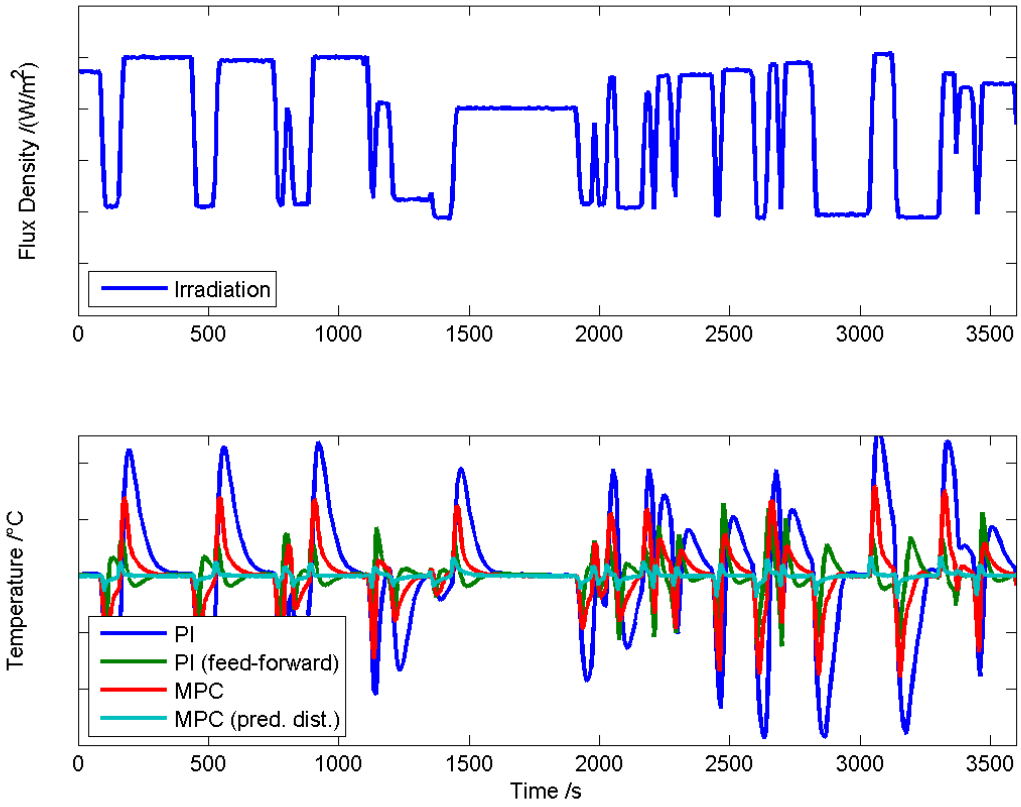

Figure IV.1-51: Stochastic disturbance

IV.2. Concept of an operator's assistance system

In the previous section it was demonstrated that advanced control methods have a clear advantage compared to conventional automation concepts based on simple PID controllers. However, it was also shown how to achieve a comparable quality of control performance by means of structural improvements, such as skillful interconnection of different signal, controllers and actuators, and also by application of feed-forward control. The subsequent sections provide an introduction and description of a system that contains a more advanced level of automation aimed at optimization of the overall operation of the power plant.

IV.2.1. Motivation

The assistance system is a system that provides the user with recommendations on how to operate the plant with the best possible efficiency, depending on the current process state and according to the current and future boundary conditions. In a solar tower power plant, this recommendation concerns in particular the operation of the thermal storage which offers large capacities for enhancing the efficiency of the overall process. A simple automation concept based on PID controllers has no such potential, since it responds only to the current state of the power plant or the current measured variables and disregards future trajectories of various values and boundary conditions.

The assistance system relies on an internal model of the power plant, which helps predict the relevant process variables of the future. The development of these variables can be assessed with a properly defined cost function. This assessment is further used to determine the required control actions, using the corresponding optimization processes, in order to minimize or maximize this cost function. This is known as *optimal control problem*.

The concept can be compared to the model-based predictive control (MPC) introduced in the previous section, which is applied however through the principle of the receding horizon in closed loop. In contrast to the MPC, the assistance system operates on a higher process level. It means that its primary task is not the direct control of the actuators. The definition of the cost function is aimed rather at economic aspects or general operation/optimization of the system over a certain time interval.

Within the framework of control engineering, the MPC is successfully deployed in several branches of industry, although not widely used, least of all at power plants. The PID controller remains the most popular algorithm applied in industrial settings.

There are at least three reasons for the prevalence of the use of the PID algorithm:

1. The PID algorithm operates satisfactorily in most types of the applications; especially with the possibility to resort to a cascade structure for dynamical decoupling in complex processes;
2. The algorithm is easy to comprehend; there is a great number of literature and software on its implementation and tuning;
3. It is readily pre-programmed in each system, whereas more advanced procedures must be often programmed additionally.

Nevertheless, investigations have shown that only a third of all control loops behave properly and almost 30% operate manually, i.e. with manual input of manipulated variables. On the other hand, according to the surveys, operators are often satisfied with the MPC, as compared to other (advanced) control processes.

Consequently, it is essential to gain an enhanced efficiency of the control as well as credence of the operating personnel and certain confidence in the system. In this respect, the assistance system can be viewed as an intermediate step to the establishment of this technology, since it helps realize comparable methods, yet without direct feedback on the process.

However, there is no reason for not operating the assistance system in a closed loop, after a certain time sufficient for its validation, as well as for not transferring the inputs directly into the control system. Furthermore, a process in the assistance system can be modeled up to the field level to allow the activation of the actuators in the closed loop directly in the assistance system.

IV.2.2. Layout

The structure of the assistance system is represented in

Figure IV.2-52. The fragment of the Dymola simulation environment on the left part exemplifies the real process (the real power plant in this case), which is controlled by means of the programmable logic controller (PLC). The right picture of the control panel of the SCADA-Software WinCC by Siemens AG stands for the process control system to which the assistance system is connected.

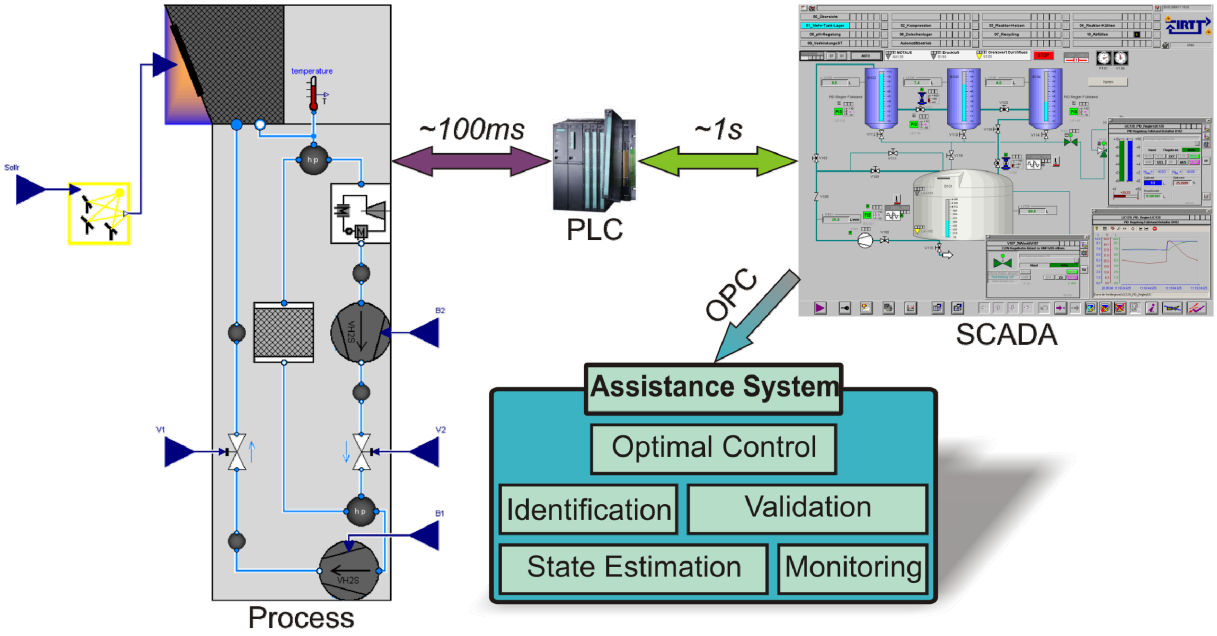

Figure IV.2-52: Layout of the assistance system

IV.2.2.1. Connection to the process control system

Control and regulation of the modern industrial processes are realized, in most cases, over programmable logic controllers (PLC) which have almost replaced the "hard-wired" controllers. Most PLCs operate cycle-oriented: in each cycle, the process image of the inputs is first updated with the subsequent calculations necessary to define the process image of the outputs, which is further transmitted to the peripherals.

The connection of the peripherals or field equipment to the PLC is often realized via a bus system. The fieldbus has replaced the conventional parallel wiring and stimulated the appearance of a number of various fieldbus systems with different properties, e. g. PROFIBUS.

The cycle times of the PLC depend on the dynamics of the associated processes. In process engineering, 90% of the required cycle times vary between 100ms and 1s, whereas other processes, such as motion-control applications, can have strict real-time requirements with isochronous cycle times of less than 1ms.

The process control system serves to operate and observe the processes and is connected to the PLC. There, processes are observed and the measured values are collected. It should be noted that the control algorithms are typically implemented in the PLC so that it can be operated autonomously, independent from the SCADA system. Hence, the requirements to the connection to the control system are not so high, as compared to the fieldbus, especially concerning the real time requirements.

The connection of the assistance system to the control system is performed via OPC, a protocol standard for manufacturer-independent communication in automation engineering. The access to the process variables in the control system proceeds (first) in read-only mode in order to prevent unintended feedback on the plant.

IV.2.2.2. Components

As seen in

Figure IV.2-52, the assistance system consists of various, partly optional elements which compose the overall system. The description of these elements is provided in the sections below.

IV.2.2.2.a. Optimal control

Finding the solution to the optimal control problem is the core task of the system. An optimal solution is calculated with respect to the defined cost function, which regards the system dynamics, i. e. fulfills the system of the differential equations, established during the modeling, as boundary conditions. Particularly, in this component a "time-table" for the storage use is generated, i. e. it contains recommendations for the operator, concerning for example the charge/discharge procedures for the course of the day.

IV.2.2.2.b. Identification

Due to the fact that the assistance system works parallel to the control system and has access to all process variables, it is possible to identify and adjust the applied internal model of the process. System identification is a process for the creation of an adequate mathematical model of the dynamical system based on the given input and output variables. This model submits the test data and the behavior also for unknown and independent validation data by making reliable generalizations. It helps secure the validity of the model and its ability for a prediction within the assistance system.

The model types applied for identification or simulation have various characteristics. There are White-Box models that make use of physical relations and expert knowledge as a-priori information. Due to the complexity of the processes, it is very difficult or sometimes impossible to obtain pure White-Box models. There also exist Black-Box models which are independent from the physical behavior of the process. Their parameters are only adapted to be able to approach the measured data well and to allow no physical interpretation

A compromise between these two extremes is provided by so-called Grey-Box models. They are capable of incorporating both qualitative expert knowledge and quantitative (data-) knowledge. For the identification, it means that the model structure is often determined a-priori and that finally a number of free parameters is estimated via adequate algorithms on the basis of the measured data. In simulation, the priority is often given to the latter modeling type, since it permits a physical interpretation of the description under its manageable complexity.

A distinctive feature in the application of the assistance system is steady-state precision. This, or offset-free tracking, is a property of a closed loop which allows obtaining a predefined setpoint for the time t towards infinity with no remaining deviation. Since the assistance system is inherently free of feedback, i. e. forms no closed loop, the definition cannot be transferred one-to-one. However, there is a similar problem: if the process is in a steady state, the recommendations of the assistance systems should be to leave the manipulated variables unchanged, despite of the model errors, in order to remain in this state. In the classical sense of the term "steady-state precision", the task is to adjust the manipulated variable, given the known setpoint, so that the process variable receives a certain value (the setpoint value). In the assistance system, the simulated output must coincide with the real output variable, given the known manipulated variable. This property plays the same role in the acceptance of the system by the operating personnel as the steady-state precision in the closed loop.

IV.2.2.2.c. Model validation

Coupling of the assistance system to the control systems also permits to validate the identified models. The essential demand for the separation of identification and validation data can be fulfilled by the assistance system by switching between identification and validation phases. To obtain reliable results, appropriate dynamic excitations of the process within a single phase must occur, corresponding to the task.

For validation, the same input variables as in the real process can be applied to the model over a past time horizon, in order to compare the model output with the real output, respectively. The result of the validation can be visualized to show the operator the quality of the

internal model performance at a certain time point to give a hint about the reliability of the prediction.

IV.2.2.2.d. *State estimation*

Almost every advanced control method requires the knowledge of the overall system state. Since this state can be measured only in a few cases, appropriate state observers must be used to estimate the system state.

In case of linear systems, the separation principle and the duality of pole placement apply to both observers and state controllers, which means that the same configuration procedures are valid for both of them. The Luenberger observer and the Kalman filter are examples of linear observers. In nonlinear systems, the extended Kalman filter (EKF) is an extension whereby the system is linearized about the current estimated value in each step.

Nonlinear optimization used in solving the optimal control problem can also be applied for state estimation (Moving Horizon Estimation (MHE)). The MHE problem is, in a way, the dual problem of predictive control. Instead of predicting the future, one looks at the in- and output data over a past (finite) horizon and estimates the state trajectories which are consistent with the model and reflect the measured data as precise as possible. This allows considering constraints explicitly also during the state estimation, so that in most cases the MHE submits better estimations and is more robust, as compared to e. g. extended Kalman filter.

IV.2.2.2.e. *Monitoring*

If the peripheral equipment is also modeled in the assistance system, the latter allows designing the current real control cycles thus implementing performance monitoring. This may help finding control cycles which are unable to achieve the optimal quality due to poor parameterization. Moreover, (gradual) changes in the real system can be detected which are regulated by the control system and thus remain unnoticed to the operator, e. g. by occurance of drift of an identified parameter which has normally been constant. Therefore, impending failures of the components can be detected at an early stage.

IV.3. Optimization of receiver operation

During the operation of the power plant, the normal operating condition is an uneven flow distribution over the receiver surface. This means that the different subreceivers will receive a different flow and need to be controlled independently to avoid overheating. By using valves in the subreceivers, it is thus possible to control the mass flow distribution. This leads to the question of finding an appropriate operation strategy. Assuming a given mixed exit air temperature from the receiver, the simplest strategy would be to let each submodule be controlled in an independent manner as to obtain this temperature. More efficient strategies can, however, be found by posing the problem as a optimal control problem. The problem formulation is here that, given an output temperature (of the air from all the subreceivers), to find a suitable mass flow distribution among the subreceivers which maximizes the total mass flow from all the subreceivers.

The problem can be posed as a discrete time optimial control problem and solved with the so-called dynamic programming (DP). Note that even though *time* is in the problem formulation, it is not physical time and the problem formulation is a static one. The DP method splits a decision making problem into a sequence of simpler decision making problems. In the present case, we start by reducing the problem to that of only two subreceivers. This is done by calculating the total (not specific) enthalpy flow from the subreceiver for every possible mass flow. This calculation is made using a simplified, static subreceiver model, deduced from the detailed one. This gives trade-off curves between enthalpy flow and mass flow as illustrated in Figure IV.3-53.

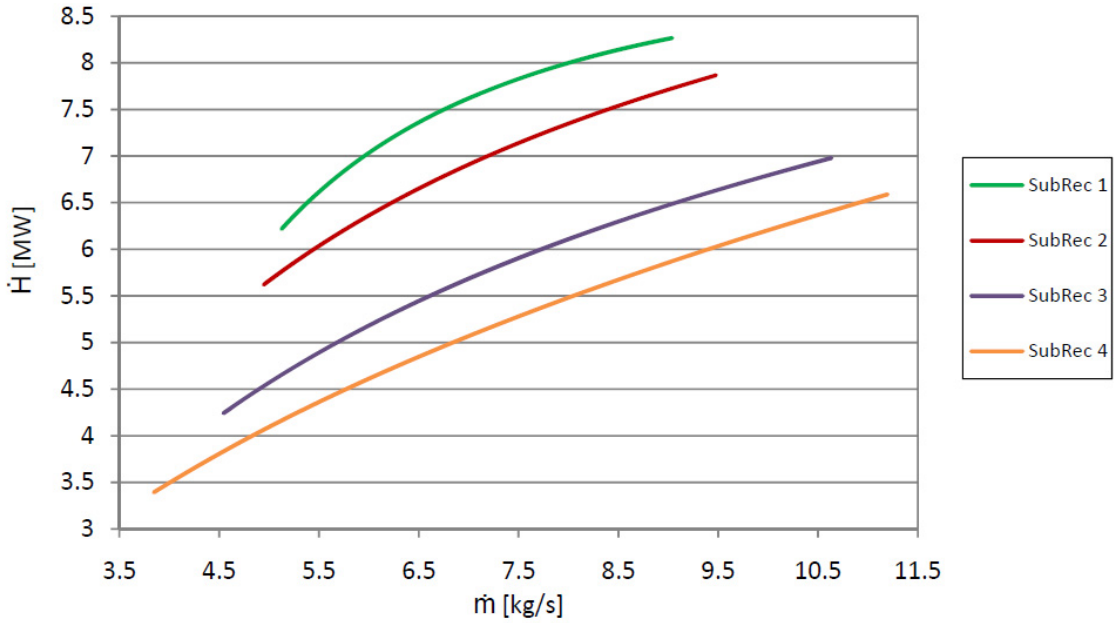

Figure IV.3-54: Enthalpy flows / mass flow trade-off for 4 different subreceivers [18]

At this point, all possible we shall combine the first two subreceivers together and obtain a similar trade-off curve for the combined mass flow and enthalpy flow. In this process, it will be possible to obtain different enthalpy flows for a given combined mass flow (by letting more mass flow though one or the other subreceiver). Interesting is however only the highest possible enthalpy flow (for a given mass flow), which allows us to eliminate a set of suboptimal solutions. This is illustrated in Figure IV.3-55.

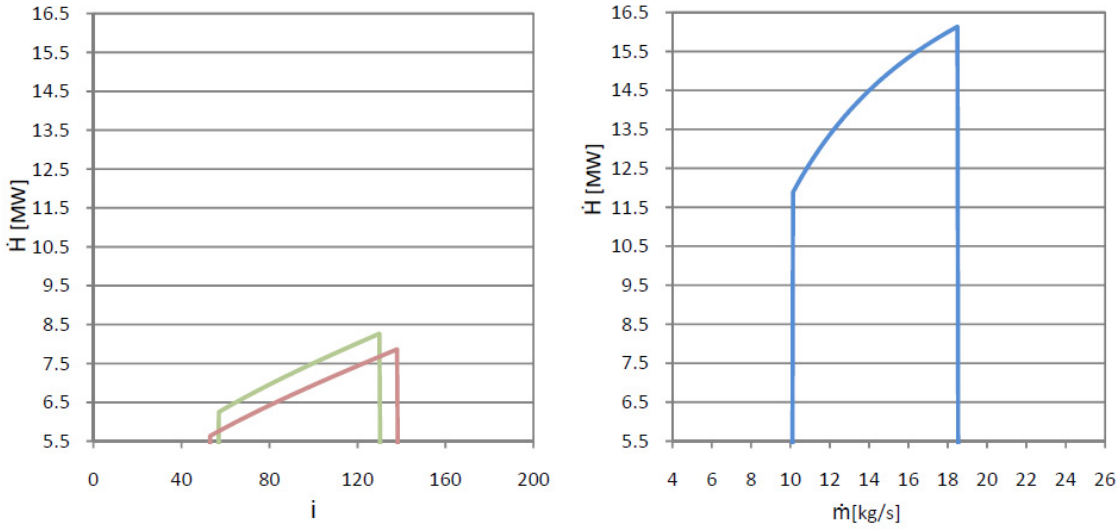

Figure IV.3-55: First step of the dynamic programming algorithm. Left: Mass/enthalpy flow trade-off for the individial subreceivers. Right: Left: Mass/enthalpy flow trade-off from both subreceivers [18]

The joint trade-off curve for subreceivers 1 and 2 will in the next step be combined with the trade-off curve for subreceiver 3, which will again exclude a set of suboptimal solutions. The procedure is continued until a trade-off curve between (optimal) enthalpy flow and mass flow

for all the subreceivers is obtained. This is shown in Figure IV.3-56. Since a mixing temperature will correspond to a curve in the enthalpy-mass flow graph, we can find the optimal mass enthalpy flow for a given mass flow by simply finding the intersection between this curve and the optimal trade-off curve just calculated. By going through all the steps in the algorithm in reverse order, it is then possible to find the individual subreceiver mass flows (and corresponding valve settings).

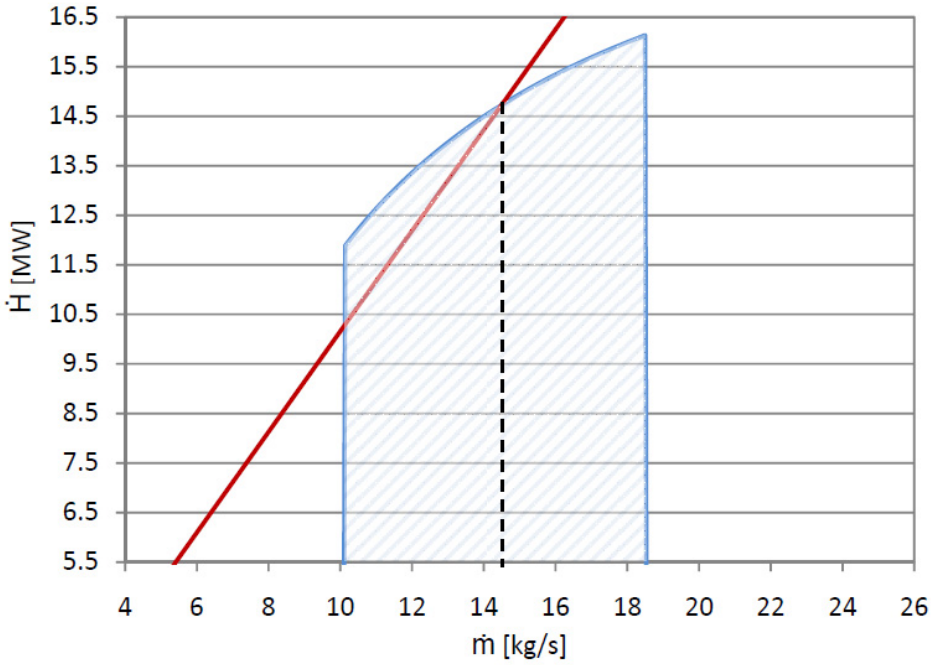

Figure IV.3-56: Mass/enthalpy flow trade-off for all subreceivers and the line corresponding to a particular temperature

IV.4. Optimization tool development

The dynamic model of the power plant, modelled in the physical modelling language Modelica, can be translated into a set of differential and algebraic equations (a *DAE*) by a compiler of Modelica code. Together with an objective function and a set of constraints (which in particular can be formulated in the Modelica language extension “Optimica”) this gives rise to an optimal control problem in differential algebraic equations.

While simulation of DAEs is a relatively developed technique, in the sense that there are robust numerical software packages that can work with a wide range of large-scale, nonlinear models, *optimization* using the same models is much less mature field.

Due to the complex geometry of the plant, temperatures ranging from ambient temperature to 800 °C or more and nonlinear dynamics such as flow reversals (e.g. in the thermal storage), even a relatively simple model of the plant would constitute a major challenge for existing tools for optimal control. Therefore it is essential to deduce as much information as possible over the model structure and, if possible, exploit this in the optimal control algorithm. For this aim, an innovative approach was developed, in which the Modelica compiler JModelica.org was used to import the Modelica code and export the DAE in a symbolic format, an extension of the Functional Mockup Interface (FMI) standard. In contrast to a more conventional approach involving the export of the DAE as a call-back function, which in turn can be linked with the optimal control problem environment, the approach used here enables auto-

matic generation of information that can be exploited in optimal control algorithms and tools. This includes sparsity information and derivative information to an arbitrary degree.

This approach was realized in the development of the software tool CasADi, which has the explicit aim to advance the state-of-the-art for optimization of complex, nonlinear and unstructured dynamic models. CasADi consists of a minimalistic computer algebra system (CAS) written in C++ which contains a number of highly efficient implementations of algorithmic differentiation using a symbolic-numeric approach [19]. This is combined with model import from JModelica.org, a highly interactive user interface in the programming language Python and interfaces to other codes from the field of numerical optimization and scientific computing.

The optimization framework was first successfully used to optimize a combined cycle power plant, where a validated first principle model in Modelica was readily available. This model, which is formulated in around 8000 lines of Modelica code, was translated into a DAE with 9 differential and 127 algebraic states. For this benchmark process, the proposed developed approach was applied successfully to find a minimal time start-up trajectory. In the solution, the robustness of the solution was improved and improvements of up to two orders o magnitude was seen in time critical calculations [20].

Two algorithmic approaches were pursued for the model based optimization, both of which belong to the group of simultaneous optimization methods. The two methods chosen were *direct collocation* and *direct multiple shooting.* These two methods can be described as representing the state-of-the-art for dynamic optimization of large-scale nonlinear processes.

A problem that can be addressed with dynamic optimization is to find an optimal plan for the loading and unloading of the four storage chambers. The goal here is to maximize the net produced electricity, possibly weighted by time dependent electricity prices. In this problem formulation, we shall furthermore introduce the *periodic* boundary condition that the temperature state of the storage is equal to its state 24 hours later. The solar radiation (which enters the problem as a *disturbance*) was taken from measurements at the Jülich location. For this problem, we assume that all dynamic behaviour other than storage dynamics can be neglected due to the relatively long time scaled involved. This in particular allows to write the mass flow from the receiver as a function of time only, which can be determined before the start of the optimization. The steam cycle was here modelled with efficiency coefficient only.

Different dynamic models, with increasing complexity, were explored for the heat storage. A very simple model is obtained when only the total heat in the storage talk is modelled, meaning that each storage talk is represented by a single state only. We used this model (which could be solved readily) as a starting point for a more realistic model based with the storage modelled using the convection-diffusion-equation. To obtain an ordinary differential equation, the spatial coordinate was discretized using the method-of-lines.

The result of the optimization is shown below for both the trivial model as well as the model which includes spatial discretization. The solution agrees with physical intuition, In this case to try to keep the mass flow to the steam turbine at a constant 80 % of its maximum value, which corresponds to the value where the steam cycle operates with the highest efficiency. The figure also shows the temperature of the storage chamber near the entry and exit respectively.

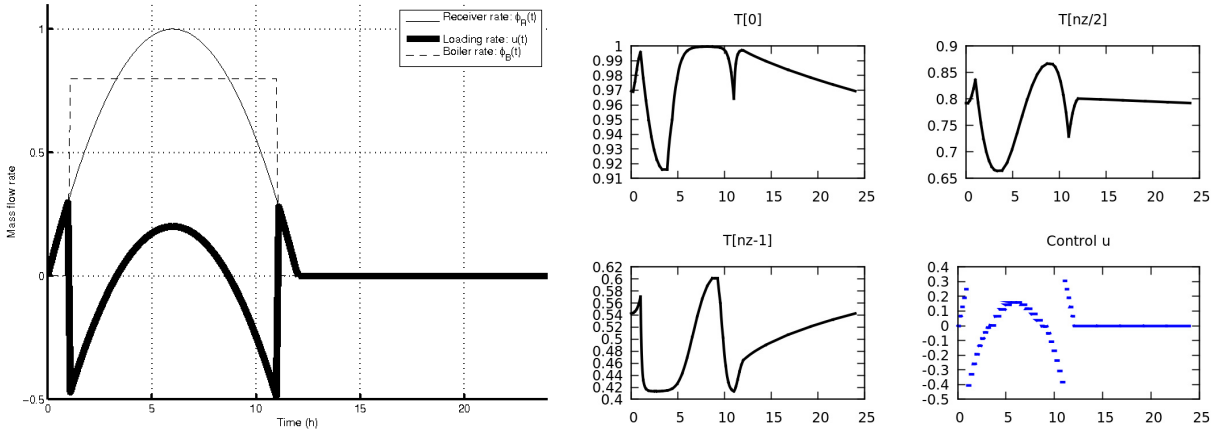

Figure IV.4-57: Optimal storage planning. Left: Solution using simplified model. Right: Solution with 1D stor-age model

V. Results of WP 4 – Impact of scale-up to larger power levels and innovative component concepts on the plant performance

V.1. Scope of the work package

The simulation studies performed in the vICERP project were closely linked to the Jülich solar Tower Configuration. Since this plant has been build as a research and demonstration facility a commercial size plant will differ in a number of aspects. These include

- The size of the plant
- The arrangement of components relative to each other
- The capacity of the storage
- Degree of plant automation

This work package intends to identify and evaluate the main differences.

V.2. Reference configuration

As a reference configuration a solar tower plant with a gross electric power of 30 MW is chosen. This is considered as a relevant size for future plants. Compared to the Jülich plant the layout shows some modifications representative for larger plants. As the thermal storage integration is one of the key benefits of the plant concept, the reference configuration assumes a thermal storage for 8 full load hours that can be used to fulfill given demand profiles. Table V-1 summarizes the main parameters of the plant.

Table V-1 Parameters of the reference configuration

		Scaled-up design
1	Turbine gross power	30 MW
2	Storage capacity in full load hours	8 h
3	Solar Multiple	2
4	Heliostat field	205 °
5	Heliostat field design power	160 MW
6	Co-firing (thermal power)	0
7	Location of boiler, turbine, and storage	Bottom of the tower
8	Boiler type	Multiple pressure
9	Design gross efficiency power block	35 – 40 %
10	Cooling	Dry
11	Operation at night	Shut-down

Some major modifications in the plant layout have to be expected for the arrangement of the components. An increase in storage capacity is not possible with a storage located inside the tower, so the reference configuration foresees the storage arranged on the ground somewhere around the tower. In the same way, the heat exchanger and the turbine will not be located in the tower. As a consequence, piping between the receiver and the heat consumers will get much longer. Large diameter pipes have to be used to meet the increased power of the system.

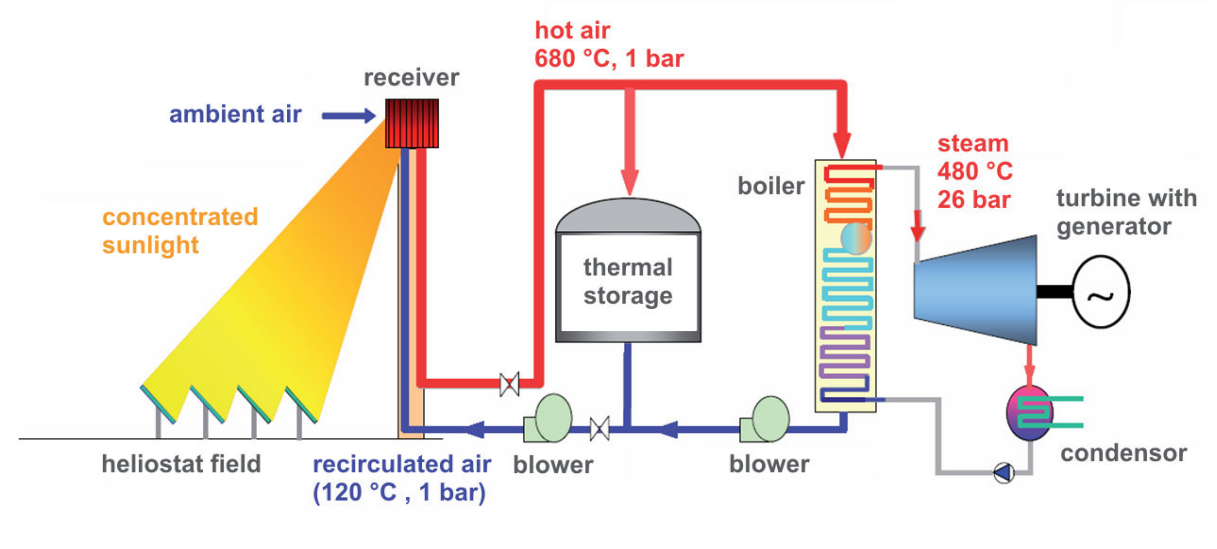

Figure V.2-58: Solar Tower Jülich plant layout

V.3. Impact of scale-up on the dynamic behaviour

V.3.1. Heliostat field

The heliostat field has as mentioned earlier a big impact on the dynamic behavior of the receiver. The impact will grow with a scale up of the power plant. The heliostat field expands most likely from a north field to a circular field. The dimensions of the field increase as well. The differences of the flux density distribution over the day enlarge.

The demand for an optimized operational strategy using a heliostat aim point configuration grows. Very good manual aim point configurations are difficult to obtain and non optimal configurations can lead to large losses. Even group configurations are very complex to handle. First results for an optimized heliostat aim point configuration are obtained indicating the big impact on the receiver performance [21].

V.3.2. Receiver

The dynamic behaviour of the receiver is mainly dependent on the adjacent flux density distribution, which local distribution changes considerably for a larger receiver. However, the subdivision of the receiver into several sub-receivers leads to a similar behaviour of the sub-receivers in a small power plant and in an up scaled power plant. The variable local distribution is handled by the sub-receivers. The changes in time are similar for a larger receiver and a smaller receiver.

However, it gets more complicated to find an optimal mass flow rate distribution for a larger receiver. With the number of sub-receivers the complexity of the mixing problem of sub-receiver air streams to reach the desired air outlet temperature increases. Different options have been evaluated to cover this effect. Especially for the start up and shut down procedures, one option might be to shut down parts of the receiver since some areas receive not enough solar energy to contribute a reasonable air stream at a specific temperature to the overall mass flow rate. Other sub-receivers would have to operate in a suboptimal area to compensate for cold sub-receivers. An optimization algorithm is applied to the problem to optimize the overall mass flow rate of the receiver at a desired air outlet temperature [21]. The approach is described in section IV.3. Further investigations are required to verify the proposed strategy.

V.3.3. Thermal storage

In further concepts the location of the storage should be on the ground. Heat losses are less if the tube connection between receiver and storage is short. But the high weights of storage mass and the installation seam not to justify the aim to bring the storage near to the receiver.

The dimension of the used storage concept has limits. For increasing the storage capacity, more storage modules are needed. There are two possibilities to install and combine more modules.

- parallel concept (system of parallel installed storage modules)
- serial concept (system of serial installed storage modules)

The parallel concept has the advantage, to enable an increase of the heat transfer power by increasing the cross sectional area. Further more pressure drop decreases by decreasing air velocity through the storage.

The serial concept has the disadvantage in increasing pressure drop. But it has the advantage to store more heat energy in the storage system per installed volume material. This advantage is reached in comparison to the parallel concept with the same boundary conditions as they exist at the solar tower Jülich (for example in respect to maximum air outlet temperature).

The best design of a large storage system, mentioned in the reference configuration, is to combine a parallel and serial concept.

Furthermore the implementation of the storage via the two blowers was observed. This configuration allows a rapid storage operation. This result is gained from work experience at solar tower Jülich. The response of the storage air mass flow by a demand of boiler inflow temperature is very fast. This configuration should be maintained.

V.3.4. Water-steam cycle

A scale-up to a plant size of 30 MW will lead to an approximated efficiency of 35%. The efficiency could be increased even further to values above 40% with a rise of the upper temperature level to 535°C and additional process enhancing arrangements, like intermediate superheating for example. These arrangements, however, will lead to a great increase in investment costs. It is further to mention that the efficiency is strongly dependent on the steam generator design, preheaters and intermediate super-heaters.

Turbines in the described power class usually operate with sliding pressure control down to 25%. Preheaters are standard components.

If the scaled-up turbine exclusively operates in times of daylight the material temperatures will approximately drop to 180-210°C during holdup at night, which requires a cold start-up which takes about one hour. For this reason, a heat energy storage with a capacity enabling the complete power plant to operate 24 hours would significantly increase the system flexibility since ramp up is possible in warm start-up mode.

Instead of the air cooled condenser a wet cooling system should be implemented. This would lead to more constant temperatures and an estimated pressure of 60 mbar. With a case-specified adaption the pressure level in the condenser could be reduced down to 40 mbar.

For the steam generator a 64t standard boiler should be used. Favourable, would be a single-duct and upright erected steam generator.

V.3.5. Operation and control

Since the overall plant layout is not affected by the scale-up, there are no necessary changes in the structural design of the automation scheme. The differences in the dynamic behavior of the various components do result only in a different parameterization of the transfer blocks.

Considering the model-based control algorithms, these have to be equipped with the adapted models for the scaled-up system to work properly. However, it may be necessary to carry out small changes in the cost function of the optimization problem (in the assistance system), e. g. to avoid frequent start-up and shutdown of the turbine, which is more harmful to a larger version than to the small one in Jülich.

References

[1] Harlow, F. H. und Welch, J. E.: *Numerical Calculation of Time-Dependent Viscous Incompressible Flow of Fluid with Free Surfaces*. Phys. Fluids, Vol. 8, (1965) p. 2182-2189

[2] Tummescheid, H.: *Design and Implementation of Object-Oriented Model Libraries using Modelica.* Lund Institute of Technology Lund, Sweden (2002)

[3] Belhomme, B. und Pitz-Paal, R. und Schwarzbozl, P. und Ulmer, S.: *A New Fast Ray Tracing Tool for High-Precision Simulation of Heliostat Fields*. Journal of Solar Energy Engineering, Vol. 131, 3 (2009) p. 031002-8

[4] Belhomme, B.: *Bewertung und Optimierung von Zielpunktstrategien für solare Turmkraftwerke.* RWTH Aachen (2010)

[5] Ahlbrink, Nils und Belhomme, Boris und Pitz-Paal, Robert: *Transient Simulation of Solar Tower Power Plants with Open Volumetric Air Receiver*. Proceedings of the SolarPACES 2009, Berlin (2009)

[6] Ahlbrink, N. und Alexopoulos, S. und Andersson, J. und Belhomme, B. und Boura, C.T. und Gall, J. und Hirsch, T.: *The virtual institute for central receiver power plants: Modeling and simulation of an open volumetric air receiver power plant*. Proceedings of the MathMod 2009, Vienna (2009)

[7] Gall, J. und Abel, Dirk und Ahlbrink, N. und Pitz-Paal, R. und Andersson, J. und Diehl, Moritz und Boura, C.T. und Schmitz, M. und Hoffschmidt, B.: *Optimized Control of Hot-Gas Cycle for Solar Thermal Power Plants*. Proceedings of the 7th International Modelica Conference, Como, Italien (2009)

[8] Shah, R.K. und London, A.L.: *Laminar Flow Forced Convection in Ducts.* Academic Press New York (1978)

[9] Kreith, Frank und Bohn, M.S.: *Principles of Heat Transfer.* Harper and Row New York (1986)

[10] Böswirth, L.: *Technische Strömungslehre.* Vieweg Wiesbaden (2005)

[11] VDI: *VDI-Wärmeatlas: Berechnungsblätter für den Wärmeübergang* Verein Deutscher Ingenieure; VDI-Gesellschaft Verfahrenstechnik und Chemieingenieurwesen (GVC), 9. Auflage Aufl. (2002)

[12] Casella, F. und Leva, A.: *Modelica open library for power plant simulation: design and experimental validation*. Proceedings of the 3rd International Modelica Conference Linköping, Schweden (2003) p. 41-50

[13] Leva, Alberto und Maffezzoni, Claudio und Benelli, Giancarlo: *Validation of drum boiler model through complete dynamic tests*. Control Engineering Practice, Vol. 7, (1999) p. 11-26

[14] Göhring, F. und Bender, O. und Röger, M. und Nettlau, J. und Schwarzbözl, P.: *Flux Density Measurement on Open Volumetric Receivers*. Proceedings of the SolarPACES 2011, Granada (2011)

[15] Schwarzbötzl, Peter und Hack, Udo und Ebert, Miriam: *Improvement of ceramic absorber material for open volumetric receivers*. Proceedings of the SolarPACES 2011, Granada (2011)

[16] Thomey, Dennis: *Entwicklung und Aufbau eines Teststand für Solarabsorber in hochkonzentrierter Solarstrahlung.* Diplomarbeit, RWTH Aachen Aachen (2008)

[17] Pomp, Stefan und Schwarzbötzl, Peter und Koll, Gerrit und Göhring, Felix und Hartz, Thomas und Schmitz, Mark und Hoffschmidt, Bernhard: *The Solar Tower Jülich-First operational experiences and test results*. Proceedings of the 16th CSP SolarPACES Symposium, Perpignan, France (2010)

[18] Maldonado Quint, Daniel: *Zielpunktoptimierung unter Berücksichtigung des thermischen Verhaltens eines offenen volumetrischen Receivers.* Diplomarbeit, RWTH Aachen Aachen (2010)

[19] Andersson, Joel und Houska, Boris und Diehl, Moritz: *Towards a Computer Algebra System with Automatic Differentiation for use with Object-Oriented modelling languages*. Proceedings of the 3rd International Workshop on Equation-Based Object-Oriented Modeling Languages and Tools*,* Oslo, Norwegen (2010)

[20] Andersson, Joel und Åkesson, Johan und Casella, Fracesco und Diehl, Moritz: *Integration of CasADi and JModelica.org*. Proceedings of the 8th International Modelica Conference Dresden, Deutschland (2011)

[21] Ahlbrink, Nils und Andersson, Joel und Diehl, Moritz und Pitz-Paal, Robert: *Optimized operatin of an open volumetric receiver*. 16th SolarPaces*,* Perpignon (2010)